Natural Resources Canada   Ressources naturelles Canada

GEOLOGICAL SURVEY OF CANADA
OPEN FILE 7665

Seismic velocity modelling, fixed point optimization, and evaluation of positioning uncertainty in the central Labrador Sea region: methods, a software tool, and an application

Q. Li, J. Shimeld, K. Dickie, S.A. Dehler, D. Mosher, and K. Desroches

2015

Canada

GEOLOGICAL SURVEY OF CANADA
OPEN FILE 7665

Seismic velocity modelling, fixed point optimization, and evaluation of positioning uncertainty in the central Labrador Sea region: methods, a software tool, and an application

Q. Li, J. Shimeld, K. Dickie, S.A. Dehler, D. Mosher, and K. Desroches

2015

ABSTRACT

Conversion between seismic two-way time (TWT) and sediment thickness is required to implement Article 76 of the United Nations Convention on the Law of the Sea. The deep water sedimentary succession of the central Labrador Sea is used to illustrate our approach to this problem. Multiple available sources of sediment seismic velocity information are assembled and analyzed with their cons and pros for this purpose, including scientific boreholes, seismic wide-angle reflection/refraction data, and proxy observations based on the normal moveout of seismic reflections. The latter exhibit a high degree of scatter and are subject to many caveats. Therefore we preprocessed the borehole and wide-angle reflection/refraction measurements from widely distributed locations across the region of interest to create a regional model of sediment velocity versus burial depth.

The velocity model is constructed by numerical fitting of the observations with a slowness (inverse velocity) function that has strong theoretical and empirical linkages with the first-order porosity reduction behaviour documented for deep water successions around the world. The mathematical form of the model is attractive because it yields physically plausible velocities at depths beyond the range of observation, and because the model parameters are readily interpretable in terms of geologically significant physical properties.

The fitting procedure of sediment velocity model accommodates measurement error in both velocity and depth by employing the reduced major axis (RMA) method. With RMA modeling, the bootstrapping method is used to estimate confidence bounds. For the example from the Labrador Sea, the bootstrapping results indicate an overall certainty of ±6.0% at the 95% level of confidence. An analytical function is derived that allows the model to be used for precise depth-to-time conversion. For time-to-depth conversion, the Newton-Raphson method is employed that provides a predefined accuracy, such as within ±1.0 cm with computing efficiency.

Comparison of the velocity model with global results from deep sea drilling and also deep water marine shales of the Gulf of Mexico demonstrates a remarkable level of correspondence. In addition to providing support for the velocity model and its underlying methodology, the comparison provide strong evidence that porosity reduction due to compaction is the predominant factor controlling seismic velocity within the deep water marine successions.

The purpose of invoking Article 76 is to define outermost fixed points along the margin. There are several criteria. One is the maximum of 2500 m bathymetry isoline plus 60 nm criterion; another is the sediment thickness formula which requires the sediment thickness to be greater than 1% of its distance to the nearest foot of continental slope (FOS). Implementation of sediment thickness criteria is significantly optimized in this work by integrating the interpreted seismic horizons (seafloor and top of basement), FOS points, and the conversion between TWT and sediment thickness using the constructed velocity model.

Positioning uncertainty is unavoidable for current techniques in the identification of outmost fixed points. The sources of uncertainty include FOS identification, positioning of survey equipment, seismic data processing, horizon identification, and conversion between TWT and sediment thickness. These uncertainty sources are integrated into the net positioning uncertainty according to the methodology suggested by United Nations agencies.

A software tool kit is provided for the construction of the velocity model, conversion between TWT and sediment thickness, optimization the identification of fixed point, and uncertainty evaluation. They are characterized flexibility as well as efficiency, such as one page web application and look up table enabling to be embedded them in a document, batch processing of all seismic profiles in one region, interactive graphic application. A user manual is also provided with giving step by step demonstration in this report.

Key words:

Two-way time to thickness; optimize fixed point; positioning uncertainty; extended continental shelf; velocity modeling; sediment compaction; Labrador Sea; The United Nation Convention on the Law of the Sea (UNCLOS)

TABLE OF CONTENTS

LIST OF FIGURES

LIST OF TABLES

LIST OF SYMBOLS AND ABBREVIATIONS

AGS	Atlantic Geoscience Centre which was renamed as Geological Survey of Canada, Atlantic in early 1990s
BGR	German Federal Institute for Geosciences and Natural Resources
$\Delta Y_{vertical}$	vertical uncertainty by integrating uncertainty of seafloor and basement identification and sediment thickness estimation with a velocity model
$\Delta Y_{vertseafloor}$	uncertainty during seafloor horizon identification on a seismic profile
$\Delta Y_{basment}$	uncertainty during top of basement horizon identification on a seismic profile
$\Delta Y_{VelocitymModel}$	sediment thickness uncertainty caused from velocity model uncertainty
$\Delta X_{fromVertical}$	transformed vertical uncertainty from the $\Delta Y_{vertical}$ using apparent dipping angles of seafloor and basement
FOS	Foot of Continental Slope
ΔX_{FOS}	uncertainty in FOS identification, including bathymetry acquiring, data processing, and other factors
$\Delta X_{shipNavigation}$	Uncertainty of seismic reflection cruise navigation
$\Delta X_{streamer}$	positioning uncertainty of streamer; it is important in an environment such as the Arctic Ocean where floating ice will affect streamers
$\Delta X_{processing}$	positioning uncertainty caused during seismic data processing, such as stacking, binning, etc.
DSDP	Deep Sea Drilling Program
mbsf	metres below the seafloor
ms	milliseconds
GEUS	Geological Survey of Denmark and Greenland
GSC	Geological Survey of Canada
IODP	Integrated Ocean Drilling Program
ODP	Ocean Drilling Program
RMA	reduced major axis
RMS	root-mean-square
SIGNAL	Seismic Investigations of Greenland, Newfoundland and Labrador
QLine	indicator horizon of fixed point overlain on seismic profile for outmost fixed point optimization
TWT	two-way time
V_0	initial velocity (*i.e.* sedimentary velocity at the surface of deposition)
$V_\infty, V_g,$	final velocity (*i.e.* sedimentary velocity at great depth within the Earth)
V_{INT}	interval velocity
V_{NMO}	normal moveout velocity
V_{RMS}	root-mean-square velocity
V_{STK}	stacking velocity

ACKNOWLEDGEMENTS

1   Introduction

This report contains detailed information about the data, methodology, and the developed software tool for : (1) fitting a model of seismic velocity for the sedimentary succession beneath central Labrador Sea along the Canadian Atlantic margin; (2) optimizing of the fixed point, (3) analyzing positioning uncertainty.

The velocity model is required to determine sedimentary thickness so that paragraph 4(a)(i) of Article 76 may be applied for the UNCLOS program.

The most accurate measurements of sedimentary thickness are obtained from boreholes penetrating the entire sedimentary succession. However at the scale of a continental margin it is impractical to determine sedimentary thickness using only information derived from boreholes (Persand 2012). As outlined in their technical guidelines and training manual (UN-CLCS 1999, paragraph 8.2.1; UN-DOALOS 2006, page VI-11), United Nations agencies regard the information provided by seismic reflection and refraction surveys as the primary source of evidence for mapping sedimentary thickness. Moreover, the UN Commission on the Limits of the Continental Shelf regards multi-channel reflection data as the most authoritative source of evidence for the determination of sedimentary thickness (UN-CLCS 1999, paragraph 8.2.4).

Seismic reflection surveying is an invaluable technique for identifying and mapping geologically significant interfaces such as the base of the sedimentary succession. However, such interfaces are imaged using the TWT of vertically incident seismic waves. To convert this to an accurate depth, seismic velocity must be adequately characterized along the associated raypath. As will be discussed in this report, velocities derived from multi-channel reflection data are in some cases inaccurate for central Labrador Sea because of the relatively deep water and thick sedimentary succession. As a substitute, a regional model of velocity versus depth is created using measurements from seismic wide-angle reflection and refraction records based on the relatively homogenous lithology of deep water sediments and sedimentation history of the study area.

1.1   Central Labrador Sea

Knowledge of sedimentary thickness is required beneath the central, deep water region of Labrador Sea where water depths are greater than about 3000 m (Figure 1.1). Regional tectonic studies based on gravity, magnetic, and seismic data identify the presence of oceanic crust beneath most of this area (Srivastava and Tapscott 1986; Roest and Srivastava 1989; Chalmers and Laursen 1995; Chian *et al.* 1995a; Chalmers and Pulvertaft 2001; Oakey *et al.*, 2001; Oakey and Chalmers 2005). Unequivocal oceanic crust extends to magnetic Anomaly 27 (Danian) (Chalmers and Laursen 1995; Chalmers and Pulvertaft 2001), but some studies identify older oceanic crust to Anomaly 31

(Maastrichtian) (Chian *et al.* 1995) and possibly to as far as Anomaly 33 (Campanian) (Roest and Srivastava 1989).

The sedimentary succession was sampled at five sites in the study area where scientific boreholes were drilled as part of the Deep Sea Drilling Program (DSDP), the Ocean Drilling Program (ODP), and the Integrated Ocean Drilling Program (IODP) (Figure 1.1). The oldest geological samples are from DSDP Site 112 which is situated in a water depth of 3657 m. Here oceanic basalt occurs at 661 metres below the seafloor (mbsf) and it is overlain by early Paleocene claystone (Laughton *et al.* 1972). Above this, the Eocene to Miocene succession includes indurated clay, marl, silt, and siliceous ooze deposited under pelagic and hemipelagic conditions. The uppermost 115 mbsf is comprised of unconsolidated Pliocene to Pleistocene terrigenous clay and silt with occasional ice-rafted pebbles.

At ODP Site 647, where the water depth is 3862 m, oceanic basalt lies beneath an early Eocene and younger sedimentary succession that is 699 m in thickness (Srivastava *et al.* 1987). The succession consists predominantly of hemipelagic and pelagic clay, siliceous ooze, nannofossil ooze, biogenic clay, and silt. Much as at DSDP Site 112, the uppermost 116 mbsf is characterized as late Pliocene to Holocene unconsolidated terrigenous clay, mud, and silt with occasional ice-rafted pebbles.

Further north, DSDP Site 113 is situated in 3619 m of water (Laughton *et al.* 1972). Drilling at this site sampled 923 m of possible Miocene to Pleistocene aged sediments before deteriorating drilling conditions forced abandonment of the hole. The Miocene succession, which occurs below 550 mbsf, includes laminated mudstones with load casts, cross-bedding, and convolute lamination indicating the influence of deep ocean currents. The overlying Pliocene–Pleistocene succession includes a wide range of lithologies including silty clay, graded sand, clay, and conglomerate that were deposited as turbidites offshore of a glaciated margin.

The sedimentary succession sampled at IODP Site U1305 (water depth 3459 m) is characterized as 287 m of uppermost Pliocene to Holocene silty clay, silty clay with nannofossils, and nannofossil ooze (Channell *et al.* 2006). These lithologies are the result of pelagic and hemipelagic deposition under the influence of deep ocean currents and the surrounding seafloor topography. Occasional cross-bedded laminae of sandy silt throughout the sampled interval manifest either the influence of turbidity currents or the intensification of regional bottom currents. Ice-rafted pebbles, at a concentration of about 1 pebble within each 3 m core interval, are also present.

Northernmost and also closest to Greenland, ODP Site 646 is located in 3451 m of water (Srivastava *et al.* 1987). The deepest sampled interval, from 236 to 767 mbsf, consists of a homogenous succession of late Miocene to late Pliocene nannofossil-rich claystone and siltstone with minor intervals of chalk and limestone interpreted to be the result of contourite deposition. The overlying late Pliocene to Holocene succession, from 0 to 236 mbsf, contains evidence for deposition by ice rafting, bottom currents, low-concentration turbidity currents, and off-shelf lutite flows. Lithologies are predominantly

2

terrigenous silty clay and clayey silt with occasional sand- to cobble-sized clasts. Calcareous nannofossils, foraminifers, sponge spicules, and diatoms are also abundant, typically comprising 5 to 40% of the sedimentary grains. Throughout the entire Miocene to Holocene succession, concentrations of $CaCO_3$ average about 10% by weight, but are as high as 20–30% within several intervals ranging between 5 and 25 m in thickness.
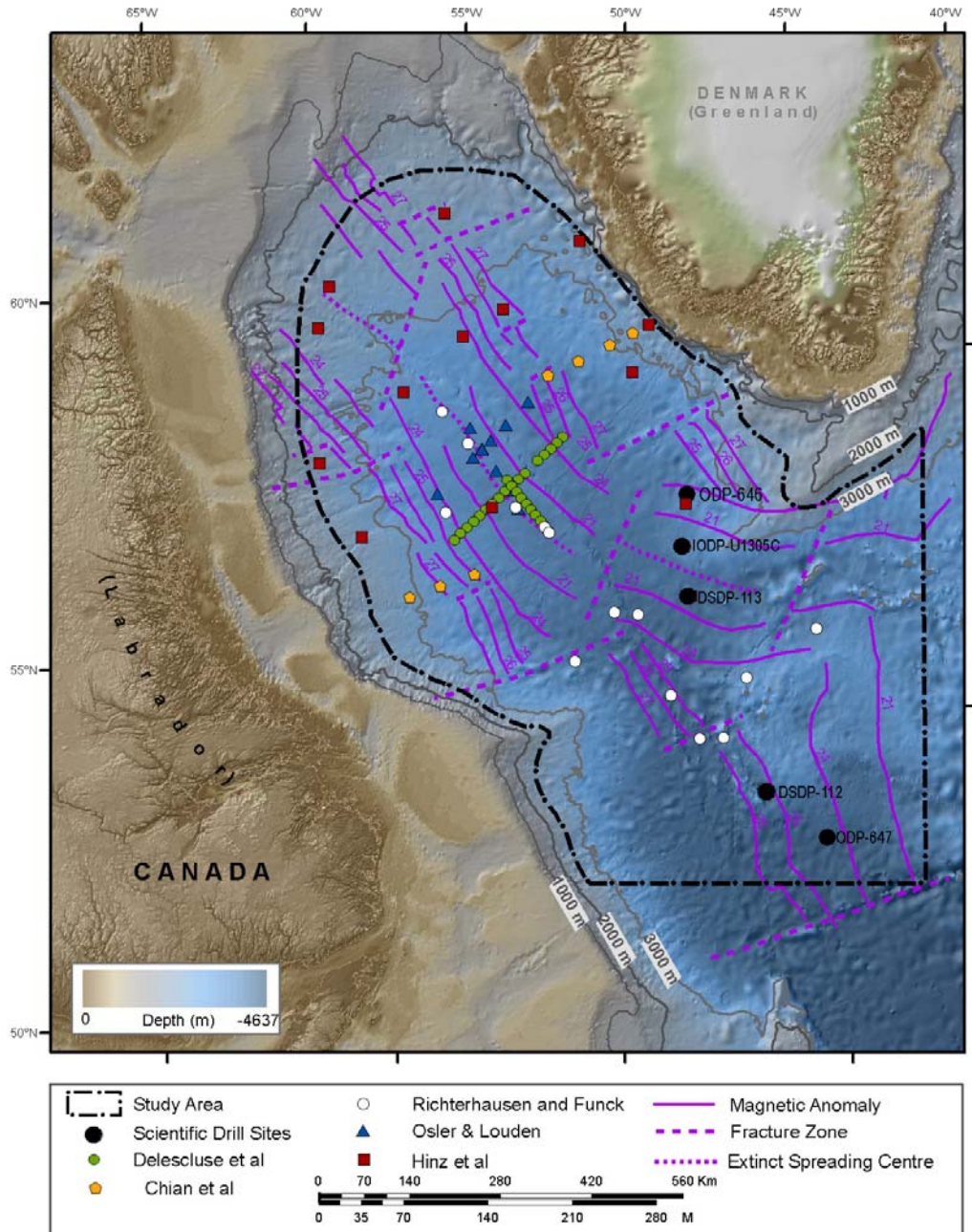
Figure 1.1. Bathymetric map showing the principal physiographic and tectonic features of the Labrador Sea region with the sources of published seismic velocity data. Bathymetric data are from the GEBCO-08 digital elevation model (http://www.gebco.net).

An extensive data set of 2D multichannel seismic reflection profiles totalling 15,438 line km is compiled for the Labrador Sea region. It includes regional surveys acquired for scientific purposes, commercial surveys for hydrocarbon exploration, and also a survey conducted by the Geological Survey of Canada (GSC) in 2009 for preparing Canada's UNCLOS submission. According to the scientific collaboration and arrangements for data exchange between Denmark and Canada, the seismic compilation is augmented with surveys collected by the Geological Survey of Denmark and Greenland (GEUS) in 2003 and 2006.

The seismic stratigraphy of the deep water central Labrador Sea region is described in published studies by Davies and Laughton (1972), Hinz *et al.* (1979), Arthur *et al.* (1989), Cremer *et al.* (1989), Srivastava *et al.* (1989), Chalmers and Pulvertaft (2001), Keen *et al.* (1994), and Dickie *et al.* (2011). This work demonstrates that the vertical time thickness of the sedimentary succession across the study area averages 1541 ms (Figure 1.2). It is continuous along all seismic profiles except over the steep flanks of isolated basement ridges where it thins to within the vertical resolution of the data. Seismic facies interpretation confirms that deep water open marine depositional processes operated during most if not the entire geological history of the basin.

There are various techniques for determining seismic velocity so that sedimentary thickness measured in two-way travel time can be converted to an actual distance. In the next section these are discussed along with the rationale for the methodology that is adopted for this report.
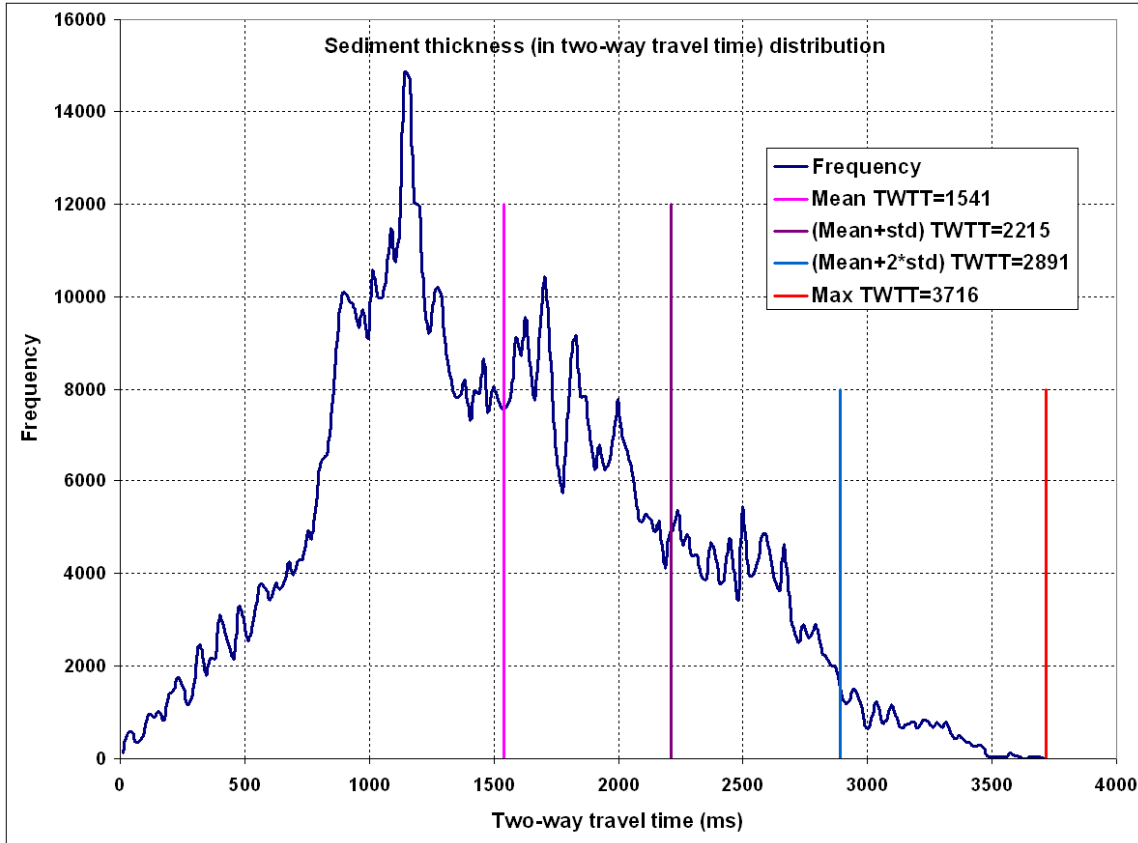
Figure 1.2. Distribution of vertical time thickness in TWT (two-way time) for the total sedimentary succession measured along all seismic profiles in the study area.

1.2 Techniques for determining seismic velocity

To convert seismic travel time to depth, it is necessary to know the average velocity of the seismic ray along its travel path. The velocity depends on elastic moduli and also density, which are interrelated physical properties. Both are affected by the composition, shape, and packing of the rock grains, the degree and type of cementation between grains, the volume of pore space, the degree and type of fracturing, the chemistry of the pore fluids, and the magnitude of pore pressures (Keary and Brooks 1984; Sheriff and Geldart 1995; Fowler 2005). The following discussion focuses on seismic energy travelling in the form of compressional waves since this applies to most depth conversion problems, but the same principles also apply to energy travelling in the form of transverse waves.

There can be a significant degree of natural variability in the elasticity and density of rocks, so it is generally impractical or impossible to determine velocity for every point along a seismic raypath. In practice, some form of layer averaging must be employed using any of the many geophysical techniques employed for measuring seismic velocity. At a general level, these are classified as either direct, indirect, or proxy techniques (Table 1.1). The accuracy and precision of each technique depend on case specific factors such as available technology, data quality, analytical methodology, and geological complexity.

1.2.1 Direct observation

This class encompasses a broad range of borehole techniques (Table 1.1). Direct measurements are made along well constrained seismic raypaths within a rock mass of known geometry. For example, laboratory methods typically use samples with a volume of 10 to 1000 cm^3. These are essentially point measurements of velocity at specific sample locations. Other techniques such as borehole sonic well logging provide interval measurements: measurements of average velocity along a fixed length of the borehole wall (1–4 m depending on the specific tool used). Still other techniques, such as vertical seismic profiling and cross-well seismic surveying, yield average velocities within much larger but nonetheless well defined rock volumes between the borehole and the Earth surface or between one borehole and another borehole.

The resolution of a direct measurement depends on the dominant frequency of the seismic energy and also on the spatial distribution of the rock samples. Laboratory measurements have potentially centimetre scale resolution but, due to expense, samples are available only from select layers. In contrast, a borehole sonic tool typically provides measurements with a resolution 0.1–0.6 m and a regular sampling interval of 0.15 m along most or all the entire length of the borehole. Relative to other classes, the accuracy and precision of direct techniques are straightforward to quantify. The main sources of error typically relate to timing and positioning constraints of the equipment which, with modern technology, are likely negligible with respect to the magnitude of the measurement.

Table 1.1. Geophysical techniques for determining seismic velocity beneath the surface of the Earth. The techniques are classified by the nature of the observation and are listed in approximate order of decreasing accuracy.

CLASS	TECHNIQUE	COMMENTS
Direct observation	1) laboratory measurements on samples	- point measurements (average velocity within samples of about 1000 cm^3) - distribution of samples can be a significant limitation - recovered samples may not be representative of *in-situ* conditions and corrections may be necessary for pressure, pore fluid, etc. - random sources of error are generally insignificant
	2) borehole sonic well logging	- interval measurement (average velocity along 1–4 m section of borehole wall) - typically provides measurements at 15 cm spacing along length of borehole - data quality can be negatively affected by borehole conditions - random sources of error are generally insignificant
	3) borehole seismic surveys (numerous configurations with either single or multiple boreholes)	- bulk volume measurement (average velocity within known geometry) - accuracy and precision are dependent on specific experimental configuration, but are generally straightforward to determine - in some configurations, random sources of error may be significant
Indirect observation	4) seismic trace inversion	- 2D or 3D seismic data used in conjunction with detailed borehole measurements to determine spatial variations in velocity away from the borehole - random sources of error are often significant - level of uncertainty may be difficult or impossible to quantify
	5) seismic refraction and wide-angle reflection	- simplifying assumptions are typically necessary (*e.g.*, homogeneous and isotropic layer velocities) - interpretation of the basic data and selection of the modelling methodology introduces subjectivity - refraction techniques can be insensitive to decreases in velocity with depth - multiple plausible solutions are possible - random sources of error are significant - level of uncertainty is difficult to quantify
	6) tomographic inversion	- subjective interpretation of the data is minimized - multiple statistically valid solutions will result - random sources of error are significant - statistical estimates of uncertainty are possible
	7) τ-p inversion	- results can be sensitive to data processing methodology - interpretation of the basic data and selection of the modeling methodology introduces subjectivity - random sources of error are significant - level of uncertainty can be quantified
Proxies	8) migration velocity (includes focusing analyses and residual moveout methods)	- results can be sensitive to data processing methodology - random sources of error are significant - level of uncertainty is difficult to quantify
	9) normal moveout velocity, stacking velocity	- results are very sensitive to noise and processing errors when offset is small - results can be sensitive to data processing methodology - simplifying assumptions of the technique (flat-lying, vertically and horizontally homogeneous, isotropic layer) are invalid, but may produce reasonable results for cases where these assumptions are most closely met - random sources of error are significant - level of uncertainty is difficult to quantify

1.2.2 Indirect observation

Since direct observations are difficult and costly to acquire on a regional scale, a wide array of modelling techniques are used to infer seismic velocity from other information (Table 1.1). Modelling invariably requires simplifying assumptions for tractability of the problem, and these assumptions will have a direct impact on the accuracy of the technique. In comparison with direct observation, modelling also requires greater levels of data processing and interpretation, which can introduce an additional element of subjectivity. Alternatively, some modelling techniques rely on statistical methodologies to identify, usually within constraints, non-unique solution sets of velocities that adequately explain the observed characteristics of the seismic data.

The resolution of indirect methods depends on numerous factors including the signal-to-noise ratio, the sampling rate, the dominant seismic frequency, the velocity contrast between adjacent layers, the distance travelled by seismic rays within a layer of interest, the source-to-receiver offset, and various details of the methodology. The net effect of all the relevant factors is difficult to quantify, but upper bounds can often be determined (*e.g.* Lebedeva-Ivanova 2010). In general, the vertical resolution is on the order of tens to hundreds of metres and the horizontal resolution is on the order of kilometres to tens of kilometres. Although these are relatively coarse scales of resolution, indirect methods are invaluable for studying the geology of large features like sedimentary basins.

As in all classes of velocity determination, significant effort is made with modelling techniques to identify and remove systematic errors or at least characterize the potential magnitude of the errors if they cannot be removed. However, in contrast with the situation encountered for direct methods, the magnitude of the errors associated with indirect methods is usually significant and the level of uncertainty is correspondingly higher. Factors contributing to the uncertainty include the assumptions used for modelling and also natural variability due to heterogeneity and/or anisotropy at the spatial scale of the measurement. With careful analysis it may be possible to estimate the uncertainty and perhaps also characterize the natural variability, but this is a less straightforward exercise than for direct methods.

1.2.3 Proxies

A number of methods are used in the processing of seismic reflection data to obtain measurements that, under specific conditions and assumptions, can be used as proxies for seismic velocity (Table 1.1). These include measurements such as normal moveout velocity, stacking velocity, and migration velocity. There are also variants, such as semblance velocity which is a particular type of stacking velocity. Full details are given in standard texts such as Yilmaz (1987) but the salient points for this discussion are: 1) these measurements are derived from a phenomenon called moveout; and 2)

moveout-based velocities are a reasonable proxy for true seismic velocity if and only if certain conditions are satisfied.

As the distance (*i.e.*, offset) between a seismic source and receiver increases, so too does the amount of time that the energy travels within the Earth. If the Earth is considered to be homogeneous and isotropic, then the total travel time T of a seismic ray travelling downward from the source to a flat horizontal reflector and then upward to the receiver is given by a simple hyperbolic relationship:

$$T^2 = \frac{4z^2}{v^2} + \frac{x^2}{v^2} \qquad (1)$$

where x is the offset, z is the depth of the reflector, and v is the velocity (Keary and Brooks 1984). *Moveout* is defined as the difference between the travel times T_1 and T_2 of two reflected ray arrivals at two offset distances x_1 and x_2. If the time difference is measured from $x = 0$ to an arbitrary offset x this is known as *normal moveout*, which is a fundamental concept widely used for processing of seismic reflection data. Substituting $x = 0$ into Equation 1 yields $T_0 = 2z/v$ and the equation can therefore be rewritten as:

$$T^2 = T_0^2 + \frac{x^2}{v^2} \qquad (2)$$

Examples of this hyperbolic normal moveout relationship are shown on Figure 1.3. Since offsets are known and travel times can be measured from the data, Equation 2 is applied (through statistical analysis and data visualization techniques) to determine velocities. These should however be understood as apparent velocities: they are the velocities, measured in the direction of the seismic profile, that best conform to the hyperbolic model of normal moveout. They are called *normal moveout velocities* (V_{NMO}) in order to distinguish them from true velocities.

The velocity structure of the Earth is generally assumed to be layered, in which case the travel time is given by an infinite power series of the following form (Taner and Koehler 1969):

$$T_n^2 = C_0 + C_1 x^2 + C_2 x^4 + C_3 x^6 + C_4 x^8 \dots \qquad (3)$$

where T_n is the total travel time of the ray reflected from the base of the nth layer. The coefficients C_0, C_1, C_2, C_3, C_4 … depend on the travel time and velocity (V_{INT}) across the depth interval of each layer. For offsets that are small with respect to the depth of the reflector, the infinite series of Equation 3 can be truncated after just the first two terms without incurring significant error (Taner and Koehler 1969; Yilmaz 1987). In practice, this *small-offset approximation* is generally considered accurate for offsets less than or equal to the reflector depth. It is convenient for numerical computation since the higher order coefficients C_2, C_3, C_4, … are complex functions.

9

Using the small-offset approximation, Equation 3 becomes:

$$T_n^2 = T_0^2 + \frac{\sum_{k=1}^{n} t_k}{\sum_{k=1}^{n} t_k V_{INT_k}^2} x^2,$$

$$\equiv T_0^2 + \frac{x^2}{V_{RMS}^2}$$

(4)

where t_k is the travel time within each of the layers above and including the nth layer. The velocity V_{RMS} (commonly referred to as the *root-mean-square velocity*), as defined in Equation 4, represents a time-weighted average of interval velocities taken across all these layers.

For the special case of layers that are homogeneous, isotropic, flat, and horizontal $V_{NMO} = V_{RMS}$. But geological layers rarely, if ever, truly conform to this scenario and so a mathematically well-posed relationship between V_{RMS} and V_{NMO} does not exist in reality (Dix 1955; Al-Chalabi 1974; Al-Chalabi 1979; Yilmaz 1987; Amery 1993; Al-Chalabi 1994; UN-DOALOS 2006). Nonetheless, lacking any better source of information, the hyperbolic model of normal moveout is frequently adopted as a proxy. Through explicit avoidance of regions with significant geological complexity like steeply dipping, heterogeneous, or curved layers, and by employing careful data processing techniques, empirical studies demonstrate that V_{NMO} can be substituted for V_{RMS} (*e.g.*, Blackburn 1980; Lizarralde and Buffler 1992; Cameron *et al.* 2008).

Another measurement, known as *stacking velocity* (V_{STK}) is often considered equivalent to V_{NMO}. Strictly speaking, the two measurements relate to subtly different types of moveout. Methods for determining stacking velocities involve optimizing the alignment of reflection events along hyperbolic trajectories on seismic traces recorded at the same point in the Earth. For each reflection event, V_{STK} is essentially the velocity that best focuses the seismic energy recorded on multiple traces. It can be thought of as a best-fit approximation to the moveout curve which, as a consequence, means that V_{STK} always exceeds V_{RMS} particularly with increasing source-to-receiver offset (Al-Chalabi 1974; UN-DOALAS 2006). Nonetheless, in practical applications, V_{STK} is frequently used as an estimate of V_{RMS} (Yilmaz 1987). The interval velocities for discrete layers in the multilayer case, are then calculated using the following equation which is based on the small-offset assumption (Dix 1955):

$$V_{INT_n} = \left[\frac{V_{RMS_n}^2 t_n - V_{RMS_{n-1}}^2 t_{n-1}}{t_n - t_{n-1}} \right]^{1/2}$$

(5)

The resolution of moveout-based velocities is a function of the seismic sampling rate, frequency, signal-to-noise ratio, velocity, and also the depth of the measurement. For central Labrador Sea, it is instructive to consider a simple model comprised of a single sedimentary layer beneath 3.5 km of water with an average velocity of 1500 m/s. The seismic travel time to the base of the sedimentary layer is plotted on Figure 1.3 for three different scenarios of sedimentary thickness and average velocity: 1) 2.0 km and 2200 m/s; 2) 2.1 km and 2281 m/s; and 3) 2.2 km and 2359 m/s. Scenario 2 represents a 5% increase in sedimentary, and scenario 3 represents a 10% increase, both with respect to scenario 1. The average velocities, which are reasonable for the region, are chosen such that the zero offset travel time is the same under each scenario (Figure 1.3).

The dominant seismic frequency from the base of a 2 km sedimentary succession is typically about 20 Hz. Two layers within the Earth are resolvable as distinct seismic reflections so long as their vertical separation is greater than about one-quarter of the seismic wavelength (Yilmaz 1987). Therefore, assuming a 2 ms sampling interval, the best achievable timing resolution is about 14 ms (one-quarter of the inverse of 20 Hz, rounded upward to the nearest 2 ms). For the example of a 2 km sedimentary succession beneath 3.5 km of water, we see on Figure 1.4 shows that a minimum offset of 4.0 km is required to detect the 5% variation in thickness, and an offset of 2.8 km is required to detect the 10% variation. Complicating factors such as noise, positioning errors, or geological complexity would reduce these levels of resolution accordingly.
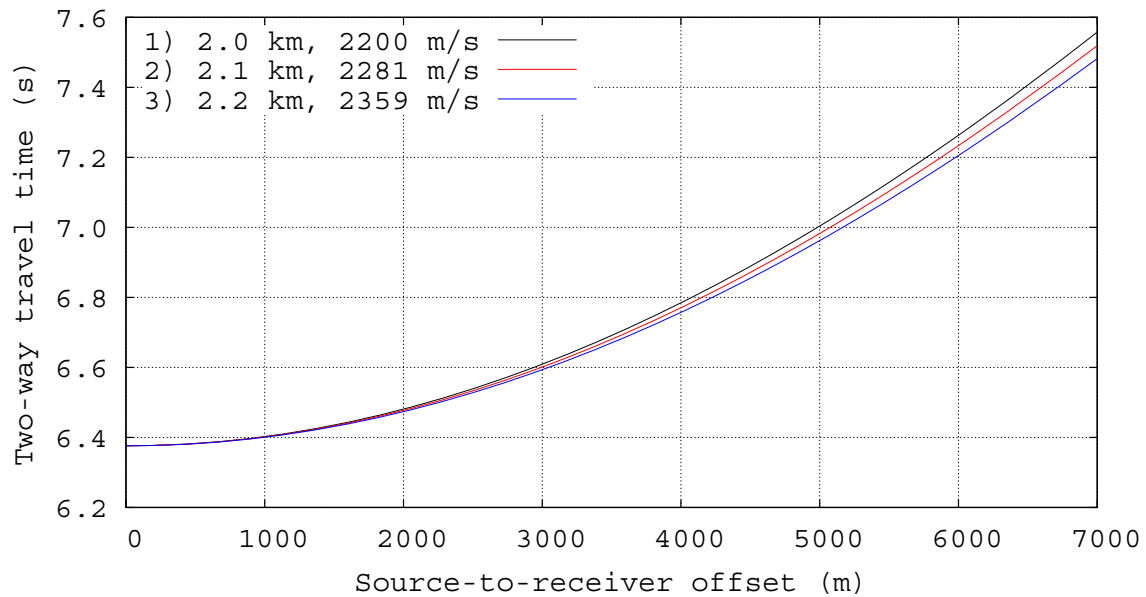
Figure 1.3. Travel time versus offset, from Equation 4, for reflections from the base of a sedimentary layer beneath 3.5 km of water assuming three scenarios for the sedimentary thickness and velocity.

11
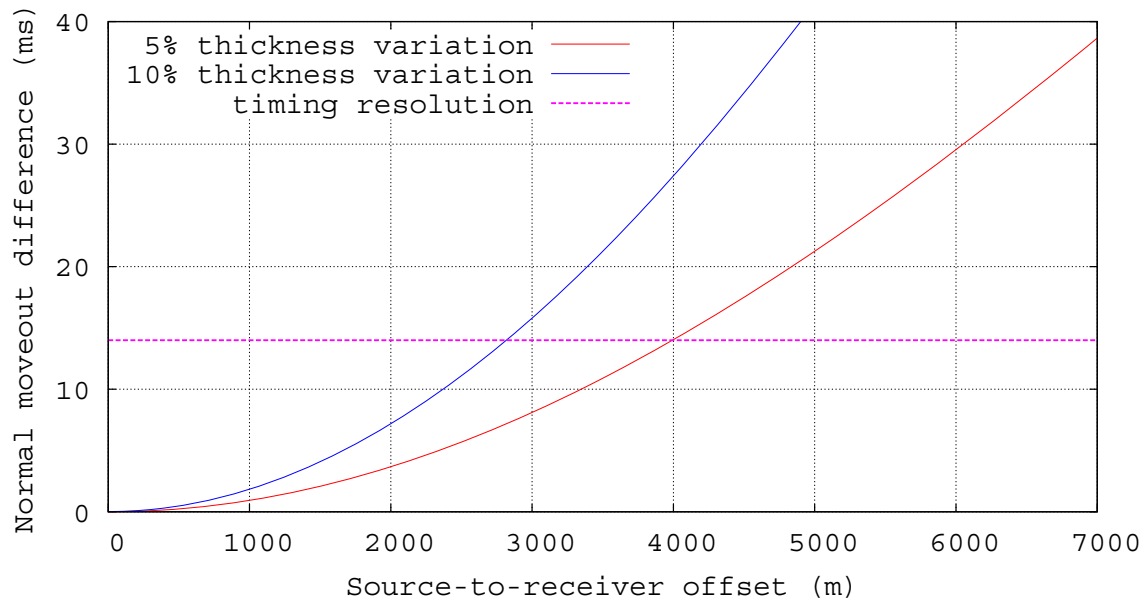
Figure 1.4. Differences in normal moveout versus offset with respect to scenario 1 of figure 1.3.

It is difficult to quantify the magnitude of the uncertainties associated with proxy measurements. Significant factors that affect the accuracy and precision include (Al-Chalabi 1979; Hajnal and Sereda 1981; Yilmaz 1987; UN-DOALOS 2006):

- offset range used for velocity analyses,
- offset-to-depth ratio,
- redundancy in spatial sampling (known as stacking fold),
- signal-to-noise ratio,
- frequency,
- correct muting of unwanted signals,
- ratio of the velocity layer thickness to its depth,
- velocity contrast between adjacent layers,
- average velocity profile within the section of interest,
- choice of statistical method used to determine moveout, and
- departures from hyperbolic moveout caused by geological complexity.

Nonetheless, practical experience within the petroleum industry indicates that moveout-based velocities can be within ±0.5–10% of the true value if seismic data are acquired with favourable conditions, analyzed data are carefully selected, and appropriate processing methodologies are applied (UN-DOALOS 2006).

1.3   Conversion between TWT and depth

It is required that conversion from sediment thickness to TWT with a velocity model when overlaying the QLine as a sediment criterion indicator of fixed points (see chapter 5 for details) on seismic profiles which is traditionally plotted in TWT. An analytical function is derived for converting sediment thickness to TWT from the fitted slowness model (see Section 4.1 for details).

Similarly, converting TWT to sediment thickness is also required for sediment thickness calculation. However, no analytical formula exists (Al-Chalabi, 1997b) and could be derived from the slowness model for this purpose. Therefore, the steepest gradient optimization Newton-Raphson numerical iteration method (Press *et al*., 1992) is used in this report for TWT to sediment thickness conversion. The test demonstrated that this method can convert the TWT to sediment thickness accurately with computing efficiency, such as it can get 0.01 m accuracy within 4 iterations (see Section 4.2).

1.4   Optimize the identification of fixed points

Fixed point comes from the fixed line concept of the Article 76 on the Law of the Sea (UN-CLCS 1999). Many criteria can be used to as the fixed point as the limit candidate for coast nations and the out-most one will be selected as the UNCLOS boundaries. The sediment thickness criterion is addressed here which states that, to be a fixed point (location) candidate, the location where the sediment thickness must be greater than its 1% of distance to its nearest FOS (UN-CLCS 1999). Fixed points can also be defined from other criteria, such as the FOS plus 60 NM criterion (UN-CLCS 1999). Fixed points defined from the sediment thickness formula is termed sediment thickness points.

To identify the outer-most sediment points, it is required to search the nearest FOS from FOS collection for every sounding point (CDP), calculate the geodetic distances, and then compare every sounding point spatially. Because of the huge amount of CDP collection and many FOS points, this procedure is tedious and error prone, or even worse when the identifying procedure is required to be repeated again and again with the updated seismic horizon interpretation, velocity models, and FOS.

Therefore, a series of methods were developed in this report to optimizing the out-most fixed points identification using automatic graphical visualization and batch processing techniques. Details can be found in the Chapter 5 and the software user manual (Appendix 4).

1.5   Evaluate the positioning uncertainty

Uncertainty in the positioning of the fixed point comes from many sources, such as in every phase of data acquisition, processing, and interpretation. For example, errors may come from the procedure of acquiring bathometry data, identifying FOS, acquiring seismic data (ship navigation and streamers biasing), processing (binning and stacking) seismic data, identifying horizons of seafloor and top of basement, and converting TWT to sediment thickness using a velocity model. All of these errors should be analyzed and integrated into the net positioning uncertainty.

Above error sources can be categorized as vertical and horizontal uncertainty groups. The vertical group includes errors from identification of horizontals of seafloor and basement, and construction of the velocity model. They can be integrated into net vertical uncertainty and then transformed as transformed horizontal uncertainty using the dipping angles of seafloor and top of basement. The horizontal uncertainty group includes errors from the FOS identification, seismic navigation, streamer floating, seismic data processing, and other procedures. The net positioning uncertainty of a fixed point is evaluated by integrating transformed horizontal uncertainty from the net vertical uncertainties and uncertainties of horizontal group. Detailed description can be found in the Chapter 6 and the user manual in Appendix 4.

2   Sources of velocity information and data preprocessing

All available sources of information for central Labrador Sea were compiled, preprocessed, and assessed to develop the velocity model. Reports and published articles were used to evaluate the accuracy and precision of each data set and consideration was given to possible sources of error that might be associated with particular field methods or survey equipment. To test for systematic error the variance, range, and sample values of each data set were compared with those of the entire sample population.

Complete listings of the station locations and velocity samples used for the model are provided in appendices 1 and 2. The compilation consists of 165 samples from 51 stations distributed widely across the region where time-to-depth conversion is required (figures 1.1 and 2.1; Table 2.1). A majority of the samples (75%) are from depths of 76 to 1690 mbsf, but there are many samples between 1690 and 4790 mbsf which provide valuable constraints for the velocity of the most deeply buried interval of the sedimentary succession (Figure 2.2).

Data preprocessing was necessary in some instances in order to edit erroneous values, avoid sample bias, and to obtain meaningful values at the sample spatial resolution of the seismic data (Table 2.2). Further details are given in the following sections.

Table 2.1. Data sets compiled to construct a velocity-depth model for central Labrador Sea. Acronyms: SB—sonobuoy; OBS—ocean bottom seismometer; ODP—Ocean Drilling Program; BGR—German Federal Institute for Geosciences and Natural Resources; GSC—Geological Survey of Canada; GEUS—Geological Survey of Denmark and Greenland.

DATA SUBSET	TYPE	# STATIONS	DEPTH RANGE (km)	DATA OWNER(S)	YEAR	REFERENCE(S)
ODP 646B	sonic log	1	[0.216, 0.719]	ODP	1985	Srivastava *et al.* (1987)
ODP 647A	core	1	[0.216, 0.696]	ODP	1985	Srivastava *et al.* (1987)
Delescluse *et al.*	OBS	13	[0.249, 2.292]	GSC & GEUS	2009	Funck *et al.* (2010) Delescluse *et al.* (2012)
Richterhausen & Funck	SB	13	[0.076, 3.443]	GEUS	2006	not included in the data set
Chian *et al.*	OBS	8	[0.598, 3.139]	Atlantic Geoscience Centre & Dalhousie University	1990	Chian & Louden (1994) Chian *et al.* (1995a) Chian *et al.* (1995b)
Osler & Louden	OBS	18	[0.156, 2.237]	Dalhousie University & Atlantic Geoscience Centre	1987	Osler & Louden (1992); Osler (1993); Osler & Louden (1995)
Hinz *et al.*	SB	10	[0.610, 4790]	BGR	1979	Hinz *et al.* (1979)
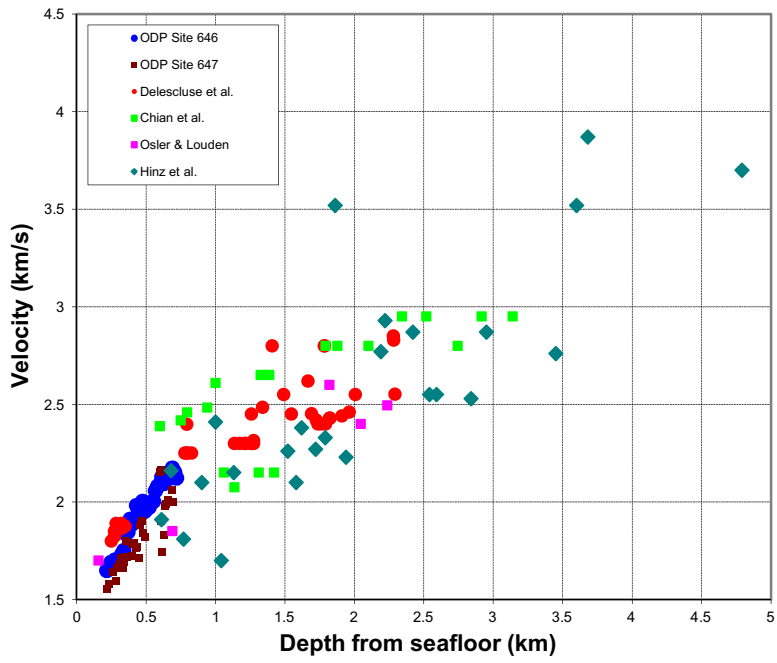
Figure 2.1. Velocity samples included in the data compilation.
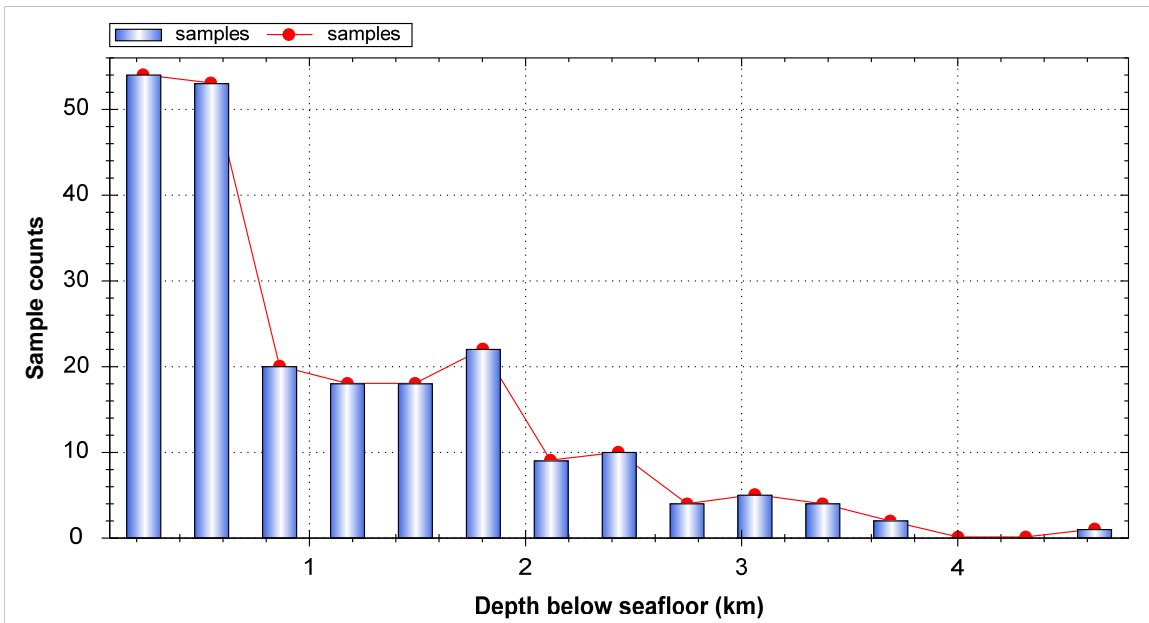
Figure 2.2. Depth distribution of velocity samples included in the data compilation.

Table 2.2. Preprocessing applied to data subsets before incorporation into the final compilation for regression modelling.

DATA SUBSET	PREPROCESSING APPLIED	# SAMPLES (ORIGINAL)	# SAMPLES (FINAL)
ODP 646B Borehole Sonic Well Logging	(1) applied 15 m median filter to smooth the data to the typical vertical resolution of seismic data; (2) resampled the smoothed curve at 15 m intervals	3463	34
ODP 647 Core analysis	One erroneous measurement excluded	35	34
Delescluse *et al.*	none	47	47
Chian *et al.*	Stations outside the study area were excluded	36	20
Osler & Louden	Clustered samples were binned and averaged	52	5
Hinz *et al.*	none	25	25

2.1 Direct observations

A total of 31 petroleum wells have been drilled into the seaward thinning wedge of continental clastics that has accumulated along the Labrador and southern Baffin margin since the initiation of rifting and seafloor spreading. The wells, all located in modern water depths of less than 600 m, sample a diverse range of shallow- and deep water lithologies and also volcanogenic sequences. The tectonostratigraphy is substantially different from that of central Labrador Sea, so measurements from the petroleum wells are not suitable for direct use in the velocity model. However, as described in the following sections, pertinent data are available from deep water scientific boreholes at two sites in the region.

2.1.1 ODP Site 646

Borehole logs of long-spaced sonic transit time at Hole 646B provide compressional wave velocity measurements for the interval between 216 and 719 mbsf (Figure 2.3; Srivastava *et al.* 1987). As discussed in Section 1.2.1, the spatial resolution of these measurements is much finer than that of seismic reflection and refraction data. Therefore, the sonic log velocities were smoothed using a 15 m median filter and then resampled at 15 m intervals.

Velocities measured on core samples from holes 646A and 646B are also plotted on Figure 2.3 for comparison with the long-spaced sonic log. These samples experienced a significant amount of damage due to the drilling and recovery process (Srivastava *et al.* 1987; Busch 1989), which likely explains why the velocities are systematically low and exhibit a high degree of scatter with respect to the sonic log. Recovery from the *in-situ* temperature and pressure conditions of the borehole is well known to sometimes cause

significant core expansion (*e.g.* Hamilton 1971), which in turn causes underestimation of the true sedimentary velocity. The core measurements from holes 646A and 646B are therefore considered erroneous and are excluded from the velocity model.
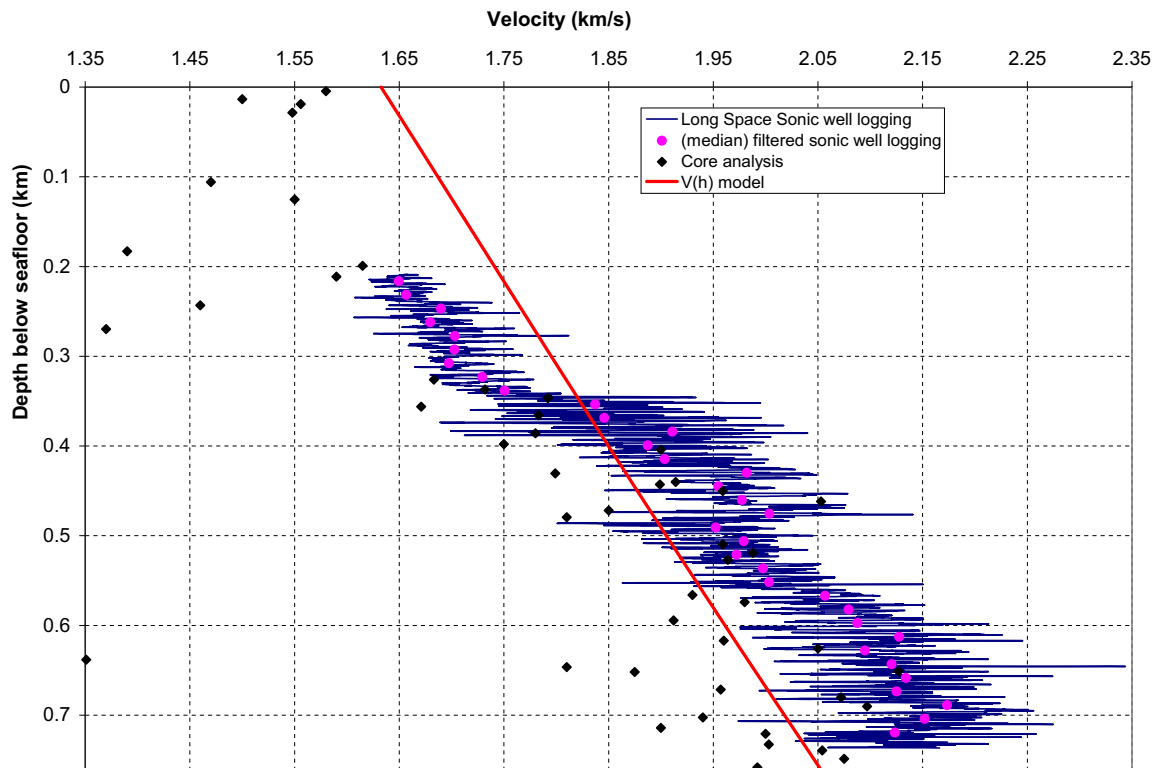
Figure 2.3. Compressional wave velocities from core measurements at ODP Site 646 and from the long-spaced sonic transit time log at 646B (Srivastava et al. 1987). For reference, the velocity model derived in the present study is indicated with the red line.

2.1.2 ODP Site 647

Borehole logs of long-spaced sonic transit time are available from Hole 647A, but the logging was terminated prematurely at a depth of 227 mbsf due to hole collapse. These data are not used for the model since the logged interval is relatively shallow. No logging was conducted at Hole 647B.

Core measurements are available from both holes 647A and 647B for the depths between 216 and 696 mbsf (Figure *2.4*). Drilling disturbance of the samples is variable, but generally low and there is good correspondence with the available sonic log measurements (Srivastava *et al.* 1987). As with Site 646, the measurements are not corrected for *in-situ* pressure and temperature. However such corrections are generally not significant for shallow depths and, at worst, the uncorrected measurements will underestimate true values by a small amount. Therefore Site 647 core measurements are used for the velocity model with the exception of one measurement that is excluded because the value is significantly lower than water velocity (Table 2.2; Figure *2.4*).
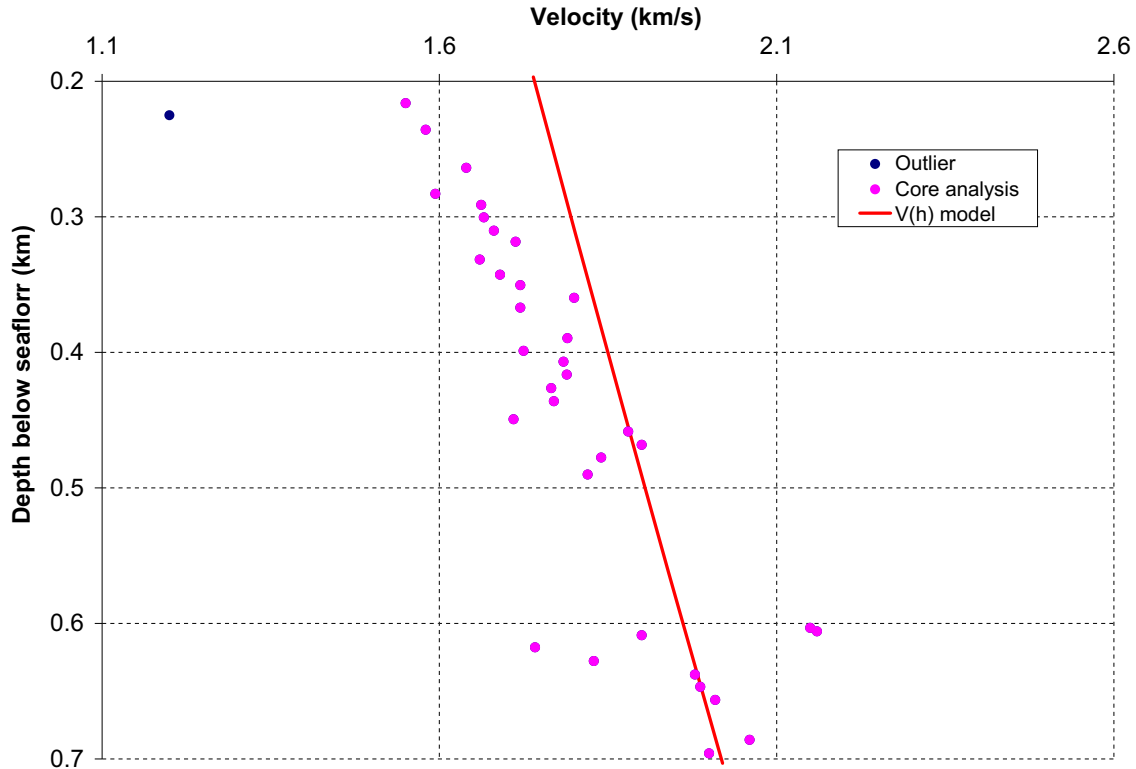
Figure 2.4. Compressional-wave velocity measurements conducted on cores from ODP Site 647. For reference, the velocity model derived in the present study is indicated with the red line.

2.1.3 IODP Site U1305

Cores were collected to a depth of 280 mbsf at this site but gas within the cores caused significant expansion of the samples and the average core recovery rate is reported well (Channell *et al.* 2006). Also several technical problems were encountered with the laboratory equipment which lowers confidence in the measurements (Channell *et al.* 2006). This data set is excluded from the model.

2.1.4 DSDP Sites 112 and 113

These sites were drilled in 1970 during an early phase of the DSDP when its capabilities for borehole logging, core recovery, and physical property measurement were still rudimentary. Borehole logging was not conducted at either site and the core samples manifest a significant degree of drilling disturbance. Velocities were measured on the core samples but the requisite corrections for *in-situ* pressures and temperatures are unknown (Witmarsh 1972). This data set is excluded from the model.

2.2 Indirect observations

Velocity measurements determined by modelling of wide-angle reflection and refraction seismic records are available from the studies described below and summarized in Table 2.1. Combined, these measurements are the most comprehensive source of velocity information in the study area since the complete sedimentary succession is sampled, from seafloor to basement, and since the observation stations have a wide geographic distribution (Figure 1.1).

2.2.1 Delescluse et al. (2012)

In 2009 a survey entitled Seismic Investigations of Greenland, Newfoundland and Labrador (SIGNAL) was conducted through collaboration between the Geological Survey of Canada and the Geological Survey of Denmark and Greenland, with scientific participation from Dalhousie University (Funck *et al.* 2010). The survey was designed specifically to acquire wide-angle reflection and refraction data in support of the Extended Continental Shelf programs of the two geological surveys. Ocean bottom seismometers and sonobuoys were used to record signals from a 6240 in^3 seismic source, resulting in a high density of measurements along each line. Lines 4 and 5 are located within the Labrador Sea study area (Figure 1.1). The associated compressional wave velocity models, shown on figures 2.5 and 2.6, were derived by Delescluse *et al.* (2012) through a two-dimensional raytracing technique. No preprocessing of these data was performed.

2.2.2 Richterhausen and Funck (2009)

During acquisition of their 2006 multichannel seismic survey over Labrador Sea, the Geological Survey of Denmark and Greenland also deployed 21 sonobuoys to record wide-angle reflections and refractions from the 1310 in^3 source. Two-dimensional raytracing was used by Richterhausen and Funck (2009) to derive the compressional wave velocity models. They are not included in this report as it is not publically available data.

2.2.3 Chian et al. (1995)

Chian and Louden (1994), Chian *et al.* (1995a), and Chian *et al.* (1995b) used two-dimensional raytracing techniques to derive compressional wave velocity models from a compilation of ocean bottom seismometer and sonobuoy records acquired along the crustal-scale multichannel seismic reflection profile collected by the Atlantic Geoscience Centre in 1990. These velocity models are shown on Figure 2.7. Other than selection of the velocity stations located in the study area, no preprocessing was applied.

2.2.4 Osler (1993)

In 1987 wide-angle reflection and refractions from a 6000 in^3 seismic source were recorded using ocean bottom seismometers along two profiles crossing the extinct spreading centre beneath central Labrador Sea (Osler and Louden 1992). Two-dimensional compressional wave velocity models were derived using raytracing techniques (Osler 1993; Osler and Louden 1995). The models are well constrained with stations at roughly 20 km intervals, but the data are reported as average velocities within five sedimentary layers of spatially varying thickness (Figure 2.8). To derive representative average velocities at the average layer depth, the data were binned and averaged as shown on Figure 2.9.

2.2.5 Hinz et al. (1979)

Hinz *et al.* (1979) derived velocity measurements from one-dimensional modelling of sonobuoy data collected in 1977 (Figure 2.10). The relatively small source-to-receiver offset and the vintage of these data likely contribute to the observed scatter. However, the data are particularly useful because of their wide geographic distribution (Figure 1.1) and because they provide control for burial depths of greater than 3.5 km. Therefore they are included in the model. No preprocessing steps were applied.
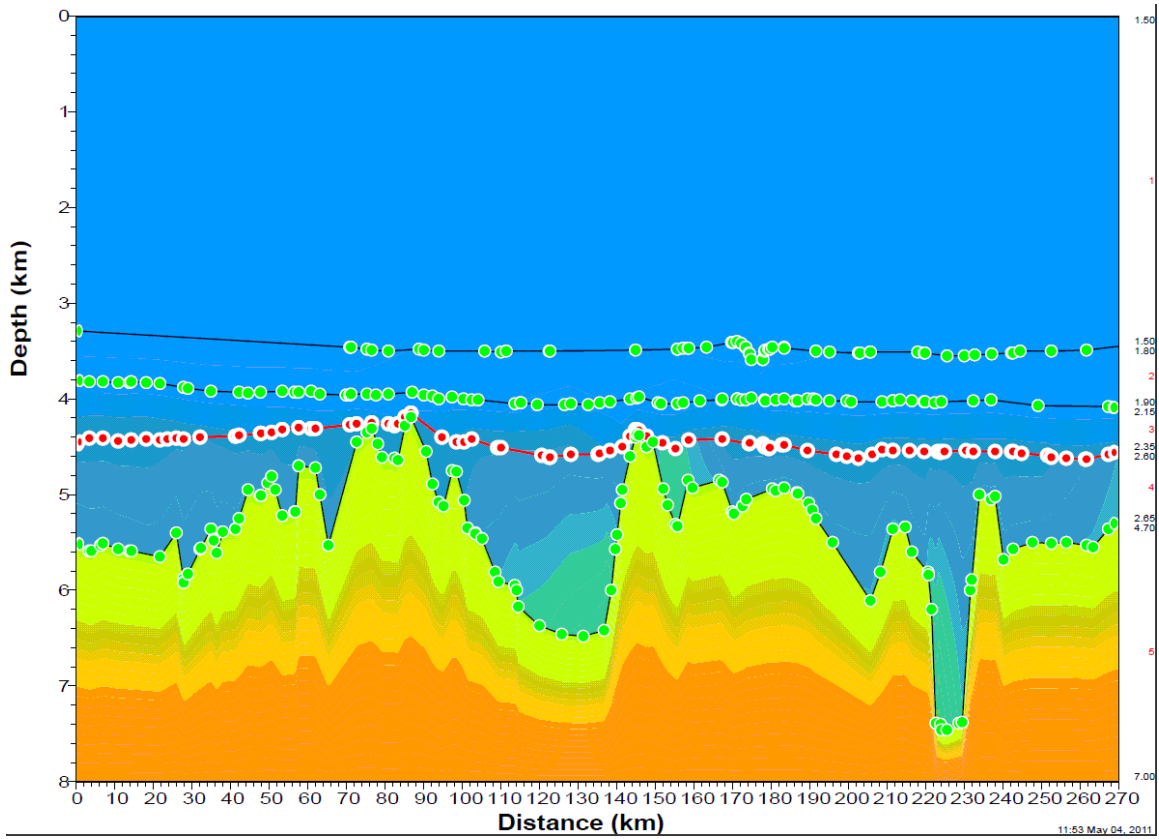
Figure 2.5. Velocity model published for SIGNAL Line 4 by Funck et al. (2010) and Delescluse et al. (2012).
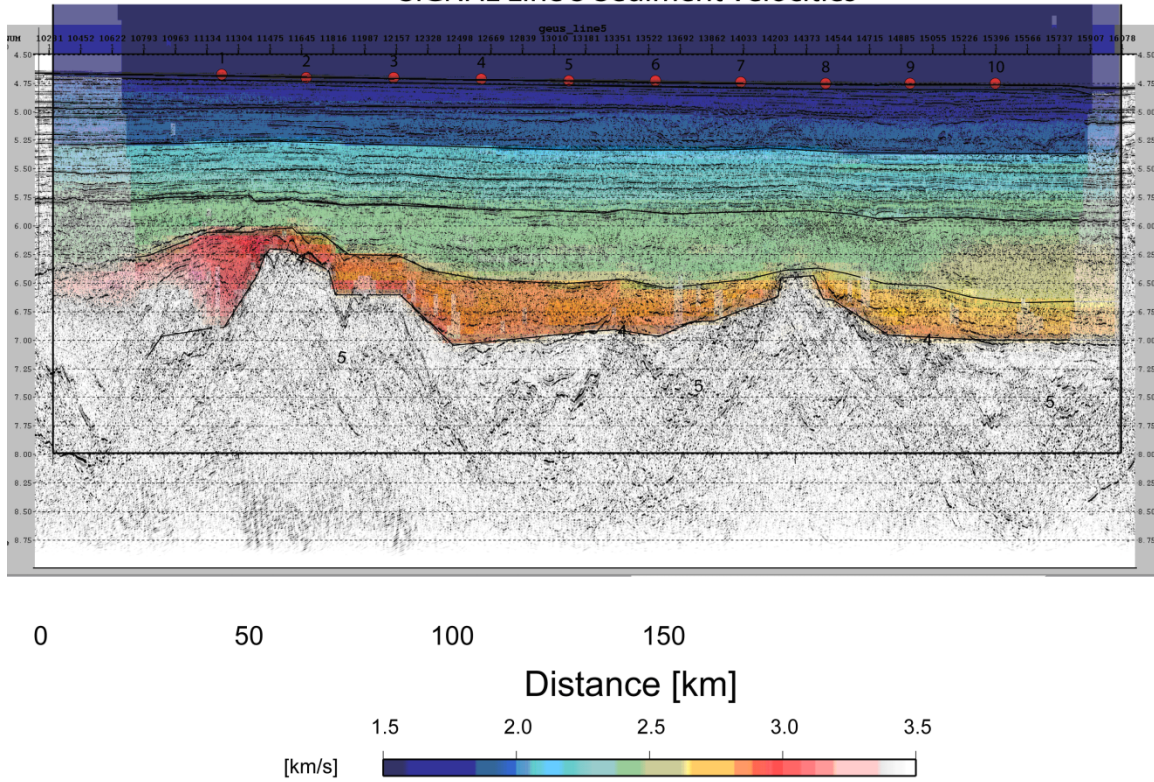
Figure 2.6. Velocity model published for SIGNAL Line 5 by Funck et al. (2010) and Delescluse et al. (2012).
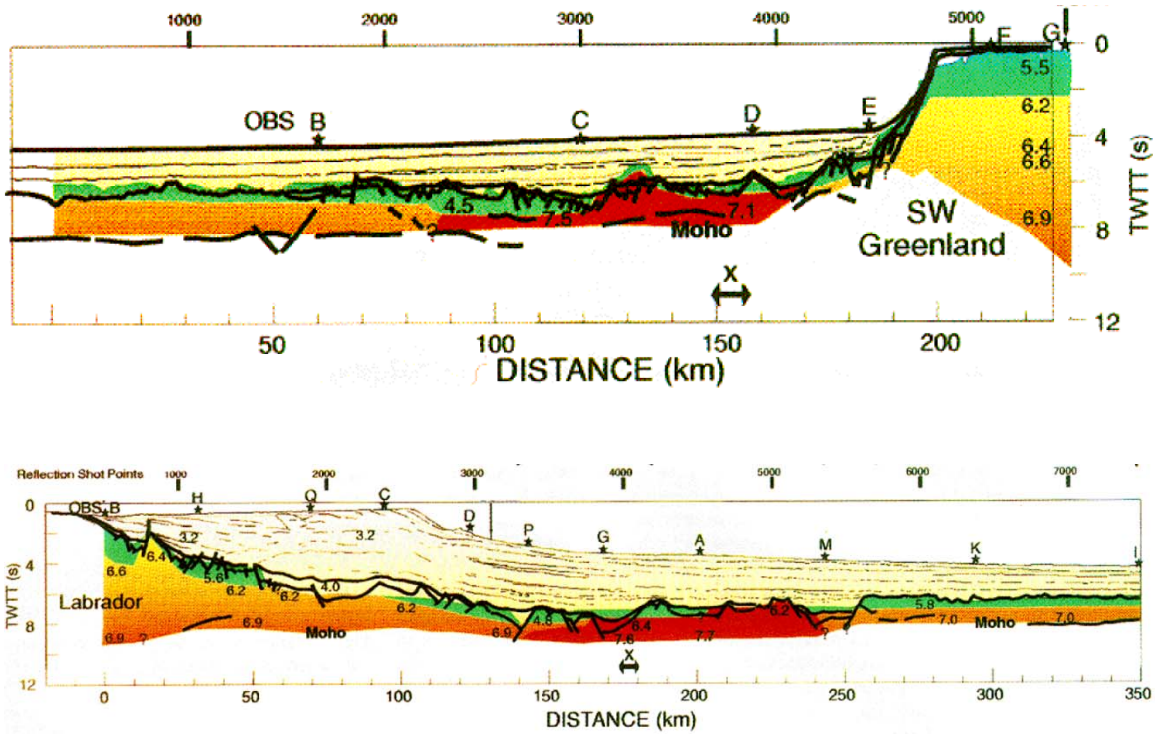
Figure 2.7. Compilation of velocity models by Chian and Louden (1994), Chian et al. (1995a) and Chian et al. (1995b) for the multichannel seismic reflection profile collected by the AGS in 1990.
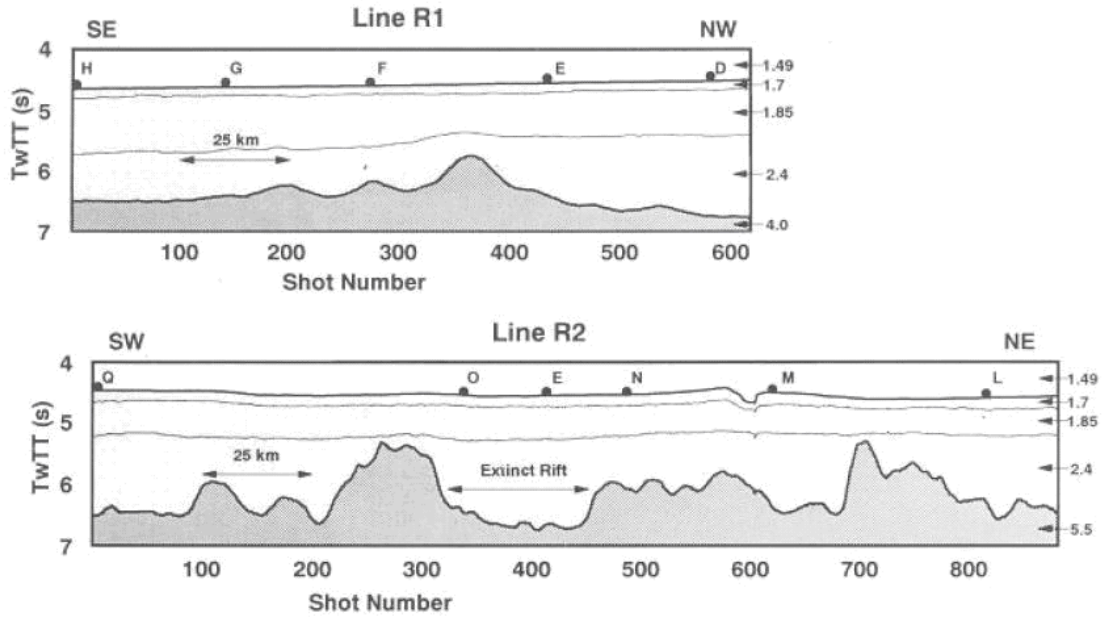
Figure 2.8. Velocity models by Osler (1993) and Osler and Louden (1995) from ocean bottom seismometer records along two profiles over the central Labrador Sea extinct spreading centre (TwTT on y axes of these figures re the same as TWT).
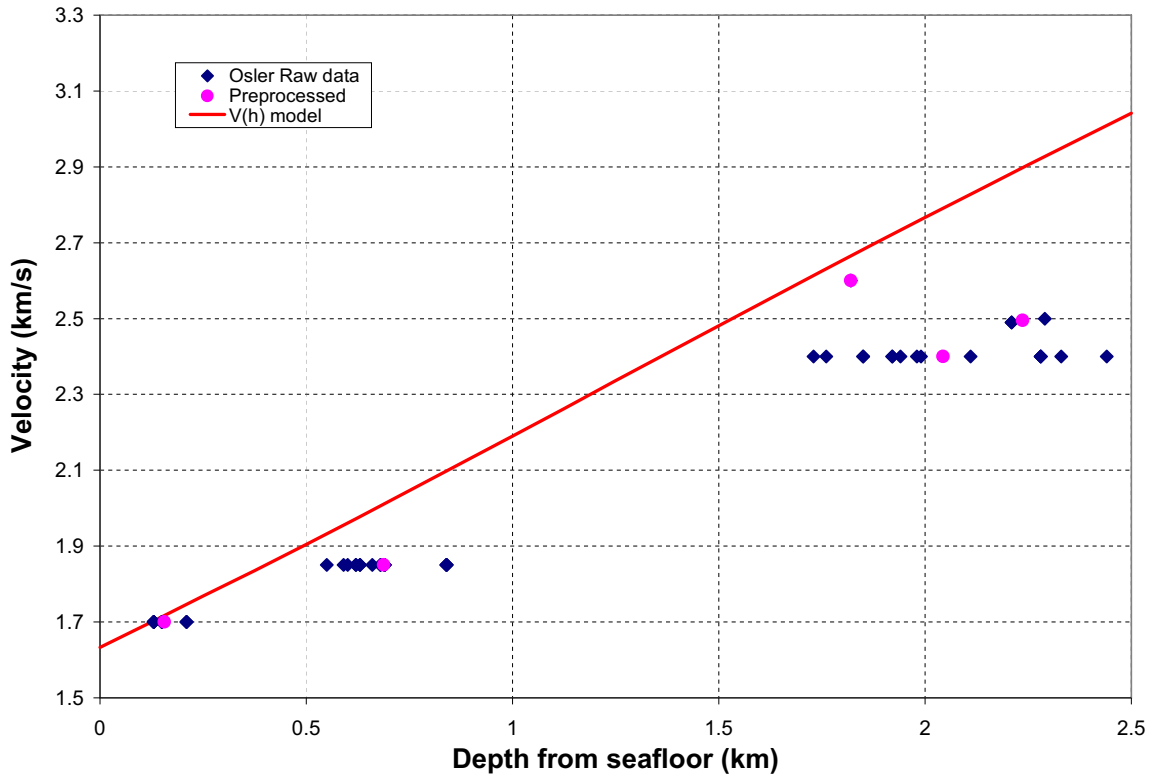
Figure 2.9. Binning and averaging of the Osler (1993) and Osler and Louden (1995) data set. For reference, the velocity model derived in the present study is indicated with the red line.
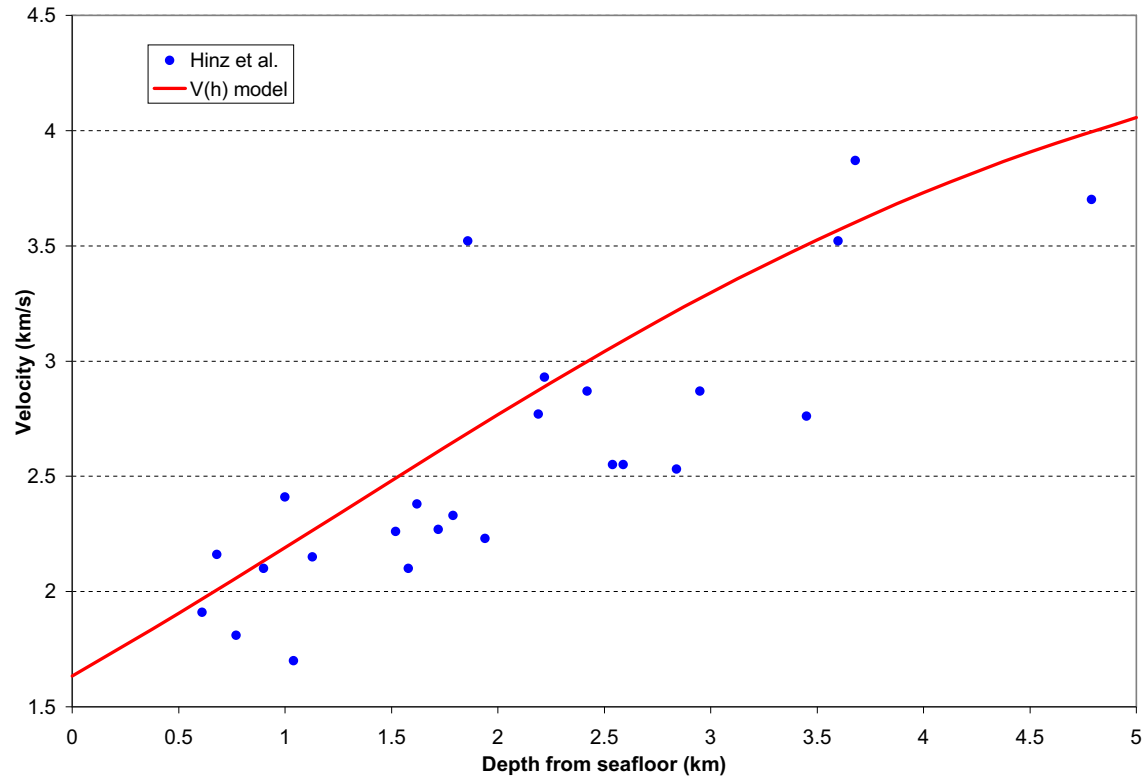
Figure 2.10. Velocities derived by Hinz et al. (1979) from sonobuoy records acquired in 1977. For reference, the velocity model derived in the present study is indicated with the red line.

2.3   Proxy observations

Moveout-based velocities derived from processing of 2-D multichannel seismic surveys in the survey area are a potential source of data. For example, locations of velocity analyses from the 2009 GSC survey are shown on Figure 2.11. However, minimum source-to-receiver offsets of 2.8 to 4.0 km are required in order to resolve sedimentary thickness variations of 5–10% under ideal conditions in the central Labrador Sea region (*c.f.* Section 1.2.3) where characterized deep water depth. This is close to the limit that is available for some surveys and, in practice, the true resolution is sensitive to numerous complications such as noise, positioning error, or geological complexity. Thus careful selection and preprocessing of the moveout-based velocities may derive convincing proxies with great uncertainty for the true sedimentary velocity. Therefore we chose not to include moveout-based velocities in the model, but they are used in Section 7.3 for independent confirmation of the modelling results.
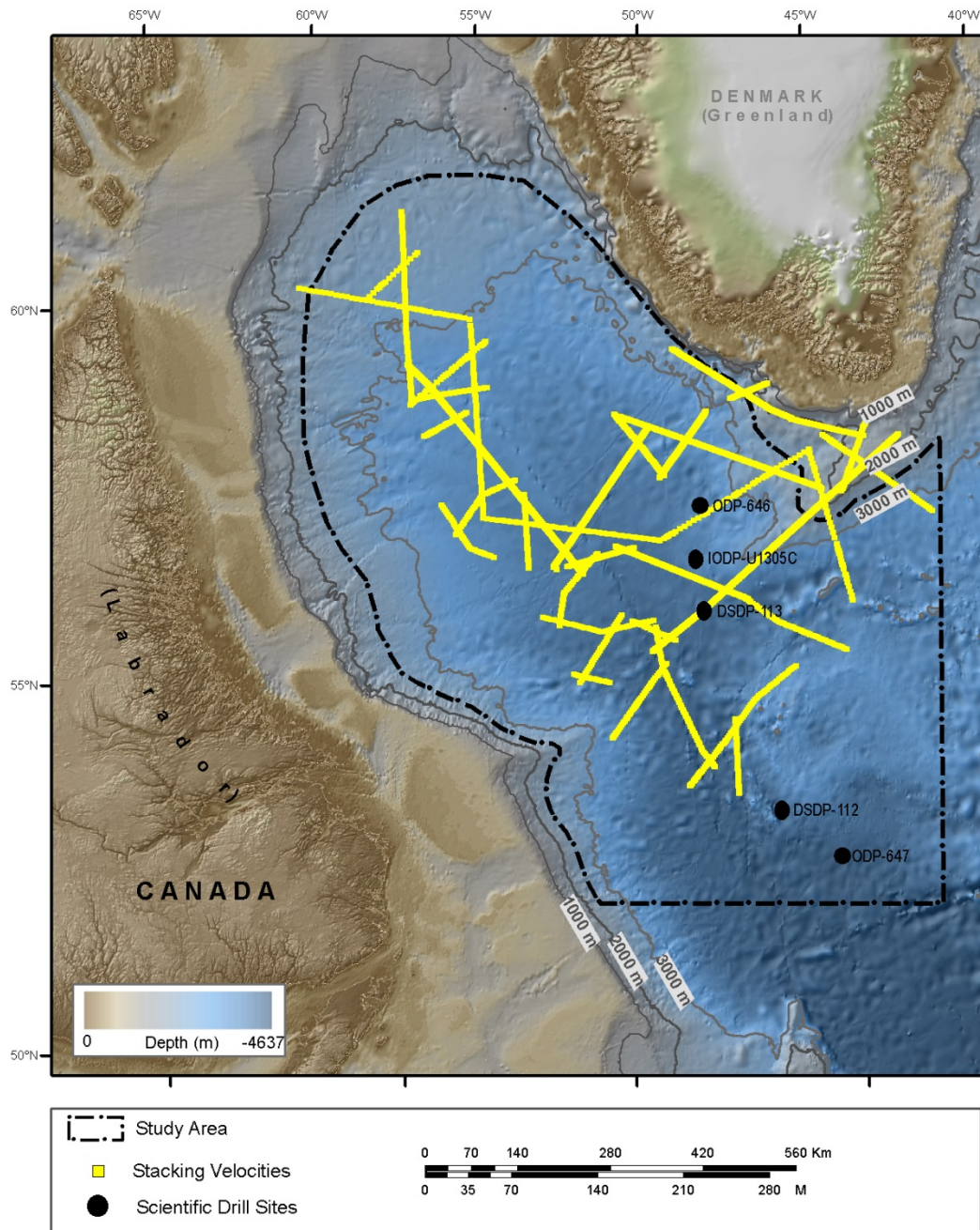
Figure 2.11. Station locations for moveout-based velocities derived from processing of the multichannel seismic reflection dataset acquired for the GSC in 2009.

28

3 RMA Velocity modelling

Velocity measurements are not available at every geographic station for which we wish to calculate sedimentary thickness. Therefore it is necessary to create a model that enables well-constrained interpolation between measurement points. Since the measurements include error, an important objective is to fit the observations to within a specified level of certainty (as opposed to trying to fit the observations exactly). Provided there is a representative sample population of measurements and provided there is no significant bias in the model formulation, such a statistical approach will minimize random errors. The resultant model is useful for accurate time-to-depth conversion within the geographic region represented by the observations. The model can also be employed to investigate localized deviations from the modelled behaviour.

3.1 Functional form of the velocity model

Indirect and proxy measurements of seismic velocity typically sample the Earth at vertical scales of tens to hundreds of metres (Section 1.2). At this scale a well known control on seismic velocity is the reduction of porosity due to increasing burial of the sediment. At the deposition surface , initial porosity is typically 40–70% for sandstones or shales (Japsen *et al.* 2007). Porosity is reduced with time, with increasing stress and temperature, by various mechanical and chemical processes. The process is *normal compaction* when there is no significant erosion (*i.e.* sedimentary thickness increases monotonically with time) and no fluid is trapped within the pores (*i.e.* pore pressure is close to hydrostatic with time).

Many empirical and theoretical studies demonstrate that porosity reduction due to normal compaction can be approximated by an exponential curve (*e.g.* Athy 1930; Rubey and Hubbert 1959; Weller 1959; Magara 1978; Sclater and Christie 1980; Yang 2001; Revil et al. 2002). Then, it is logical to try/use the exponential function to model seismic velocity. Numerous empirical studies of seismic velocity support this choice especially for deep water successions similar to those of the central Labrador Sea (*e.g.* Hottman and Johnson 1965; Matthews and Kelly 1967; Chapman 1983; Carlson *et al.* 1986; Japsen 1999; Japsen 1993, 2000; Japsen *et al.* 2007; Dutta *et al.* 2009).

For this study, the following exponential function of instantaneous slowness (the inverse of instantaneous velocity) versus burial depth is adapted from examples provided by Al-Chalabi (1997b):

$$\frac{1}{V(h)} = \frac{1}{V_\infty} + (\frac{1}{V_0} - \frac{1}{V_\infty})e^{-\alpha h} \tag{6}$$

where h, $V(h)$, V_0, and V_∞ are burial depth, velocity at depth h, velocity at $h = 0$, and velocity at $h = \infty$, respectively.

Compared with other functions that might be considered for modelling purposes, such as any polynomial of arbitrary order, Equation 6 is attractive for two reasons. Firstly, as h approaches infinity, the velocity limit is V_∞. As a result, the equation yields physically plausible values of velocity for any depth range. Secondly, the parameters of the equation are well suited for geologically meaningful interpretation. Initial velocity V_0 is a physical property of the sediments at the surface of deposition before any significant degree of compaction has occurred (Japsen *et al.* 2007). Final velocity V_∞ is an approximation of the bulk velocity of the sedimentary minerals under conditions of high pressure and temperature (Japsen *et al.* 2007). Both V_0 and V_∞ are constrained by theoretical and empirical knowledge. The exponential coefficient α controls the rate of exponential attenuation, thus providing the ability to replicate a wide range of observed behaviours from linear to strongly curvilinear. α may also have geological significance related to regional trends in porosity, lithology, pore pressure, cementation, etc.

The three equation parameters in Equation 6 can be varied so that the model predictions match the observations to within a specified level of certainty. The overriding control on the model is therefore the distribution of the observations. The exponential form of the model equation is simply a practical assumption—for which there is strong theoretical and empirical support—that constrains the nature of interpolation between the observations.

3.2   Number of functions used for the velocity model

The final compilation of velocity samples is considered representative of the region indicated on Figure 1.1. Samples located within this region plot along a smooth curvilinear trend with a small degree of scatter and there is little evidence for discrete layering (Figure 2.1). In other words, the sedimentary succession of this region exhibits a reasonably consistent velocity-depth profile and multiple functions of instantaneous slowness with depth would not improve the predictive capacity of the model.

Adoption of a single function simply means that the averaged behaviour of the succession can be modelled as a one unit. This does not exclude the possibility that localized subunits are present. Indeed characteristic sedimentary velocity layers can sometimes be correlated with seismic reflection data over horizontal scales of tens of kilometres. However reflections are caused by discrete changes in density and/or velocity whereas refractions tend to be associated with changes in velocity gradient (Kennett 2009). Typically, on seismic records from central Labrador Sea, there are many more reflections than refractions and they frequently do not coincide, particularly when sharp velocity contrasts are not present. As a result, it is not possible to correlate characteristic sedimentary velocity layers across the region and so, again, there is no basis for defining more than one function in the velocity model.

3.3 Model linearization

Without losing generality, Equation 6 can be rearranged as follows:

$$\frac{1}{V(h)} = \frac{1}{V_\infty} + \frac{1}{V_\infty}\left(\frac{V_\infty}{V_0} - 1\right)e^{-\alpha h}$$

$$= \frac{1}{V_\infty} + \frac{1}{V_\infty} e^{\ln\left(\frac{V_\infty}{V_0} - 1\right)} e^{-\alpha h} \tag{7}$$

$$= \frac{1}{V_\infty} + \frac{1}{V_\infty} e^{\beta - \alpha h}$$

where $\beta = \ln\left(\frac{V_\infty}{V_0} - 1\right)$. We then define a variable $V'(h)$ using the natural logarithm:

$$V'(h) = \ln\left(\frac{V_\infty}{V(h)} - 1\right) \tag{8}$$

Applying this transformation, Equation 7 is now a simple linear function of h with three parameters α, V_0 and V_∞ (the latter two are expressed by β):

$$V'(h) = \beta - \alpha h \tag{9}$$

3.4 Estimation of the velocity model parameters

In the data set used for modelling, errors associated with depth are likely to be about as significant as those associated with velocity. Therefore the reduced major axis (RMA) regression technique which accounts for bivariate error (*e.g.* Press *et al.* 1982; McArdle 1988) is better suited for estimation of the model parameters than is ordinary regression in which only the dependent variable is assumed to be subject to error. We used a computer software implementation of RMA regression by Bohonak (2004) which is at a mature stage of development (version 1.17) and which has been successfully employed in various peer-reviewed studies (*e.g.*, González-Solís 2004; Guillemain *et al.* 2004). As will be described in Section 3.5, the software also implements a statistical method called bootstrapping to estimate 95% confidence bounds for the RMA regression parameters.

Theoretical and empirical knowledge can be used to constrain both the initial and the final velocities. In a marine setting V_0 should generally be greater than or equal to the velocity of water, which is in the range of about 1.4 to 1.5 km/s (Keary and Brooks 1984). For example, using well established rock physics with typical shales and clayey

31

sandstones, V_0 is calculated to be about 1.6 km/s (*e.g.* Japsen *et al.* 2007). In calcareous or siliceous sediments V_0 might be slightly higher. Likewise, estimates of V_∞ can be obtained from laboratory measurements of common sedimentary minerals or from empirical studies. Measurements from deep boreholes suggest that V_∞ for shale successions is roughly 5 km/s (*e.g.* Storvall *et al.* 2005). A practical lower limit on V_∞ is necessitated by Equation 8 which requires that V_∞ must be greater than the highest value of *V(h)* in the data set.

Rather than arbitrarily specifying values for V_0 and V_∞ from the above constraints we chose to estimate the values using the following iterative procedure:

1. define a V_∞ series from 4.660 to 6.600 km/s at increments of 0.0005 km/s;
2. for each V_∞, apply RMA regression with the linearized velocity model to estimate the model parameters;
3. calculate the sample correlation coefficient R between the observed and predicted velocity/depth pairs;
4. select as the best-fit model that which has the highest R after verifying that the corresponding V_0 is within a plausible range of 1.4 to 1.8 km/s.

The above procedure essentially allows just two degrees of freedom in the model by choosing V_∞ through an optimization criterion. Within the specified range, the solution space appears to vary smoothly with a broadly defined maximum R at $V_\infty = 4.856$ (Figure 3.1). Through rearrangement of Equation 7 the best-fit velocity model is therefore expressed as follows:

$$V(h) = \frac{4.856}{1 + e^{0.66675 - 0.43799 * h}} \tag{10}$$

The best-fit RMA regression parameters and correlation coefficients corresponding to $V_\infty = 4.856$ are listed in Table 3.1 and the corresponding curves of *V'(h)* and *V(h)* are shown on figures 3.2 and 3.3. Plots of the residuals are given on figures 3.4 and 3.5 and descriptive statistics for the residuals are listed in Table 3.2.

Table 3.1. Best-fit parameters and 95% confidence bounds obtained using the RMA regression technique with 30,000 bootstrap iterations.

	Bestfit	**95% confidence bounds**
R	0.79	[0.72, 0.86]
α	0.43799	[0.39889, 0.49127]
β	0.66675	[0.63032, 0.70858]
V_0	1.647	[1.6020, 1.6872]
V_∞	4.856	n/a

Table 3.2. Statistics of the velocity residuals plotted on figures 3.4 and 3.5.

Count	165
mean residual (km/s)	0.0016
standard deviation	0.2026
minimum	-0.636
maximum	0.913
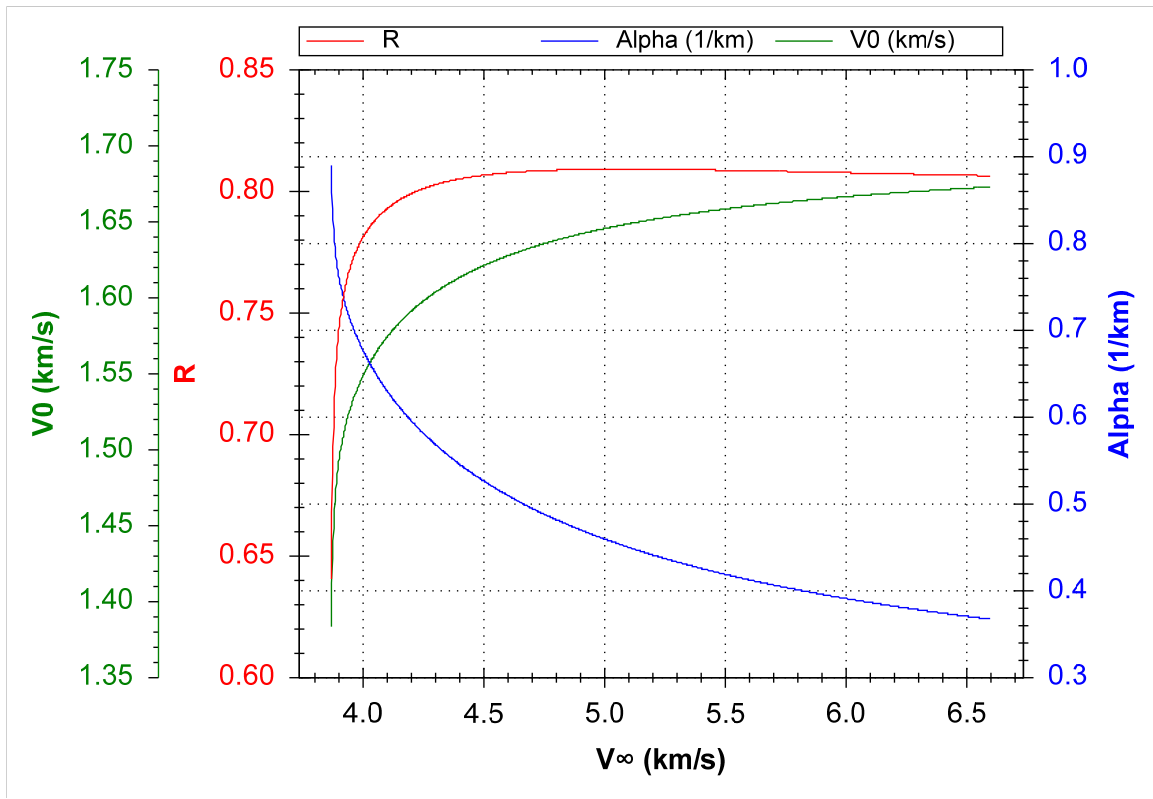
Figure 3.1. Solution space obtained by iterated RMA regression of the model with two degrees of freedom (V_0 and α).
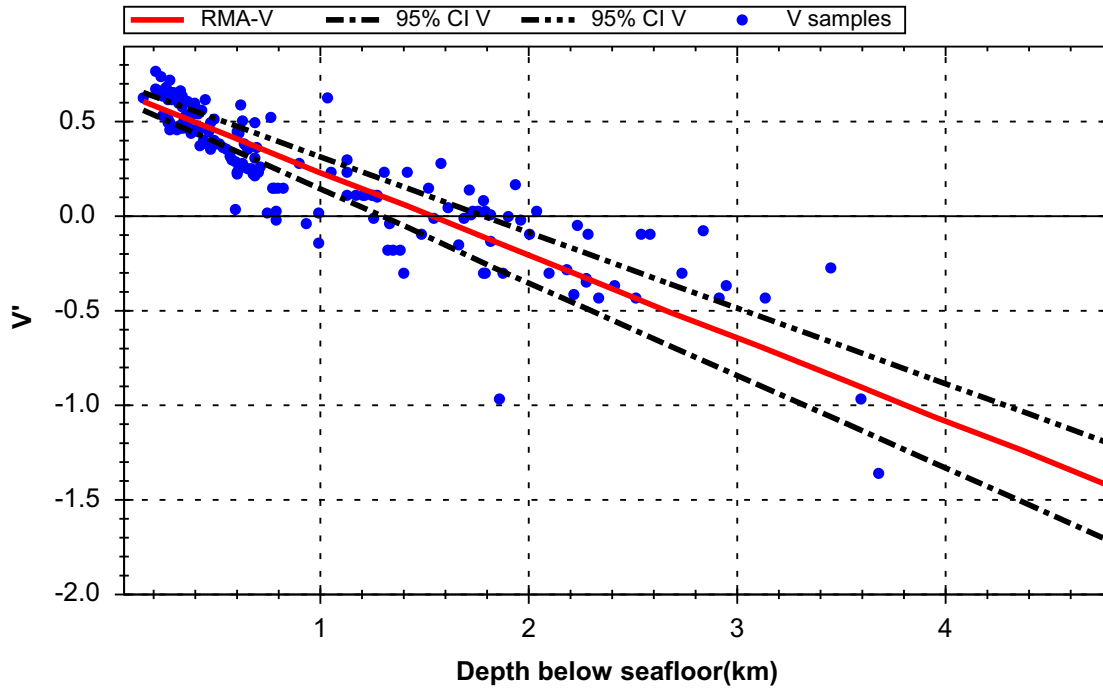
Figure 3.2. RMA regression results for $V'(h)$ including the estimated 95% confidence interval.
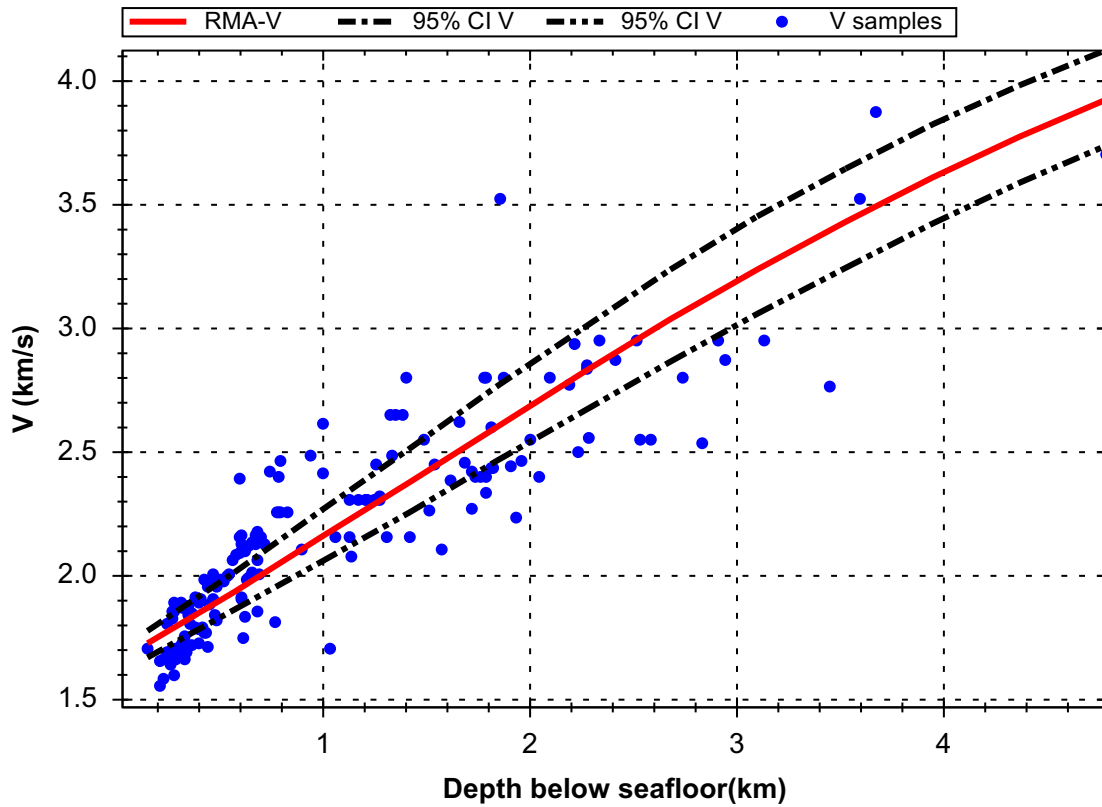
Figure 3.3. RMA regression results for $V(h)$ including the estimated 95% confidence interval.
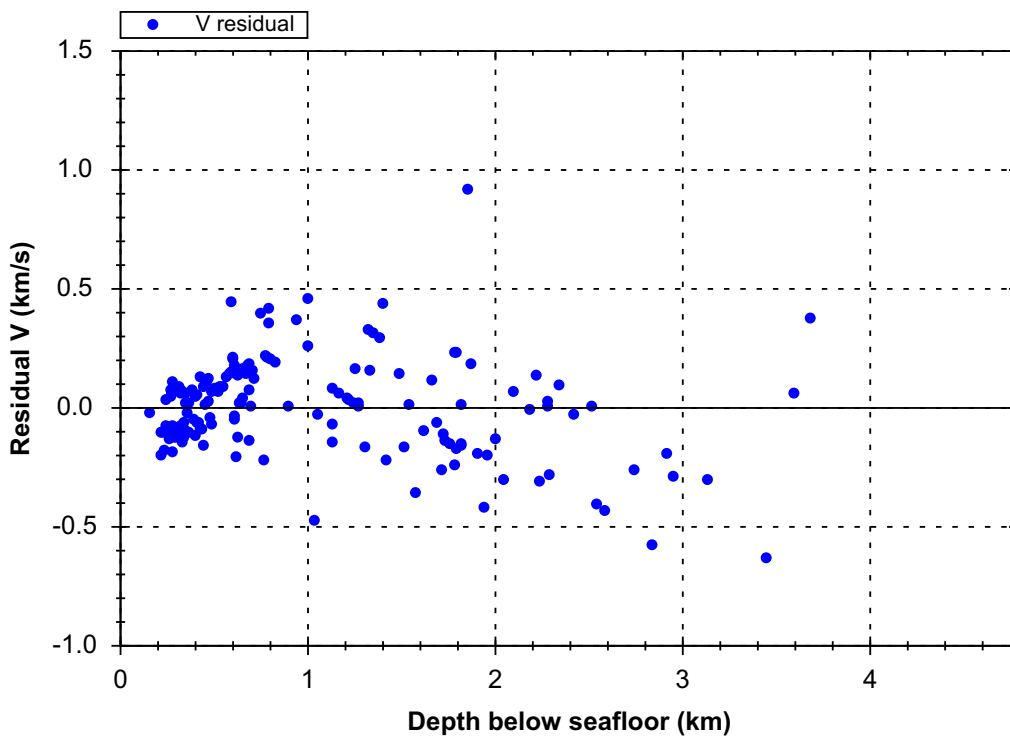
Figure 3.4. Observed minus modelled velocity versus depth below seafloor.

35
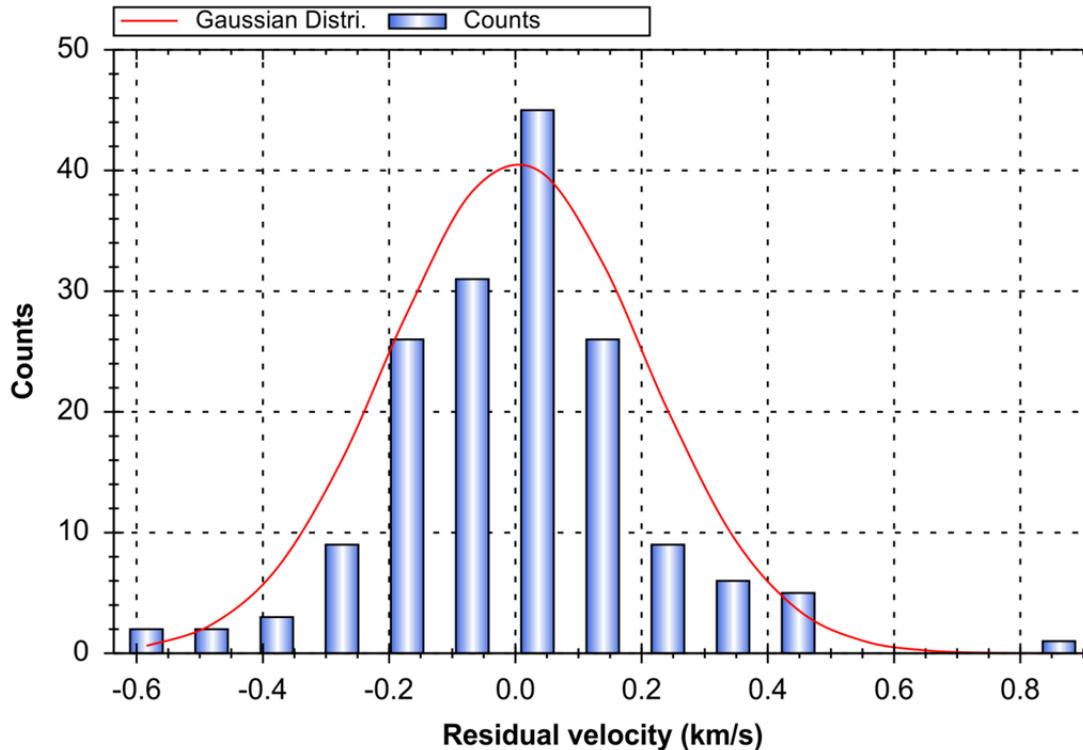
Figure 3.5. Histogram of residual velocities and the Gaussian distribution having the same standard deviation.

3.5 Estimation of the 95% confidence bounds

It is challenging to estimate confidence bounds for the model using traditional statistical methods because the sample size is limited, and also because the distributions of the measurement errors are unknown and possibly non-normal. Therefore we chose a nonparametric computational technique called bootstrapping (*e.g.* Efron 1979) which offers several advantages over traditional statistical inference techniques (Davison and Hinkley 1997; Press *et al.* 1992). Bootstrapping does not require assumptions regarding the distributions of the samples or the measurement errors. As a result, it can be applied to relatively small sample sizes and also to distributions that are difficult to derive even asymptotically. Also, the methodology is straightforward to apply regardless of the complexity of the data set.

The following steps are used to incorporate bootstrapping with the RMA regression technique (Bohonak 2004):

1. randomly sample the depth/velocity pairs, with replacement, to create a new sample population that is the same size as the original (replacement means that there may be duplication of the depth/velocity pairs);

2. apply RMA regression to the new sample population and store the regression parameters;
3. repeat steps 1 and 2 *m* times (the choice of *m* is described below);
4. sort the RMA regression parameters to determine their mean values and the associated range of certainty at the desired level of confidence according to the *t*-distribution (95% confidence bounds were used for the present study);
5. export the mean and the confidence bounds as the final RMA regression results.

One assumption of the above methodology is that the RMA regression parameters derived from *m* bootstrap iterations are distributed about their means in close to the same manner that the final model parameters are distributed about the true values for and α and β (and therefore also V_0 and V_∞). This assumption is valid if the original measurements are independent and identically distributed. Strictly speaking this may not be true, but it is a practical assumption that enables reasonable estimates of the confidence bounds (Press *et al.* 1992).

Selection of an appropriate value for *m* depends on the sample population. To investigate this further we tested estimation of the 95% confidence bounds on α and β for *m* ranging from 3 to 90,000 (Figure 3.6). The results demonstrate that the estimates are remarkably close to their stable values after just 100 iterations and that there are no significant changes after 1000 iterations. For the present study we chose 30,000 iterations.
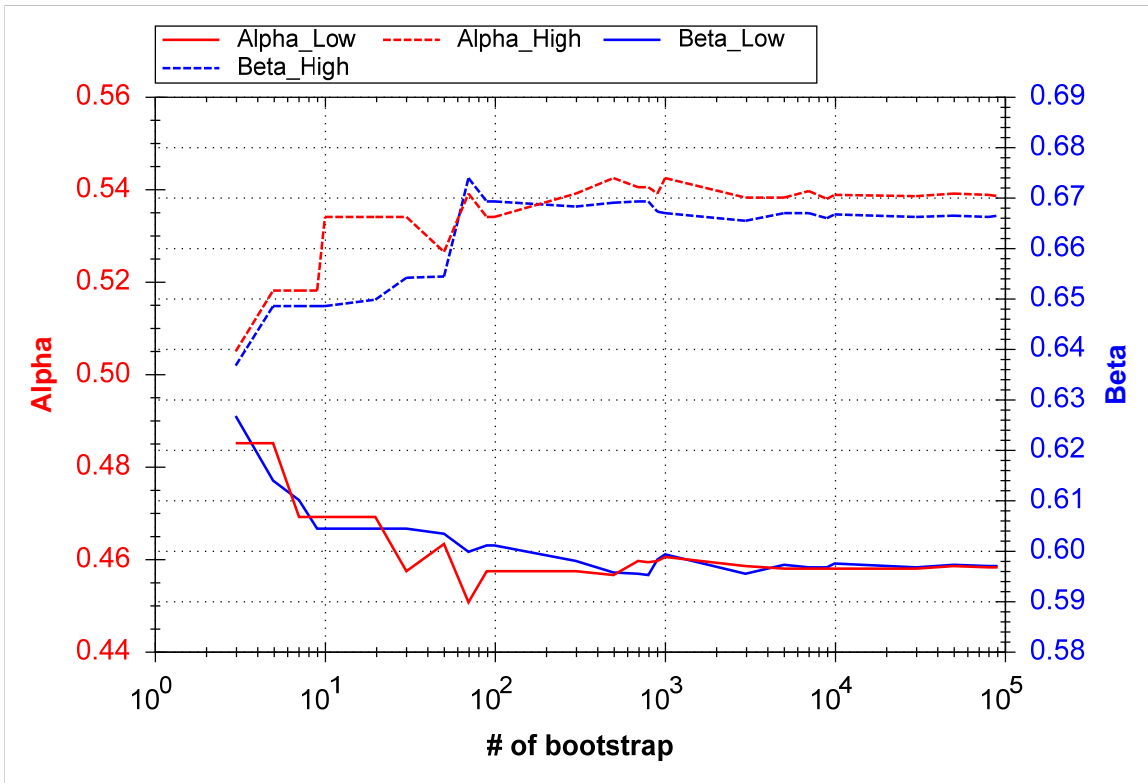
Figure 3.6. The effect of the number of bootstrap iterations on estimation of 95% confidence bounds for α and β.

4 Conversion between TWT and depth

4.1 Conversion of sedimentary thickness to two-way time

To use the velocity model for depth-to-time conversion we start with the following definition of velocity:

$$V = \frac{dh}{dt}$$

(11)

If a seismic wave travels from the seafloor to an arbitrary depth H which corresponds to a two-way time of TWT, we get:

$$\int_0^{twt/2} dt = \int_0^H \frac{dh}{V(h)}$$

(12)

By substituting Equation 7 for $V(h)$ we obtain the following analytical formula that allows us to calculate TWT at any H:

$$twt = \frac{2}{V_\infty}\left(H + \frac{e^\beta - e^{\beta - \alpha H}}{\alpha}\right)$$

(13)

4.2 Conversion of two-way travel time to sedimentary thickness

For time-to-depth conversion, we need to find the roots of following equation (from Eqn. 13):

$$f(H) = \alpha H - e^{\beta - \alpha H} + \left(e^\beta - \alpha \frac{V_\infty \cdot twt}{2}\right) = 0$$

(14)

We solved this problem in an iterative fashion using Newton-Raphson's method (Press 1992) with a starting estimate of sedimentary thickness H_0 calculated as follows:

$$H_0 = \frac{(V_0 + V_\infty)}{2} \cdot \frac{twt}{2}$$

(15)

To assess the accuracy and convergence of the iteration method, we used Equation 13 to generate a synthetic series of TWT for depths of 0 to 10 km sampled at 5 m intervals. The synthetic TWT values were then converted back to depth using the iteration method.

38

Within 4 iterations, differences between the calculated and original values are within ±1 cm over the entire depth range of 0 to 10 km.

In comparison with other methods such as polynomial curve fitting, Newton-Raphson's method is well constrained for any desired depth range and it provides a high degree of accuracy in the time-to-depth conversion. For convenience, the results are plotted on Figure 4.1. In Appendix 3, a one-page web application using JavaScript characterizes platform independence for time-to-depth solution . For quick reference, a table of time-depth pairs is provided in Appendix 5.
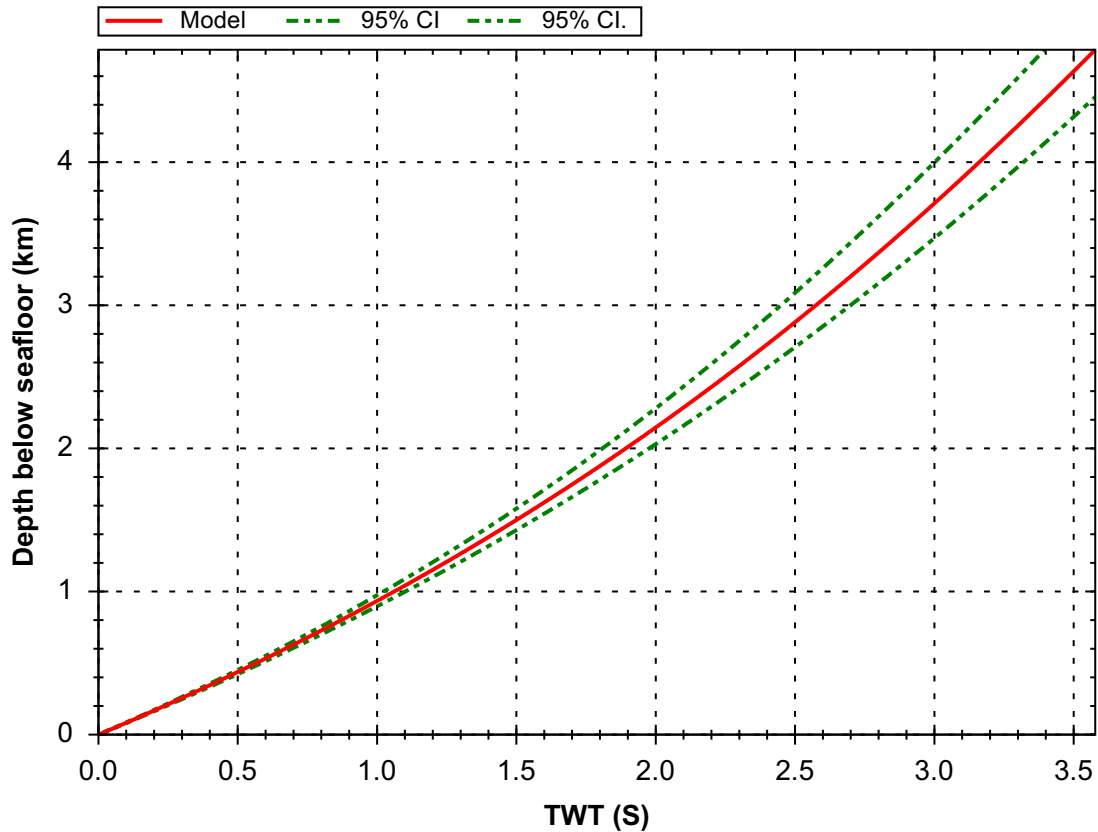
Figure 4.1. Time-depth relationship derived from the velocity model through application of Newton's method.

4.3   Uncertainty in time-to-depth conversion

Time-to-depth conversion allows closer examination of the estimated 95% confidence bounds. The total and relative thickness error ranges associated with these bounds are shown on figures 4.2 and 4.3. They indicate that the methods described in this report can be used for time-to-depth conversion with a level of certainty that is within ±0.379 km or ±7.9% over the time range of 0 to 4.8 km, which is appropriate for the region in which time-to-depth conversion is required (Figure 1.2).
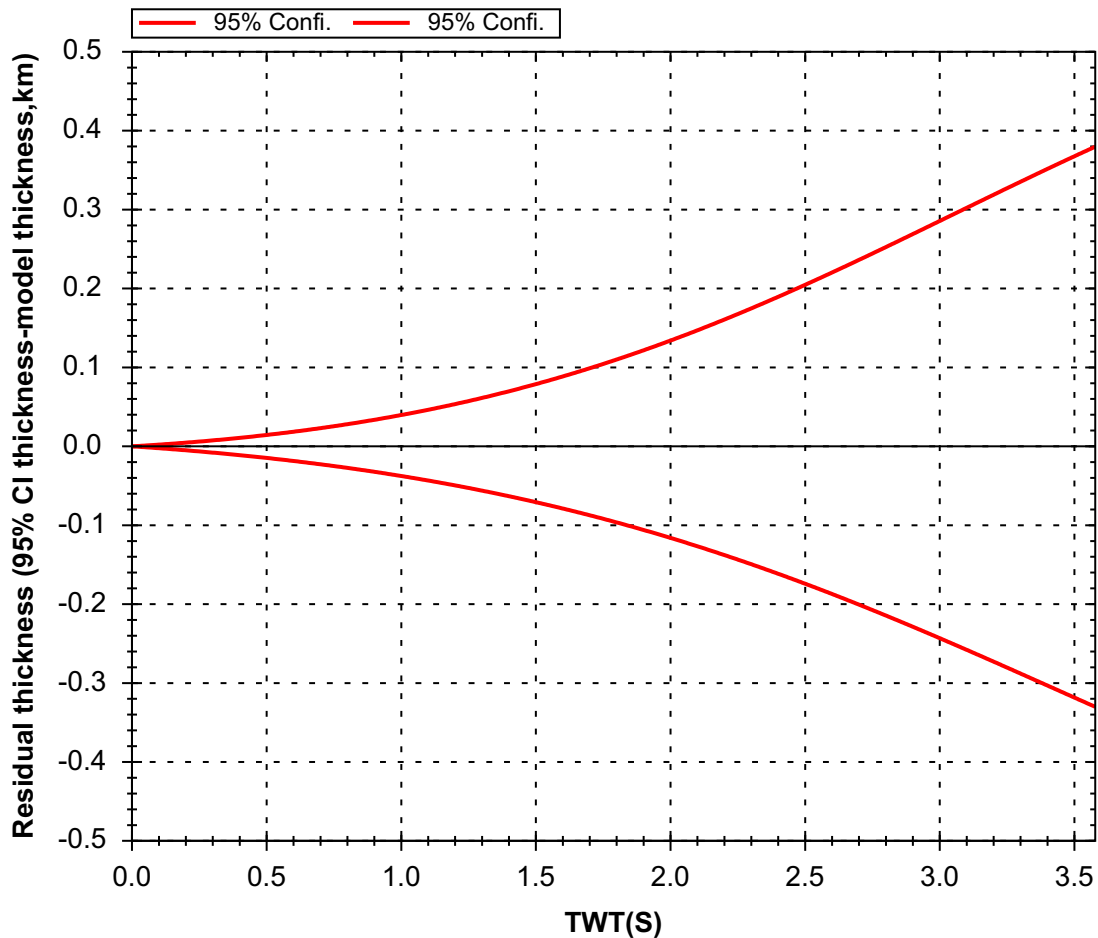
Figure 4.2. Conversion of the 95% confidence bounds to uncertainty in the total sedimentary thickness.
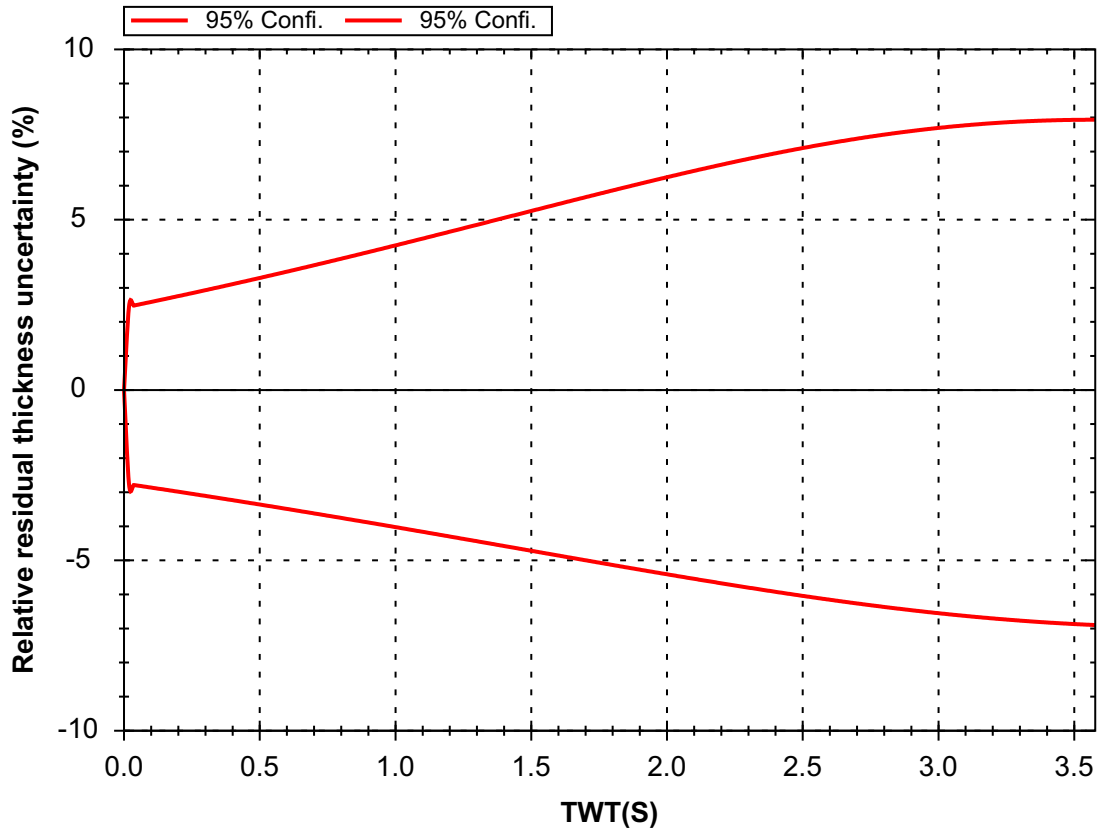
Figure 4.3. Conversion of the 95% confidence bounds to uncertainty in the relative sedimentary thickness.

5   Fixed points optimization

5.1   Fixed point and sediment point

Fixed point concept comes from the fixed line definition in Article 76 of the Law Of the Sea (UN-DOALOS 2006). One of the most important parameters in the definition of the extended continental shelf is the sediment thickness criteria, which defines the location where the sediment thickness is greater than 1% of the distance to its nearest FOS. Fixed points can also be defined from other criteria, such as the FOS plus 60 NM formula (UN-DOALOS 2006). If the fixed points are defined from the sediment thickness formula, it is also named a sediment thickness point.

5.2   Geodetic distance

The distance between an arbitrary sounding point (CDP) and any FOS is calculated using the (ellipsoid) geodetic distance of revised Vincenty (Vincenty, 1975) equations by Veness (2012). The JavaScript of Veness (2012) is revised into C# coding for the geodetic distance calculation between arbitrary two points on the ellipsoid earth. The maximum uncertainty is within 5 millimeters for any two points on the ellipsoid earth according to Veness (2012).

5.3   QLine and overlaying on seismic profile

The common way to identify the outermost sediment points is to inspect every depth sounding point (CDP) by finding its nearest FOS and calculating the geodetic distances. This procedure is not only tedious but also poorly defined in selecting the best thickness points for so many variation factors, such as seismic horizons, velocity models, and FOS. These all have uncertainties and they are often updatable in the working procedure.

The new method adopted in this work is simple and efficient by assuming any CDP could be a fixed point, thus we can evaluate the required thickness (to be a fixed point). The required sediment depth (to be a fixed point) is defined as the required thickness plus the water depth. Overlaying the required sediment depth (to be a fixed point) on seismic profile will create a horizon named QLine in this approach. If the required sediment depth (QLine) is within the sedimentary section on a seismic profile, the CDP could be a fixed point, otherwise the required sediment depth falls in basement, one CDP could not be a fixed point.

The procedure of charting QLine on a seismic profile follows:

(1) calculate the geodetic distance to all FOS points for one CDP (depth sounding point);

(2) find the smallest geodetic distance and the nearest FOS;

(3) calculate 1% of the nearest distance and name it as required sediment thickness (to be a fixed point) in metres;

(4) transform the required sediment thickness in metres to TWT in milliseconds with a velocity model (see Section 4.1);

(5) calculate required depth by sum of required thickness in TWT (milliseconds) and water depth in TWT; (5) repeat step 1-4 for every CDP and overlay these points on seismic profile as the QLine chart (see Figure. 5.1).
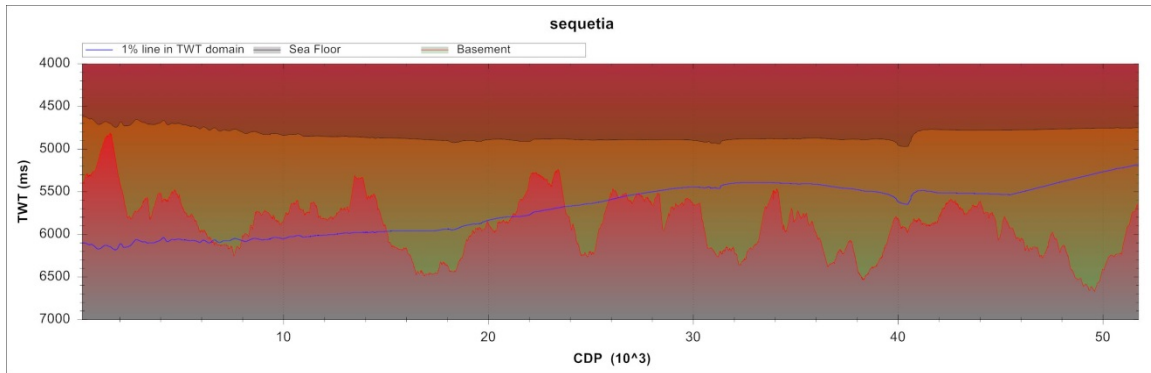
Figure 5.1 Automated QLine (blue line) for fixed point optimization (seafloor and top of basement are shown as black and red lines)

5.4   Batch processing and visualization

There might be hundreds of seismic lines or millions of depth sounding points, so batch processing is developed to facilitate the procedure of charting QLine on many seismic profiles in one area by one command in near real time. The step are

(1) prepare the interpreted seismic horizons of the seafloor and the top of basement, using seismic interpretation software (GeoFrame) GeoFrame project (the output format is a text file; see 13.3.2 for the udf file format),

(2) Prepare for FOS file with FOS points (see 13.3.3), and

(3) edit or create a velocity file with velocity models (see 13.3.5).

(4) Use the Gardiner application to dump QLine files (e.g. Fig. 13.30-32) and other files for report as well as charts overlaid on interpreted seismic profile (*e.g.* Fig. 13.32).

6   Positioning uncertainty evaluation of fixed point

A large number of factors may produce errors during fixed points positioning. Errors can be incurred at every phase of data acquisition, processing, and interpretation. Example phases include acquiring bathymetry data and identification of FOS, seismic acquiring (navigation and streamer biasing), processing (binning and stacking), identification of seafloor and basement, and sediment thickness interpretation using a velocity model. Each of these phases needs to be evaluated and integrated into the net positioning uncertainty.

The errors that could be introduced during seismic processing are innumerable, and significant processing mistakes may blur or even obliterate a seismic image. However, only a small class of errors will affect the two-way time and hence the interpreted sediment thickness.

These error sources could be categorized as vertical and horizontal uncertainties. The vertical uncertainty category includes errors in identification of seismic horizons (seafloor and top of basement) and the velocity modeling. They should be integrated and transformed into (transformed) horizontal uncertainty using the dipping angles of seafloor and top of the basement. The horizontal uncertainty category includes uncertainty originated from FOS identification, seismic navigation, streamer drift, and seismic data processing. The net positioning uncertainty of a fixed point is evaluated by integrating transformed horizontal uncertainty of the integrated vertical uncertainty and horizontal uncertainties.

6.1   Vertical uncertainty and transformed into horizontal uncertainty

The errors in identification of seafloor ($\Delta Y_{seafloor}$) and basement ($\Delta Y_{basement}$) depend on seismic profile quality, bathymetry, depth of basement, and frequency contentcompositions of processed seismic profile. They can be integrated with the sediment thickness error ($\Delta Y_{VelocitymModel}$) during the velocity modeling procedure into the integrated vertical uncertainty ($\Delta Y_{vertical}$).

$$\Delta Y_{vertical} = \sqrt{\Delta Y_{seafloor} + \Delta Y_{basement} + \Delta Y_{VelocitymModel}} \qquad (16)$$

Optimal vertical resolution is equal to one-quarter of the dominant seismic wavelength (Yilmaz, 1987), which corresponds to 5–10 m for seafloor or buried base of sediments according to the UNCLOS training manual (UN-CLCS, 1999).

$\Delta Y_{vertical}$ causes horizontal uncertainty and is estimated (UN-CLCS, 1999) as follows,

$$\Delta X_{fromVertical} = \frac{\Delta Y_{vertical}}{tan\left(Arctan\left(\frac{tan\beta_0 cos\theta}{1+tan\beta_0 sin\theta}\right)+\theta\right)+tan\alpha} \qquad (17)$$

where $\alpha, \beta_0,$ and θ are the dip of the seafloor away from the FOS, the dip of basement towards the foot of slope, and the angle of slope of the 1% line at the starting position of a horizontal basement (so, $tan\beta_0 = 0.01$ according to the definition on page VI40, UN-DOALOS, 2006)

Estimate the seafloor and basement dip angles from the averaged slopes by approximating straight lines inside a vicinity window of the potential Gardiner points, as in Figure 13.37. Inside the window, straight linear equations of $D_{seafloor} = tan\alpha * x + b$ and $D_{basement} = tan\beta * x + c$ for the seafloor and top of basement, respectively, are fitted using the ordinary least square approximation. In these two straight line equations, D is the depth of seafloor or basement, x is the distance along the profile, and c and d are constants.

An interactive visualization application is developed to evaluate the two apparent dipping angles and an example is shown in Figure 6.1. The estimated apparent dipping angles and straight line approximation of the seafloor and the top of basement are reported in the inlet window in Figure 6.1.

6.2 Net positing uncertainty for fixed point

The net positioning uncertainty is calculated using the following formula:

$$\Delta X_{Net} = \sqrt{\Delta X_{FOS}^2 + \Delta X_{shipNavigation}^2 + \Delta X_{streamer}^2 + \Delta X_{processing}^2 + \Delta X_{fromVertical}^2}$$

Where ΔX_{FOS}, $\Delta X_{shipNavigation}$, $\Delta X_{streamer}^2$, and $\Delta X_{processing}$ are errors created by identification of FOS, seismic ship navigation, streamer biasing, and seismic data processing, respectively. $\Delta X_{fromVertical}$ is the transformed uncertainty from vertical error sources (see previous section).

Finally, the net horizontal uncertainty is charted as an error box. The error box is centred near the Gardiner point and has a width of two times the horizontal uncertainty and a height of two times the integrated vertical uncertainty. An example is shown in figure 13.37-38.

The developed software tool was able to fulfill this net uncertainty analysis task with flexibility and ease of use. During the net uncertainty analysis, the apparent dipping angles of seafloor and top of basement are estimated by calculating the slope of the two fitted straight lines between the two movable vertical bars (see figures 6.1 and 13.37). The vertical error (sediment thickness error) caused during conversion from TWT and the sediment thickness using a velocity modeling was also calculated and then (their absolute value) was averaged between the two vertical bars and used as the sediment thickness error in the net positioning uncertainty integration.
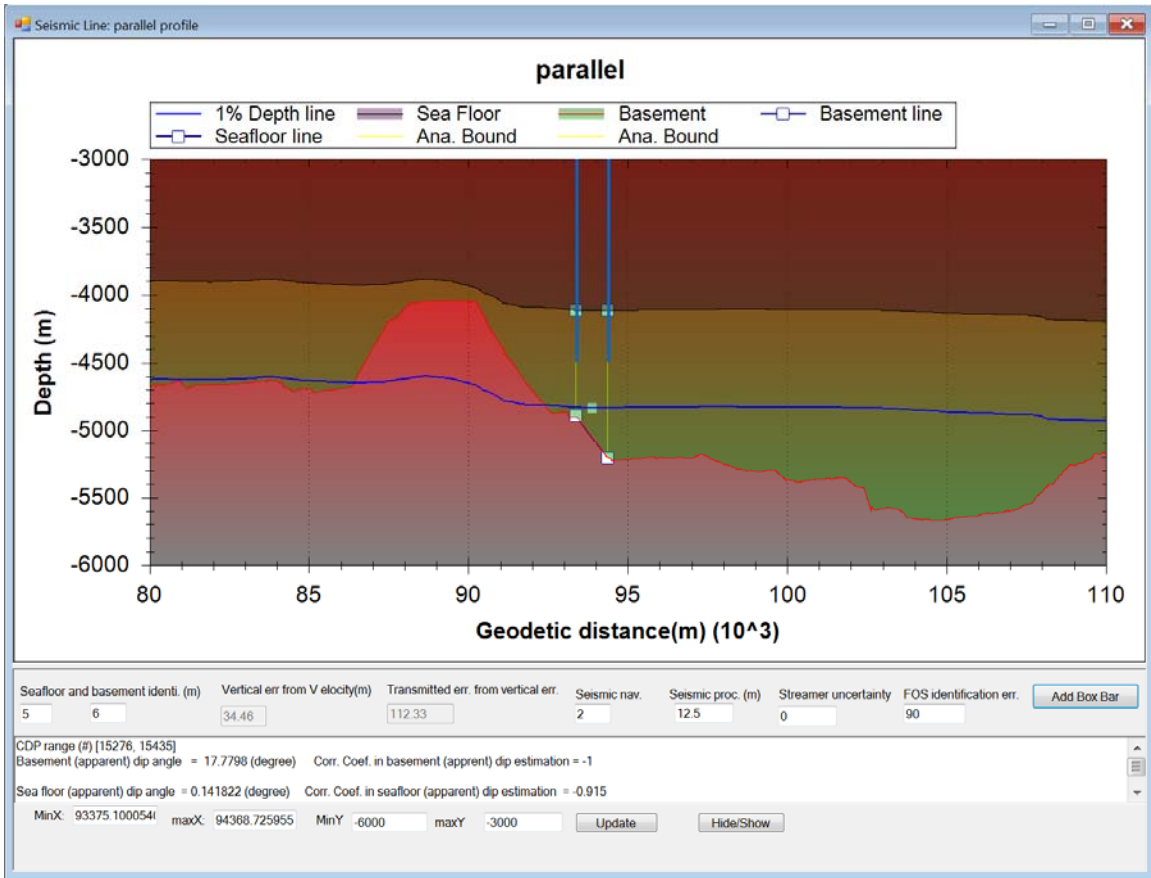
Figure 6.1 Graphic interactive net positioning uncertainty evaluation

7   Discussions

Estimation of the 95% confidence interval for the model using the bootstrap method provides one measure by which to evaluate certainty in the modelling results. In the following sections we compare the model with other independent sources of information.

7.1   Well-to-seismic correlation at ODP Hole 647A

As explained in Section 2.1.2, the data compilation used for the velocity model in the present study does not include samples from ODP Hole 647A. However, the exact thickness of the sedimentary succession is known with certainty at this location since the underlying basement was cored between 699 and 736 mbsf. This provides a valuable test of the velocity model.

At Hole 647A, basement is described as generally massive, aphyric to moderately pyroxene-phyric, fine- to medium-crystalline basalt that is probably comprised of thick flow units (Srivastava *et al.* 1987). The contact with the overlying the sedimentary succession at 699 mbsf is sharp and characterized by large calcite- and chlorite-filled vesicles. Veins in the basalt contain calcite and chlorite and, at deeper levels, massive serpentine. Otherwise the basalt appears fresh. A strong seismic reflection is generated from the top of basement in this region due to the strong impedance contrast.

A detail map is given on Figure 7.1. The hole is located 1.12 km from line 9A of a single-channel survey collected by the Atlantic Geoscience Centre during Hudson Cruise 84-030. These data were digitized from analog recordings on magnetic tape so that they could be interpreted on a digital seismic workstation. A -90° phase delay and -80 ms time shift was applied to the 84-030 survey in order to correctly tie with the modern multichannel surveys in the study area.

The basement contact at 699 mbsf corresponds to a two-way time of 770 ms below seafloor. At the projected location of Hole 647A on line 9A, the basement horizon is 756 ms below seafloor (Figure 7.2), which corresponds to a model depth of 685 mbsf. The 14 m discrepancy with the measurement at the borehole is just 2% of the total thickness and it is well within the 95% confidence interval. It is an excellent match considering that the seismic profile is 1.12 km from the borehole location and considering that the basement is neither horizontal nor flat.
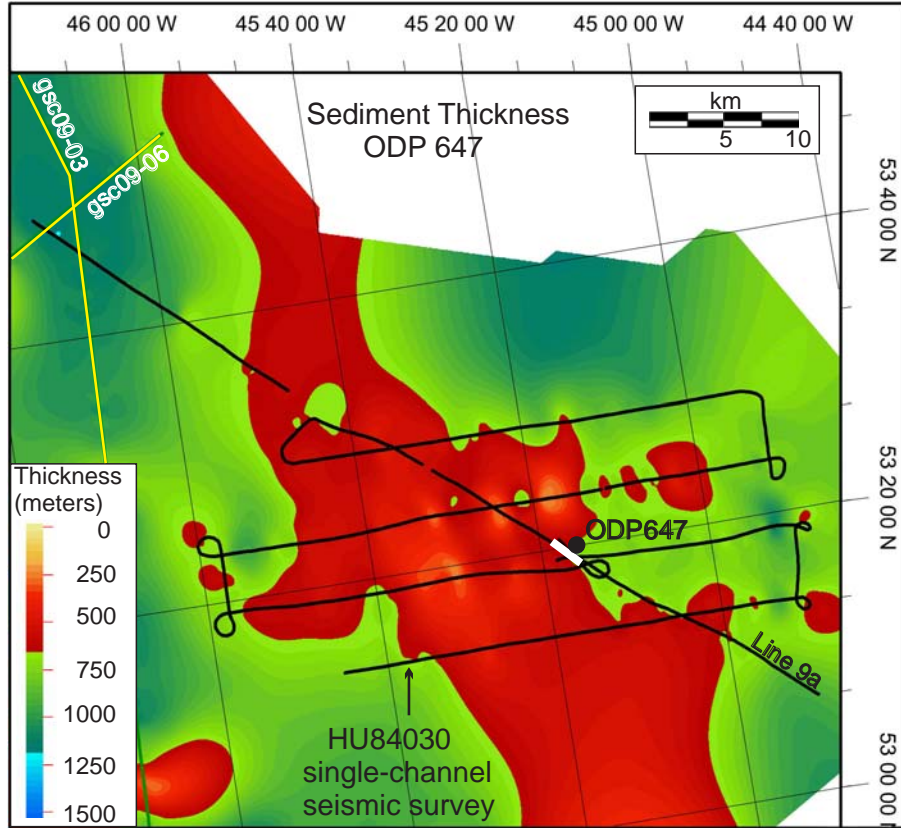
Figure 7.1. Single channel seismic reflection profiles acquired in the vicinity of ODP Site 647 by the Atlantic Geoscience Centre during the scientific cruise Hudson 84-030. Note: line 9a is incorrectly labelled as line 8 in the ODP Site report (Srivastava et al. 1987).
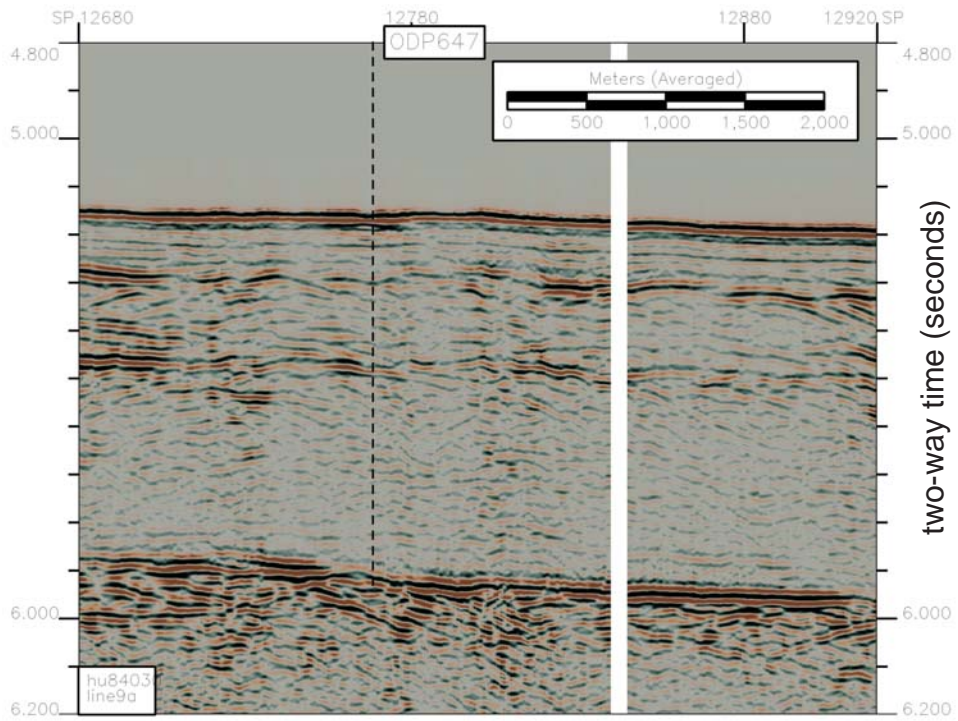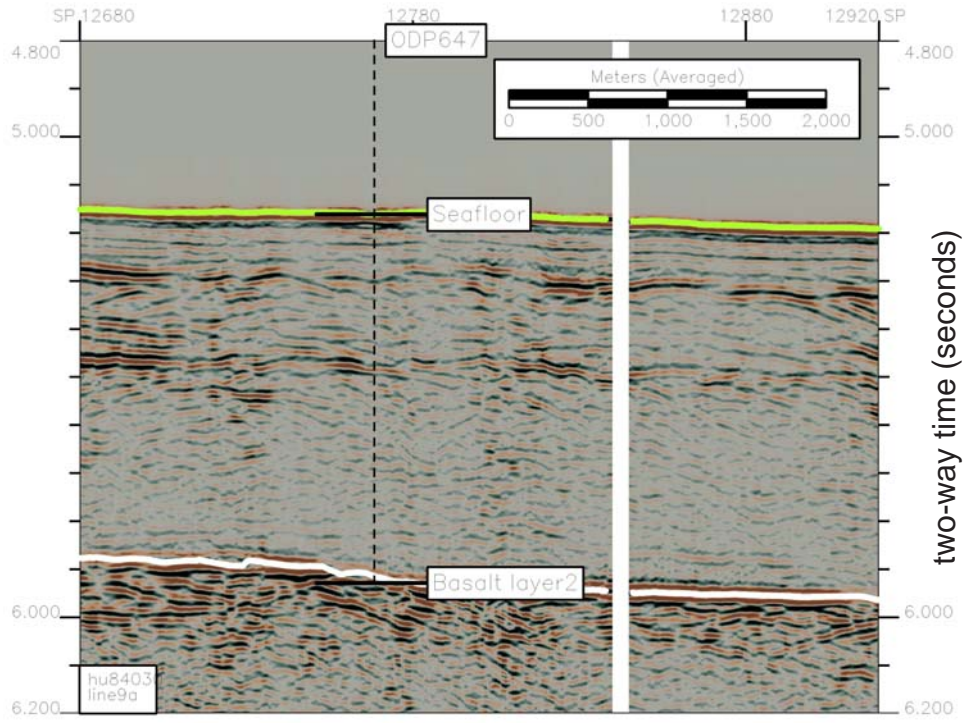
Figure 7.2. Correlation of ODP Hole 647A and Hudson 84-030 line 9A.

7.2 Comparison with direct observations from global analogues

There are relatively few publications containing direct observations of shale velocity, especially for open marine deep water settings. Carlson *et al.* (1986) published a compilation of seismic reflection travel times and the corresponding depths to the reflection interfaces intersected by DSDP boreholes. These are high quality measurements representative of deep water successions sampled at 128 DSDP sites around the world. To describe the time-depth relationship of borehole information, Carlson *et al.* (1986) used the following empirical relationship which can be applied for burial depths of up to 1.4 km:

$$DBSF = -\frac{1}{a}\ln(1 - \frac{T}{aV_0^2})$$ (18)

where *DBSF* is depth below seafloor in km, *T* is one-way travel time below seafloor in seconds, and V_0 is the velocity in km/s at the seafloor. Using a regression technique that accounts for bivariate uncertainty, Carlson *et al.* (1986) obtained the following best-fit parameters: V_0 = 1.59 ± 0.018 and *a* = 0.33 ± 0.03 s/km. The RMS error of predicted versus observed depths in the DSDP data set is 26 m. Carlson *et al.* (1986) estimated that site-to-site variability of velocity at a given depth is less than 0.20 km/s and they commented that the data exhibit remarkably little scatter.

Another source of information comes from Dutta *et al.* (2009) who used the following empirical equation to describe the depth-velocity relationship derived from borehole sonic logs of open marine deep water shale intervals in the Green Canyon region of the Gulf of Mexico:

$$V_{SHALE} = Ae^{Bz} + Ce^{Dz}$$ (19)

where V_{SHALE} is measured in ft/s and *z* is the depth below seafloor in feet. After excluding overpressured intervals and subsalt shales with complex compaction histories, Dutta *et al.* (2009) used nonlinear regression to determine *A* = 6917, *B* = 4.633E-05, *C* = -1652, and *D* = -3.646E-04. The accuracy of this empirical relationship is not given, but we assume that it is comparable to that of the Carlson *et al.* (1986) relationship. It is also important to note that Dutta *et al.* (2009) do not explicitly state the depth range for which their relationship is considered valid, although their deepest measurements appear to be at 9000 ft or about 2.7 km. The relationship may be invalid beyond that range.

A comparison between the empirical relationships of Carlson *et al.* (1986) and Dutta *et al.* versus the model of the present study demonstrates a remarkable level of agreement (Figure 7.3). Sedimentary thickness calculated from the Carlson *et al.* relationship over its constrained range of 0.0 to 1.4 km below seafloor is with ±20 m of the model. This is strong evidence that porosity and mechanical compaction are predominant controls on seismic velocity within the uppermost 1.4 km of deep water marine successions around the world.

Sedimentary thickness calculated from the Dutta *et al.* (2009) relationship is within 7.9% of the model for burial depths up to 4.5 km. This is close to the upper 95% confidence bound of the model, so there may be no statistically significant difference especially if the assumed accuracy of the Dutta *et al.* relationship is also considered. However, presuming that the difference is real, the velocity of the Gulf of Mexico succession appears to be about 7.9% higher than that of the central Labrador Sea succession and perhaps this is related to geological factors. For example, the bulk lithological and textural characteristics of sediment from the subtropical Gulf of Mexico margin is likely different from that of sediment from the glaciated margins of Labrador, Baffin Island, and Greenland. Therefore different sedimentary velocity profiles for the two regions are certainly plausible.
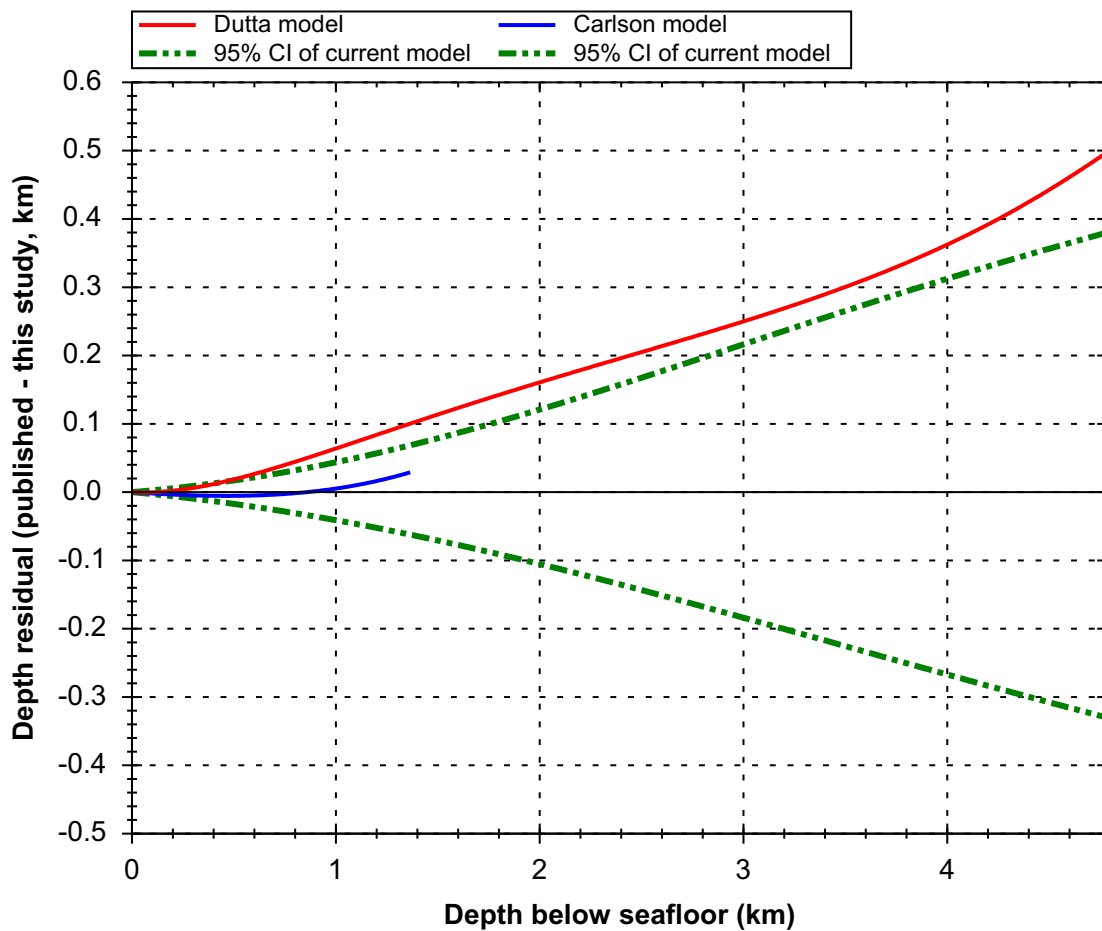
Figure 7.3. Comparison of the model with borehole velocity measurements from global deep sea drilling (Carlson et al. 1986) and with deep-water marine shales in the Green Canyon region of the Gulf of Mexico (Dutta et al. 2009).

7.3 Comparison with moveout-based velocities

Moveout-based velocities from processing of the multichannel seismic reflection data acquired for GEUS in 2003 and 2006 are shown on Figure 7.4 (see Figure 2.11 for locations). These were calculated from maximum coherency stacking velocities using the Dix equation (Equation 5). The calculation is sensitive to small variations in interval thickness, which causes a high degree of scatter, so the results were clipped at 3.6 km/s to allow meaningful comparison with the model. The scatter obscures any evidence for the curvilinear mechanical compaction trend that is expected for deep water marine successions (Section 3.1). Nonetheless, binning and averaging of the moveout-based values over 100 m intervals demonstrates a close match to burial depths of about 3.0 km (deeper than which there is bias due to the clipping; Figure 7.4). In other words, the regional statistical trend of the moveout-based velocities does provide independently derived support for the modelling results.
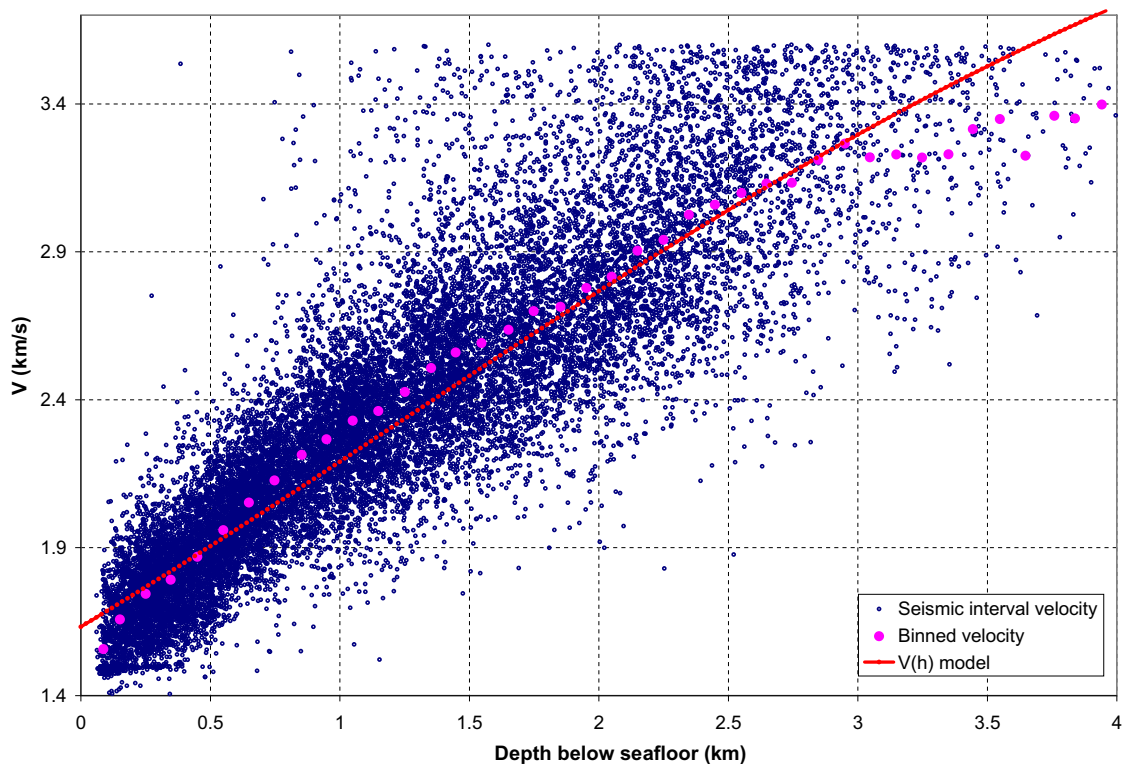
Figure 7.4. Scatter plot of moveout-based velocities derived from processing of multichannel seismic surveys collected by the Geological Survey of Denmark and Greenland in 2003 and 2006.

8   Conclusions

A total of 165 velocity samples from 33 widely distributed stations are compiled to characterize the deep water succession of central Labrador Sea where conversion between TWT and sediment thickness is required.

The data are successfully modelled using the RMA method which, minimizing errors from both velocity and depth measurements with excellent correlation and confidence limits (±7.9% at the 95% confidence level), are estimated using the nonparametric statistical bootstrapping method. Such an approach with slowness function assessed the theoretical and empirical facts of porosity reduction behaviour that is well documented for deep water marine successions around the world. Simultaneously, the model parameters are readily interpretable in terms of geologically significant physical properties.

An analytical function is derived from the model that allows exact conversion of depth to two-way time. For the inverse conversion, from two-way time to depth, a numerical method known as Newton-Raphson's method is employed. This provides a depth conversion accuracy of better than ±1.0 cm.

The constructed model yields physically plausible velocities for any depth range and therefore suitable for conversion between TWT and depth at any depth.

The model prediction for the sedimentary thickness at ODP Hole 647A is within 2% of the true value, and comparison with averaged moveout-based velocities also demonstrates a close match. These are independent validations of the model accuracy for the central Labrador Sea region. Furthermore, the model results are remarkably similar to those published for boreholes of the Deep Sea Drilling Program and from the deep water Gulf of Mexico. In addition to providing support for the model and its underlying methodology, comparison with these global analogues provides evidence that porosity reduction due to mechanical compaction is a predominant factor controlling seismic velocity within at least the uppermost 1.4 km of deep water marine successions.

Fixed points selection procedure are analyzed and programmed for optimized identification with QLine visualization in near real-time.

Net positioning uncertainty is analyzed and factors of uncertainty are integrated with a developed software tool featuring interactive graphic interactive editing according to the requirement of UNCLOS.

Software tools are developed and documented to fulfill these procedures featured interactive graphic user interface, visualization, and batch processing. The conversion between TWT and sediment depth is created as a look-up table; it is also coded for a one-page web application which features platform independence and can be embeddable in a document.

9 References

Al-Chalabi, M. 1974. An analysis of stacking, rms, average, and interval velocities over a horizontally layered ground. Geophysical Prospecting, **22:** 458–475.

Al-Chalabi, M. 1979. Velocity determination from seismic reflection data. *In* Developments In Geophysical Exploration Methods. *Edited by* A. Fitch. Applied Science Publishing, Barking, United Kingdom, pp. 1–68.

Al-Chalabi, M. 1994. Seismic velocities - a critique. First Break, **12:** 589–596.

Al-Chalabi, M. 1997a. Time-depth relationships for multilayer depth conversion. Geophysical Prospecting, **45:** 715–720.

Al-Chalabi, M. 1997b. Instantaneous slowness versus depth functions. Geophysics, **62:** 270–273.

Amery, G.B. 1993. Basics of seismic velocities. The Leading Edge, **12:** 1087–1091.

Arthur, M.A., Srivastava, S., Kaminski, M., Jarrard, R., and Osler, J. 1989. Seismic stratigraphy and history of deep circulation and sediment drift development in Baffin Bay and the Labrador Sea. *In* Proceedings of the Ocean Drilling Program, Scientific Results, Volume 105. Ocean Drilling Program, College Station, Texas, pp. 957–988.

Athy, L.F. 1930. Compaction and oil migation. American Association of Petroleum Geologists Bulletin, **14:** 25–35.

Blackburn, G. 1980. Errors in stacking velocity--true velocity conversion over complex geologic situations.. Geophysics, **45:** 1465–1488.

Bohonak, J.A. 2004. Manual of RMA-software for Reduced Major Axis Regression [online]. Available from http://www.bio.sdsu.edu/pub/andy/RMAmanual.pdf [accessed 3 January 2013].

Busch, W.H. 1989. Patterns of sediment compaction at Ocean Drilling Program sites 645, 646, and 647, Baffin Bay and Labrador Sea. *In* Proceedings of the Ocean Drilling Program, Scientific Results, Volume 105. Ocean Drilling Program, College Station, Texas, pp. 781–790.

Carlson, R.L., Gangi, A.F., and Snow, K.R. 1986. Empirical reflection travel time versus depth and velocity versus depth functions for the deep-sea sediment column. Journal of Geophysical Research, **91:** 8249–8266.

Cameron, M., Fomel, S., and Sethian, J. 2008. Time-to-depth conversion and seismic velocity estimation using time-migration velocity. Geophysics, **73:** VE205–VE210.

Chalmers, J.A. and Laursen, K.H. 1995. Labrador Sea: The extent of continental and oceanic crust and the timing of the onset of seafloor spreading. Marine and Petroleum Geology, **12:** 205–217.

Chalmers, J.A. and Pulvertaft, T.C.R. 2001. Development of the continental margins of the Labrador Sea – A review. *In* Non-Volcanic Rifting of Continental Margins: A comparison of Evidence from Land and Sea. *Edited by* R. Wilson, R. Whitmarsh, B. Taylor, and N. Froitzheim. Geological Society of London, Special Publication 187. pp. 77–105.

Channell, J. E. T., T. Kanamatsu, T. Sato, R. Stein, C. A. Alvarez Zarikian, and M. J. Malone, and the Expedition 303/306 Scientists, 2006. North Atlantic Climate, Proc. Integr. Ocean Drill. Program, 303/306, doi:10.2204/iodp.proc.303306.2006

Chapman, R.E. 1983. Elsevier Science Publishing Company,

Chian, D., Keen, C., Reid, I., and Louden, K.E. 1995a. Evolution of nonvolcanic rifted margins: new results from the conjugate margins of the Labrador Sea. Geology, **23:** 589–592.

Chian, D. and Louden, K.E. 1994. The continent-ocean crustal transition across the southwest Greenland margin. Journal of Geophysical Research, **99:** 9117–9135.

Chian, D., Louden, K.E., and Reid, I. 1995b. Crustal structure of the Labrador Sea conjugate margin and implications for the formation of nonvolcanic continental margins. Journal of Geophysical Research, **100:** 24,239–24,253.

Cremer, M., Maillet, N., and Latouche, C. 1989. Analysis of sedimentary facies and clay mineralogy of the Neogene-Quaternary sediments in ODP Site 646, Labrador Sea. *In* Proceedings of the Ocean Drilling Program, Scientific Results, Volume 105. Ocean Drilling Program, College Station, Texas, pp. 71–81.

Davies, T.A. and Laughton, A.S. 1972. Sedimentary processes in the North Atlantic. *In* Initial Reports of the Deep Sea Drilling Program, Volume XII covering Leg 12 of the Cruises of the Drilling Vessel Glomar Challenger. *Edited by* T. Davies. United States Government Printing Office, pp. 905–934.

Davison, A.C. and Hinkley, D.V. 1997. Cambridge University Press,

Delescluse, M., Funck, T., Dehler, S., and Louden, K. 2012. The oceanic crustal structure at the extinct labrador sea spreading center. *In* Joint Annual Meeting of the Geological Association of Canada and the Mineralogical Association of Canada, Abstracts, Volume 35., St. John's, Newfoundland.

Dickie, K., Keen, C.E., Williams, G.L., and Dehler, S.A. 2011. Tectonostratigraphic evolution of the labrador margin, Atlantic Canada. Marine and Petroleum Geology, **28:** 1663–1675.

Dix, C.H. 1955. Seismic velocities from surface measurements. Geophysics, **20:** 68–86.

Dutta, T., Mavko, G., Mukerji, T., and Lane, T. 2009. Compaction trends for shale and clean sandstone in shallow sediments, Gulf of Mexico. The Leading Edge, **28:** 590–596.

Efron, B. 1977. Bootstrap methods: Another look at the Jackknife. The Annals of Statistics, **7:** 1–26.

Fowler, C.M.R. 2005. Chapter 4: Seismology measuring the interior. *In* The Solid Earth. Cambridge University Press, Cambridge, United Kingdom, pp. 100–192.

Funck, T., Dehler, S.A., Chapman, C.B., Delescluse, M., Iuliucci, J., Iuliucci, R., Judge, W., Meslin, P., and Ruhnau, M. 2010. Cruise report of the SIGNAL 2009 Refraction Seismic Cruise (Hudson 2009-019), Open File 6144. Geological Survey of Canada, Dartmouth, Nova Scotia.

González-Solís, J. 2004. Sexual size dimorphism in northern giant petrels: ecological correlates and scaling. Oikos, **105:** 247–254.

Guillemain, M, Hervé, F., Klaassen, M, Johnson, A., and Heinz, H. 2004. Fuelling rates of garganey (Anas querquedula) staging in the Camargue, southern France, during spring migration. Journal of Ornithology, **145:** 152–158.

Hajnal, Z. and Sereda, I.T. 1981. Maximum uncertainty of interval velocity estimates. Geophysics, **46:** 1543–1547.

Hamilton, E.L. 1971. Prediction of in situ acoustic and elastic properties in marine sediments. Geophysics, **36:** 266–284.

Hinz, K., Schluter, H.-U., Grant, A.C., S.P., Srivastava, D., Umpleby, and J., Woodside 1979. Geophysical transects of the Labrador Sea: Labrador to southwest Greenland. Tectonophysics, **59:** 151–183. doi:10.1016/0040-1951(79)90043-X.

Hottman, C.E. and Johnson, R.K. 1965. Estimation of formation pressures from log-derived shale properties. Journal of Petroleum Technology, **17:** 717–723.

Japsen, P. 1993. Influence of lithology and Neogene uplift on seismic velocities in Denmark: Implications for depth conversion of maps. American Association of Petroleum Geologists Bulletin, **77:** 194–211.

Japsen, P. 1999. Overpressured Cenozoic shale mapped from velocity anomalies relative to a baseline for marine shale. Petroleum Geoscience, **5:** 321–336.

Japsen, P. 2000. Investigation of multi-phase erosion using reconstructed shale trends based on sonic data. Sole Pit axis, North Sea. Global and Planetary Change, **24:** 189–210.

Japsen, P., Mukerji, T., and Mavko, G. 2007. Constraints on velocity-depth trends from rock physics models. Geophysical Prospecting, **55:** 135–154.

Kearey, P. and Brooks, M. 1984. Chapter 3: Elements of seismic surveying. *In* An Introduction to Geophysical Exploration. *Edited by* A. Hallam. Blackwell Scientific Publications, Oxford, United Kingdom, Geoscience Texts Volume 4. pp. 34–56.

Keen, C.E., Potter, P., and Srivastava, S.P. 1994. Deep seismic reflection data across the conjugate margins of the Labrador Sea. Canadian Journal of Earth Sciences, **31:** 192–205.

Kennett, B.L.N 2009. Australian National University Press (originally published by Cambridge University Press, 1981),

Laughton, A.S., Berggren, W.A., and the Shipboard Scientific Party 1972. *Edited by* T. Davies. United States Government Printing Office,

Lebedeva-Ivanova, N. 2010. Geophysical Studies Bearing on the Origin of the Arctic Basin. Faculty of Science and Technology, Uppsala Universitet,

Lizarralde, D. and Buffler, R.T. 1992. Chapter 34: Comparison of velocities determined from sonobuoy, VSP, core-sample, and sonic-log data from Site 765. *In* Proceedings of the Ocean Drilling Program, Scientific Results, Leg 123, Argo Abyssal Plain/Exmouth Plateau. Ocean Drilling Program, College Station, U.S.A., pp. 625–636.

Magara, K. 1978. Compaction and Fluid Migration -- Practical Geology. Elsevier, Oxford.

Matthews, W.R. and Kelly, J. 1967. How to predict formation pressure and fraction gradient. Oil and Gas Journal, **65:** 92–106.

McArdle, B.H. 1988. The structural relationship: Regression in biology. Canadian Journal of Zoology, **66:** 2329–2339.

Oakey, G.N. and Chalmers, J.A. 2005. A new model for Paleogene motion of Greenland relative to North America; A re-evaluation of plate geometry of Baffin Bay. *In* Cenozoic Evolution and Lithosphere Dynamics of the Baffin Bay-Nares Strait region of Arctic Canada and Greenland. *Edited by* G. Oakey. Faculty of Earth Sciences, Vrije Universiteit, pp. 64–91.

Oakey, G., Forsberg, R., and Jackson, H.R. 2001. Gravity anomaly of the Labrador Region, Canadian and Greenland Arctic, Open File 3934A, scale 1:1500000. Geological Survey of Canada, Dartmouth, Nova Scotia.

Osler, J.C. 1993. Crustal structure of the extinct spreading center in the Labrador Sea: Implications for dynamic models of flow beneath mid-ocean ridges. Ph.D. thesis, Department of Geology, Dalhousie University, Halfiax, Nova Scotia.

Osler, J.C. and Louden, K.E. 1992. Crustal structure of an extinct rift axis in the Labrador Sea: preliminary results from a seismic refraction survey. Earth and Planetary Science Letters, **108:** 243–258.

Osler, J.C. and Louden, K.E. 1995. Extinct spreading center in the Labrador Sea: crustal structure from a two-dimensional seismic refraction velocity model. Journal of Geophysical Research, **100:** 2261–2278.

Persand, S. 2012. A Practical Overview of Article 76 of the United Nations Convention on the Law of the Sea [online]. Available from http://www.un.org/Depts/los/nippon/ unnff_programme_home/fellows_pages/fellows_papers/persand_0506_mauritius.pdf [accessed 7 July, 2012].

Press, W.H., Teuolsky, S.A., Vetterling, W.T., and Flannery, B.P. 1992. Cambridge University Press, Cambridge, United Kingdom.

Revil, A., Grauls, D., and Brévart, O. 2002. Mechanical compaction of sand/clay mixtures. Jounal of Geophysical Research, **107:** 1–15. doi:10.1029/2001JB000318.

Richterhausen, M. and Funck, T. 2009. Seismic velocities obtained from sonobuoy measurements in Labrador Sea, Report 2009/12. Geological Survey of Denmark and Greenland (GEUS), Copenhagen, Denmark.

Roest, W.R. and Srivastava, S.P. 1989. Sea-floor spreading in the Labrador Sea: A new reconstruction. Geology, **17:** 1000–1003.

Ruby, W.W. and Hubbert, M.K. 1959. Role of fluid pressure in mechanics of overthrust faulting, part II. Geological Society of America Bulletin, **70:** 167–206.

Sclater, J.G. and Christie, P.A.F. 1980. Continental stretching: an explanation of the post-Mid-Cretaceous subsidence of the central North Sea basin. Journal of Geophysical Research, **85:** 3711–3739.

Sheriff, R.E. and Geldart, L.P. 1995. Chapter 5: Seismic velocity. *In* Exploration Seismology. Cambridge University Press, Cambridge, United Kingdom, pp. 107–143.

Srivastava, S.P., Arthur, M., Clement, B., and the Shipboard Scientific Party 1987. Ocean Drilling Program, College Station, Texas.

Srivastava, S.P. and Keen, C.E. 1995. A deep seismic reflection profile across the extinct mid-Labrador Sea spreading center. Tectonics, **14:** 372–389.

Srivastava, S.P., Louden, K.E., Chough, S., Mosher, D., Loncarevic, B., Mudie, P., de Vernal, A., and MacLean, B. 1989. Results of detailed geological and geophysical measurements at ODP sites 645 in Baffin Bay and 646 and 647 in the Labrador Sea. *In* Proceedings of the Ocean Drilling Program, Scientific Results, Volume 105. Ocean Drilling Program, College Station, Texas, pp. 891–922.

Srivastava, S.P. and Tapscott, C.R. 1986. Plate kinematics of the North Atlantic. *In* The Geology of North America, volume M. *Edited by* P. Vogt and B. Tucholke. Geological Society of America, pp. 379–404.

Taner, M.T. and Koehler, F. 1969. Velocity spectra--digitial computer derivation and applications of velocity functions. Geophysics, **34:** 859–881.

Tucholke, B.E. and Fry, V.A. 1985. Basement structure and sediment distribution in northwest Atlantic Ocean. American Association of Petroleum Geologists Bulletin, **69:** 2077–2097.

UN-CLCS 1999. Scientific and Technical Guidelines of the Commission on the Limits of the Continental Shelf. United Nations, Commission on the Limits of the Continental Shelf, New York.

UN-DOALOS 2006. United Nations, Division for Ocean Affairs and the Law of the Sea, Office of Legal Affairs, New York, U.S.A.

Vincenty,T. 1975. Direct and Inverse Solutions of Geodesics on the ellipsoid with application of nested equations", Survey Review, Vol. XXII no. 176, http://www.ngs.noaa.gov/PUBS_LIB/inverse.pdf

Veness, C., 2012. Vincenty Inverse Solution of Geodesics on the Ellipsoid (c) Chris Veness 2002-2012, http://www.movable-type.co.uk/scripts/latlong-vincenty.html (Javascript, Open source)

Weller, J.M. 1959. Compaction of sediment. AAPG Bulletin, **43:** 273–310.

Whitmarsh, R.B. 1972. Chapter 12: Discussion and interpretation of some physical properties. *In* Initial Reports of the Deep Sea Drilling Program, Volume XII covering Leg 12 of the Cruises of the Drilling Vessel Glomar Challenger. *Edited by* T. Davies. United States Government Printing Office, pp. 935–951.

Yang, X.-S. 2001. A unified approach to mechanical compaction, pressure solution, mineral reactions, and the temperature distribution in hydrocarbon basins. Tectonophysics, **330:** 141–151.

Yilmaz, Ö. 1987. Chapter 3: Velocity analysis, statics corrections, and stacking. *In* Seismic Data Processing. *Edited by* S. Doherty. Society of Exploration Geophysicists, Tulsa, USA, Investigations in Geophysics, Volume 2. pp. 155–354.

10   Appendix 1: Geographic locations of the velocity stations

Data Set	Station Name	Latitude	Longitude
ODP Leg 105	Site 646	58° 50' 29.69" N	44° 27' 27.07" W
	Site 647	58° 41' 38.22" N	44° 24' 56.94" W
IODP Expedition 303/306	Site U1305C	58° 12' 33.48" N	48° 22' 08.76" W
DSDP Leg 12	Site 113	53° 19' 56.28" N	45° 16' 41.72" W
	Site 112	57° 28' 30.72" N	48° 32' 46.92" W
Chian et al.	88R2-A	59° 50' 26.88" N	52° 06' 11.88" W
	88R2-B	60° 03' 06.12" N	51° 17' 24.00" W
	88R2-C	60° 16' 36.12" N	50° 25' 23.88" W
	88R2-D	60° 26' 39.12" N	49° 47' 36.12" W
	88R2-E	60° 33' 05.76" N	49° 21' 05.04" W
	88R2-F	60° 39' 47.88" N	48° 55' 36.00" W
	99R1-A	56° 31' 10.63" N	56° 05' 10.32" W
	99R1-B	55° 49' 33.67" N	59° 04' 58.97" W
	99R1-C	56° 08' 42.97" N	57° 40' 05.34" W
	99R1-D	56° 14' 58.63" N	57° 15' 49.13" W
	99R1-G	56° 24' 45.00" N	56° 34' 03.25" W
	99R1-H	55° 55' 31.19" N	58° 36' 03.89" W
	99R1-I	57° 02' 32.21" N	53° 51' 00.47" W
	99R1-K	56° 50' 50.35" N	54° 42' 48.23" W
	99R1-M	56° 40' 03.90" N	55° 27' 09.72" W
	99R1-P	56° 19' 11.46" N	56° 57' 58.31" W
	99R1-Q	56° 03' 16.27" N	58° 04' 00.95" W
Delescluse *et al.*, Line 4	OBS1	56° 19' 11.46" N	56° 57' 58.31" W
	OBS2	56° 03' 16.27" N	58° 04' 00.95" W
	OBS3	58° 59' 58.72" N	51° 41' 39.67" W
	OBS4	58° 54' 42.54" N	51° 50' 12.52" W
	OBS5	58° 49' 38.24" N	52° 00' 08.13" W
	OBS7	58° 44' 33.03" N	52° 10' 01.94" W
	OBS8	58° 39' 22.56" N	52° 20' 01.03" W
	OBS9	58° 28' 39.98" N	52° 40' 28.17" W
	OBS10	58° 23' 25.60" N	52° 50' 21.64" W
	OBS11	58° 18' 10.17" N	53° 00' 12.02" W
	OBS12	58° 12' 54.63" N	53° 10' 58.81" W
	OBS13	58° 07' 42.08" N	53° 20' 36.48" W
	OBS14	58° 02' 26.97" N	53° 29' 13.35" W
	OBS15	57° 56' 55.75" N	53° 39' 15.78" W
	OBS16	57° 51' 42.39" N	53° 48' 11.88" W
	OBS17	57° 46' 32.41" N	53° 58' 32.37" W
	OBS18	57° 41' 20.93" N	54° 07' 14.43" W

Delescluse *et al.*, Line 5	OBS1	57° 35' 53.95" N	54° 17' 52.80" W
	OBS2	57° 30' 14.83" N	54° 26' 03.82" W
	OBS3	58° 22' 24.24" N	53° 08' 01.68" W
	OBS4	58° 17' 49.20" N	53° 00' 13.68" W
	OBS5	58° 13' 03.36" N	52° 52' 13.80" W
	OBS6	58° 08' 16.80" N	52° 44' 16.44" W
	OBS7	58° 03' 30.60" N	52° 36' 20.16" W
	OBS8	57° 58' 46.56" N	52° 29' 30.36" W
	OBS9	57° 54' 03.60" N	52° 21' 51.36" W
	OBS10	57° 49' 23.52" N	52° 13' 16.32" W
Richterhausen and Funck	V01S	57° 44' 44.52" N	52° 06' 45.96" W
	V02S	57° 40' 03.36" N	51° 58' 13.80" W
	V03S	59° 16' 39.11" N	54° 58' 47.92" W
	V05S	58° 51' 27.07" N	54° 12' 19.91" W
	V07s	57° 52' 45.48" N	54° 40' 17.80" W
	V09s	57° 59' 55.43" N	52° 52' 43.13" W
	V10s	56° 34' 30.22" N	50° 16' 27.80" W
	V12s	55° 52' 35.08" N	51° 15' 05.65" W
	V13s	56° 32' 23.32" N	49° 40' 11.32" W
	V141s	55° 24' 28.33" N	48° 53' 32.27" W
	V142s	54° 47' 59.06" N	47° 37' 15.42" W
	V151s	54° 47' 24.22" N	48° 11' 09.38" W
	V161s	55° 37' 09.70" N	46° 60' 35.66" W
	V162s	56° 15' 30.96" N	45° 12' 43.87" W
	V17S	58° 16' 25.32" N	43° 09' 06.70" W
Osler and Louden	R1-D	59° 04' 04.08" N	54° 10' 39.96" W
	R1-E	58° 47' 25.44" N	53° 49' 41.76" W
	R1-E SE	58° 29' 23.28" N	53° 25' 00.84" W
	R1E-SE	58° 29' 23.28" N	53° 25' 00.84" W
	F	58° 29' 23.28" N	53° 25' 00.84" W
	R1-G	58° 14' 11.40" N	53° 06' 47.04" W
	R1-G SE	58° 14' 11.40" N	53° 06' 47.04" W
	R1-H-NW	57° 58' 32.16" N	52° 47' 09.24" W
	R2-E-NE	58° 47' 11.04" N	53° 49' 39.96" W
	R2-E-SW	58° 47' 11.04" N	53° 49' 39.96" W
	R2-L-SW	59° 27' 45.00" N	52° 38' 06.72" W
	R2-M-NE	59° 07' 56.64" N	53° 12' 23.40" W
	R2-M-SW	59° 07' 56.64" N	53° 12' 23.40" W
	R2-N-SW	58° 54' 43.20" N	53° 36' 45.60" W
	R2-N-SW	58° 54' 43.20" N	53° 36' 45.60" W
	R2-O-NE	58° 39' 40.32" N	54° 02' 00.60" W
	R2-O-SW	58° 39' 40.32" N	54° 02' 00.60" W

| | R2-Q-NE | 58° 07' 33.96" N | 54° 56' 50.88" W |

11   Appendix 2: Samples used for velocity modelling

Data Set	Station Name	Depth Below Seafloor (km)	V (km/s)
ODP Leg 105	Hole 646B	0.216408	1.6497
		0.231648	1.6566
		0.246888	1.69
		0.262128	1.6797
		0.277368	1.7032
		0.292608	1.7028
		0.307848	1.6975
		0.323088	1.7295
		0.338328	1.7507
		0.353568	1.8372
		0.368808	1.8459
		0.384048	1.911
		0.399288	1.8875
		0.414528	1.9037
		0.429768	1.982
		0.445008	1.955
		0.460248	1.9775
		0.475488	2.0036
		0.490728	1.9523
		0.505968	1.9792
		0.521208	1.9723
		0.536448	1.9975
		0.551688	2.0034
		0.566928	2.0569
		0.582168	2.0794
		0.597408	2.0877
		0.612648	2.1277
		0.627888	2.0949
		0.643128	2.1203
		0.658368	2.1341
		0.673608	2.1251
		0.688848	2.1733
		0.704088	2.1518
		0.719328	2.1236
ODP Leg 105	Hole 647A	0.21621	1.55
		0.23573	1.58
		0.2639	1.64
		0.28313	1.594
		0.29125	1.662
		0.30048	1.666

Data Set	Station Name	Depth Below Seafloor (km)	V (km/s)
		0.31027	1.681
		0.3185	1.713
		0.33163	1.66
		0.34275	1.69
		0.35049	1.72
		0.35984	1.8
		0.36709	1.72
		0.38956	1.79
		0.39895	1.725
		0.40701	1.784
		0.4165	1.789
		0.4264	1.766
		0.43604	1.77
		0.44933	1.71
		0.45841	1.88
		0.46826	1.9
		0.47758	1.84
		0.49024	1.82
		0.60333	2.15
		0.60591	2.16
		0.60871	1.9
		0.61774	1.742
		0.62775	1.829
		0.63774	1.979
		0.64677	1.987
		0.65651	2.009
		0.68591	2.06
		0.69596	2
Delescluse *et al.*, Line 4	19 km	0.2485	1.8
		0.792	2.398
		1.6895	2.452
		2.292	2.552
	154.78 km	0.2845	1.89
		0.8	2.25
		1.4075	2.8
		1.783	2.8
		1.784	2.8
	182 km	0.273	1.825
		0.787	2.2505
		1.2585	2.45
		1.489	2.55
	213 km	0.2715	1.85
		0.7775	2.25

Data Set	Station Name	Depth Below Seafloor (km)	V (km/s)
		1.338	2.485
		1.664	2.62
	250 km	0.285	1.85
		0.8275	2.25
		1.545	2.45
		2.005	2.55
Delescluse *et al.*, Line 5	Station 1	0.319228662	1.89
		1.135107041	2.3
		1.909971905	2.44
		2.282820581	2.83
	Station 2	0.310360642	1.875
		1.172860642	2.3
		1.962387669	2.46
		2.280101047	2.85
	Station 3	0.323029561	1.875
		1.216610642	2.3
		1.735500372	2.4
	Station 4	0.342032939	1.875
		1.251154561	2.3
		1.76202375	2.4
	Station 5	0.348367399	1.875
		1.273029561	2.3
		1.791974426	2.4
	Station 8	0.323080236	1.875
		1.208891047	2.3
		1.724001128	2.42
	Station 9	0.327657818	1.865
		1.26009025	2.3
		1.818277669	2.43
	Station 10	0.335749155	1.875
		1.274262669	2.315
		1.824240628	2.43
Richterhausen and Funck[*]	NA	NA	
Chian *et al.*	90R1-A	1.67327	2.88
		1.4205	2.15
	90R1-I	3.1385	2.95
		1.059	2.15
	90R1-K	2.343	2.95
		1.136	2.075
	90R1-M	2.516	2.95
		1.31	2.15
	88R2-A	2.9155	2.95

Data Set	Station Name	Depth Below Seafloor (km)	V (km/s)
		0.939	2.4835
		1.3855	2.65
	88R2-B	1.8765	2.8
		0.7935	2.459
		1.325	2.65
	88R2-C	1.792	2.8
		0.749	2.4185
		1.351	2.65
	88R2-D	2.742	2.8
		0.598	2.388
		0.999	2.61
Osler and Louden	(averaged layer)	2.1005	2.8
		0.1557143	1.7
		0.6878948	1.85
		2.044	2.4
		2.236667	2.495
Hinz et al.	3_77	1.82	2.6
		0.61	1.91
		0.9	2.1
	5_77	1.86	3.52
		1.79	2.33
	6_77	2.59	2.55
		1.58	2.1
		2.19	2.77
	7_77	4.79	3.7
		1.72	2.27
	15_77	2.95	2.87
		3.45	2.76
	16_77	3.6	3.52
		1.52	2.26
		2.22	2.93
	19_77	3.68	3.87
		1.13	2.15
	22_77	2.84	2.53
		1.04	1.7
		1.62	2.38
	23_77	2.42	2.87
		0.77	1.81
	24_77	1.94	2.23
		0.68	2.16
		1	2.41
		2.54	2.55

12 Appendix 3: A platform independent tool for conversion between TWT and depth

On the following page is a listing of a computer software program written in JavaScript to perform time/depth conversion using the analytical and numerical methods described in Section 4.0 and 4.2 of this report. The program is embedded in hypertext markup language (HTML) so it can be used in a platform independent manner on any computer with a web browser.

To use the program, please do the following:

1. copy and paste the program listed below into a plain text file
2. save the file using the name of your choice and the extension .html (*e.g.* sohm_model.html)
3. open the .html file using a Java-enabled web browser such as Netscape or FireFox
4. type in the desired two-way time or depth in the appropriate input entry field and click the "calculate" button
5. the depth- or time-converted value will be displayed below the entry field

Note: If the .html file is on a network drive, its content maybe blocked by a security configuration. Copy the file to a local drive or change the security options to solve this problem. If you find that the software is still blocked, check your browser security setting to ensure execution JavaScript is enabled.
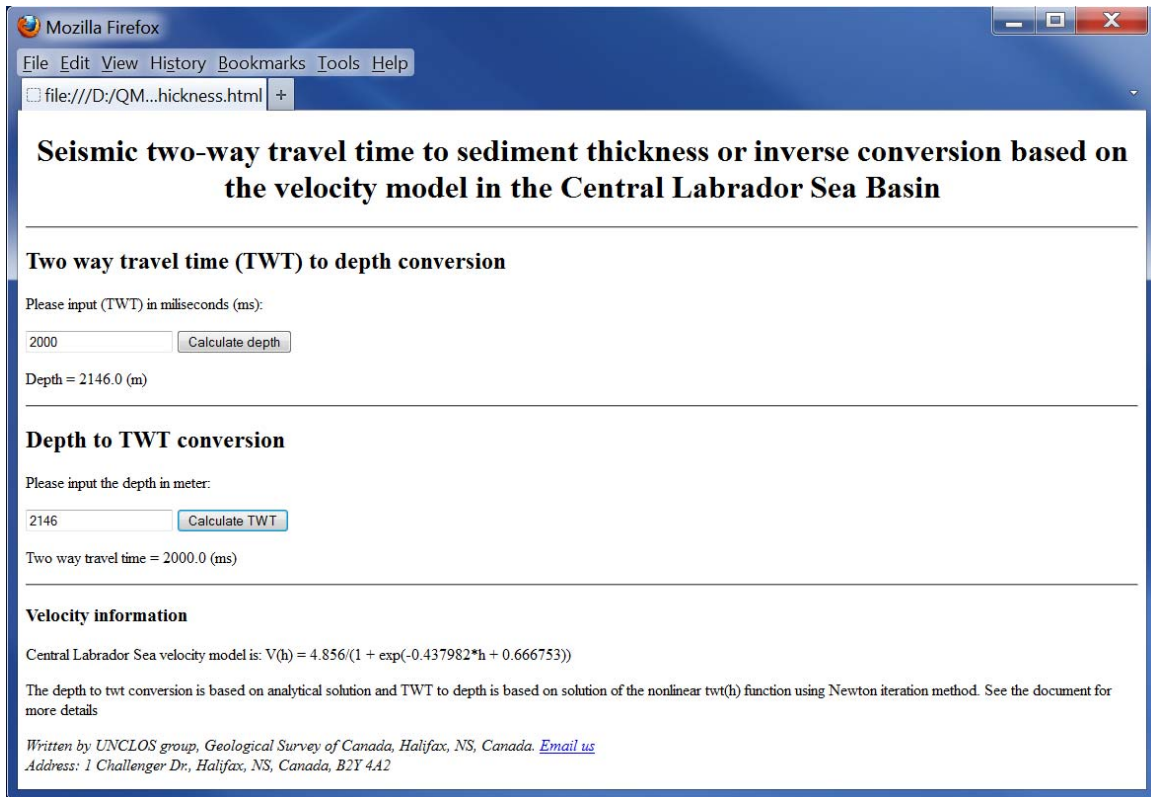
```
<!DOCTYPE html><html><body>
<h1><center>Seismic two-way travel time to sediment thickness or inverse
conversion based on the velocity model in the central Labrador Sea Basin
</center></h1><hr>
<h2>Two way travel time (TWT) to depth conversion</h2>
<p>Please input (TWT) in milliseconds (ms):</p>
<input id="TWT" type="text">
<script>
    //Sohm Plain velocity parameters
    var Vg = 4.856;    var V0 = 1.64727283409048; var Slope = -0.437981830803358;
var beta = 0.666753244321286;
    var htol  = 1E-5; var  maxNum = 100; //accuracy and maximum iteration control
parameters
 function CalculateDepth()
  {var TWT=document.getElementById("TWT").value;
  if(TWT==""||isNaN(TWT) || TWT < 0){alert("It is not an illegal two way travel
time ");} else
   {TWT =0.001*TWT; var  i = 1; var  inidep = 0.5*(Vg+V0)*0.5*TWT;  var  p =
inidep;
    while (i < maxNum){
    p = inidep - (inidep+ (Math.exp(Slope*inidep+beta)-Math.exp(beta)) / Slope -
0.5 * Vg * TWT)/(1+Math.exp(Slope*inidep+beta));
     if(Math.abs(inidep-p) <= htol)
      { break; } else{
      inidep =p;   i++; } }
     p = p * 1000; //change to meter
     x=document.getElementById("depth");
     x.innerHTML= "Depth = " + p.toFixed(1) + " (m) ";} }
 function depth2TWT()  //from depth to two way travel time
   { var depth = document.getElementById("depthB").value;
```

69

```
    if(depth == ""||isNaN(depth) || depth < 0)
        {alert("It is not an illegal depth value");}else{
    depth =0.001 * depth; var  TWT = (depth + (Math.exp(Slope * depth + beta)-
Math.exp(beta))/Slope)*2/Vg;
    TWT =TWT *1000; x=document.getElementById("TWTB");
    x.innerHTML= "Two way travel time = " + TWT.toFixed(1) + " (ms) ";}}
</script>
<button type="button" onclick="CalculateDepth()">Calculate depth</button>
<p id="depth"> Calculated depth will be put here.</p> <hr>
  <h2>Depth to TWT conversion</h2>
  <p>Please input the depth in meter:</p>
  <input id="depthB" type="text">
  <button type="button" onclick = "depth2TWT()"> Calculate TWT</button>
  <p id="TWTB"> Calculated TWT will be put here. </p> <hr>
 <h3>Velocity information</h3>
    <p>cCentral Labrador Sea velocity model is: V(h) = 4.856/(1 + exp(-0.437982*h
+ 0.666753))</p>
    <p>The depth to TWT conversion is based on analytical solution and TWT to
depth is based on solution of the nonlinear TWT(h)
        function using Newton iteration method. See the document for more details
</p>
    <address>Written by UNCLOS Group, Geological Survey of Canada, Halifax, NS,
Canada. <a href="mailto:qli@NRCan.gc.ca">Email us</a>
    <br> Address: 1 Challenger Dr., Halifax, NS, Canada, B2Y 4A2<br> </address>
 </body></html>
```

13   Appendix 4: Gardiner 1.0 user manual

13.1   Disclaim

The Gardiner software tool (version 1.0) is a revised of the version created by Natural Resources Canada for/during the United Nation Convention for the Law of the Sea (UNCLOS) Program. The tool is available at no cost from the author for personal and scientific use.

There is no guarantee that this tool work well for your data in your study area. Finding an independent way to evaluate the quality of results is important for the user's success. GSC Atlantic uses other independent procedures to assess the quality of the results.

This software tool is provided as is. The authors disclaim all warranties, expressed or implied, with regard to this software tool. In no event shall the author or the affiliate be liable for any indirect or consequential damage or any damages whatever from loss of use, data or profits, arising out of or in connection with the use or performance of the software tool.

13.2   Common information

13.2.1 MS .NET 4.0 Framework is required

Gardiner version 1.0 runs on 64-bit MS Windows system. It is a 64-bit .NET framework application and so requires MS .NET 4.0 to be installed. Microsoft Windows 7 usually has this framework as default installation or users can download MS .NET 4.0 Framework for no charge from the Microsoft web site.

13.2.2 Installation

To install the Gardiner, use setup.exe and follow its simple steps. Subfolders contain all required velocity models, demonstration files to help to use Gardiner 1.0.
Note: it is users' responsibility to install .NET 4.0 framework on the system.

13.3   Demo data

All supplied data in the dataSamples subfolder are virtual data which means it can only be used to demonstrate the program and to show how to prepare data for the application.

13.3.1 Data formats

All input data are in plain ascii text format but with different suffixes to minimize errors mistakes. Table 1 lists these suffixes. The (created) QLine files have a .txt suffix and can be imported into GeoFrame project like those with the .udf suffix.

For geographic location representation, latitude is positive in the northern hemisphere and negative in the southern sphere. The longitude can be [-180,180] or [0,180].

All distance is ellipsoid geodetic distance (Vincenty, 1975; Veness, 2012). Projection from spherical co-ordinates to plane co-ordinates is not necessary.

Table 1. File suffixes used in Gardiner

Suffix	Description	Sample File
udf	GeoFrame dumped horizon file. It can also be imported by GeoFrame in the same way. The QLine horizon dumped from Gardiner has .txt suffix and the same format with .udf file suffix	Demo_SedThickness_Geofrа meDumpedEDITED.udf
FOS	FOS file contains longitude, latitude, and name of identified foot of continental slope	FOS_Ran1.FOS
VelSample	Velocity sample file with velocity samples for velocity model construction	VelocitySamples.VelSample
ModPara	Velocity model parameter file used in the application for transformation between TWT and thickness velocity. Two types of (velocity) models are supported in version 0.9.5.0. For details	VelcityModels.ModPara

	see the following section and supplied samples (it is self-indicative)	
HTWT	The data prepared for H-TWT polynomial fitting	H_TWT_Samples.HTWT

13.3.2 udf file format

See the dialogs and sample dataset for dumping (from GeoFrame) .udf file (figs. 13.1 ~ 13.3). Note that TWT in the sediment thickness **(TWT)** udf file equals TWT of basement minus the TWT of seafloor, not the basement TWT.

The size of seafloor file and sediment thickness file must be the same and they must be in the same CDP order. Table 2 gives the column order of the udf file. The first two lines are comment and last line is a flag. They must be there and the program needs them when it create the QLine file.

Figure 13.1~3 and Table 2 list columns of this file format and how to dump them from GeoFrame.

Table 2. Field description used in .udf file

Field name	Column range	Comments
X	[1-16]	Projected coordinate, not used but it must be there
Y	[17,32]	Projected coordinate, not used but it must be there
Latitude	[122,137]	In degree, see the sample file for the format
Longitude	[140,155]	In degree, see the sample file for the format
Z	[39,47]	Seafloor, sediment, or QLine horizons (TWT) in ms
Seismic trace number	[66,71]	
Shot point Number	[49,57]	
CDP	[59,64]	
Amplitude	[73,86]	Not used, but it must be there

.

Figure 13.1 Control parameter definition in GeoFrame

User Defined Output Format

Format definition file

```
2d_ci7m_geocap3.iudf => 2D Card Image 7 multi-horizon expor
2d_ci7m_gf.ifdf => 2D Card Image 7 multi-horizon export (XY
2d_ci7m_latlonzspcdp.iudf => For Qingmou Li_UNCLOS_Lat_Long
2d_ci7m_latlonzspcdpsurvey.iudf => For Qingmou Li_UNCLOS_La
2d_ci7m_latlon_z.iudf => For Walli_Lat_Long_Z_
2d_ci7m_los1.iudf => UNCLOS bulk horizon Export-Import
```

Define Header Format

Profile information	Label	Card Num	Start Col	End Col
■ Profile Label	PROFILE	1	1	7
■ Profile Name		1	9	28
■ Profile Description		1	40	72
■ Type Label	TYPE	1	30	33
■ Profile Type		1	35	35
■ Posting Color		1	37	38
☐ Contact Symbol		0	0	0
☐ Line Label		0	0	0
☐ Line name (2D)		0	0	0
☐ InLine (3D)		0	0	0
☐ Line Type		0	0	0
☐ Survey Name		0	0	0
■ Snapping label	SNAPPING PARAMETERS	2	1	19
■ Snap position		2	21	21
■ Snap window		2	23	27
■ Event picked		2	29	29
■ Format file name		1	74	96
■ X/Y units		1	98	99
■ Z units		1	101	102

Reset   OK   Cancel

Figure 13.2 Definition of header information in a udf file

74

User Defined Output Format

Format definition file

```
2d_ci7m_geocap3.iudf => 2D Card Image 7 multi-horizon expor
2d_ci7m_gf.ifdf => 2D Card Image 7 multi-horizon export (XY
2d_ci7m_latlonzspcdp.iudf => For Qingmou Li_UNCLOS_Lat_Long
2d_ci7m_latlonzspcdpsurvey.iudf => For Qingmou Li_UNCLOS_La
2d_ci7m_latlon_z.iudf => For Walli_Lat_Long_Z_
2d_ci7m_los1.iudf => UNCLOS bulk horizon Export-Import
2d_ci7m_patch_gf.ifdf => 2D Card Image 7 multi-patch export
2d_ci7m_xyz1.iudf => x-y: UTM21_WGS84  z:TWT in msec
```

Format file name

2d_ci7m_los1.iudf

Define Data Format

Data Item	Units	Start Col	End Col	Data type	Decimal
■ X Coordinate	Meter	1	16	Exponent	8
■ Y Coordinate	Meter	17	32	Exponent	8
■ Latitude		122	137	Degree	7
■ Longitude		140	155	Degree	7
■ Z Coordinate (Time/Depth)	Msec	39	47	Float	2
■ Seismic Trace Number		66	71	Integer	0
■ Shot Point Number		49	57	Float	2
■ CDP		59	64	Integer	0
■ Amplitude		73	86	Exponent	7
⊔ Other Attribute 1		0	0	Exponent	0
⊔ Other Attribute 2		0	0	Exponent	0
⊔ Other Attribute 3		0	0	Exponent	0

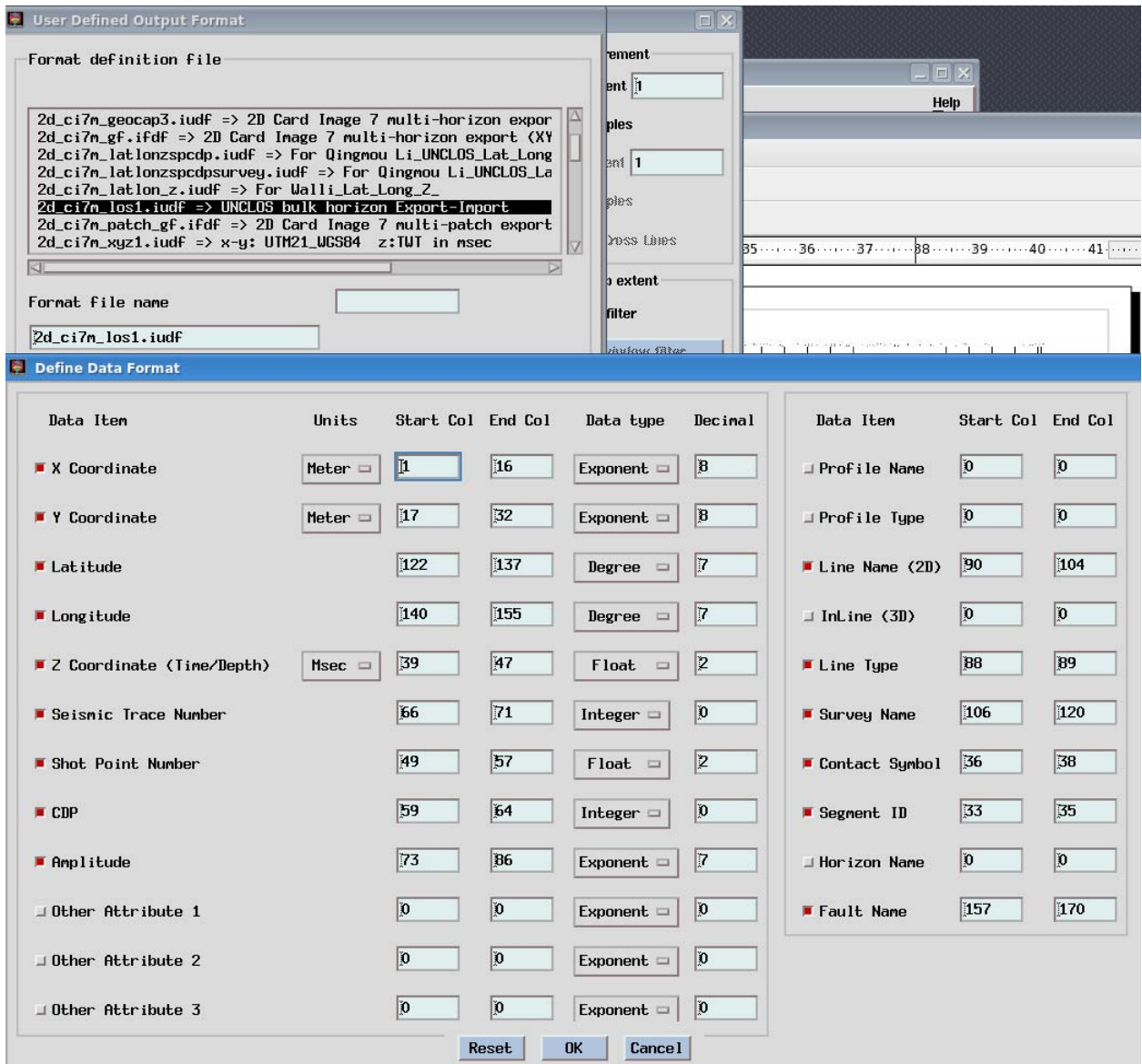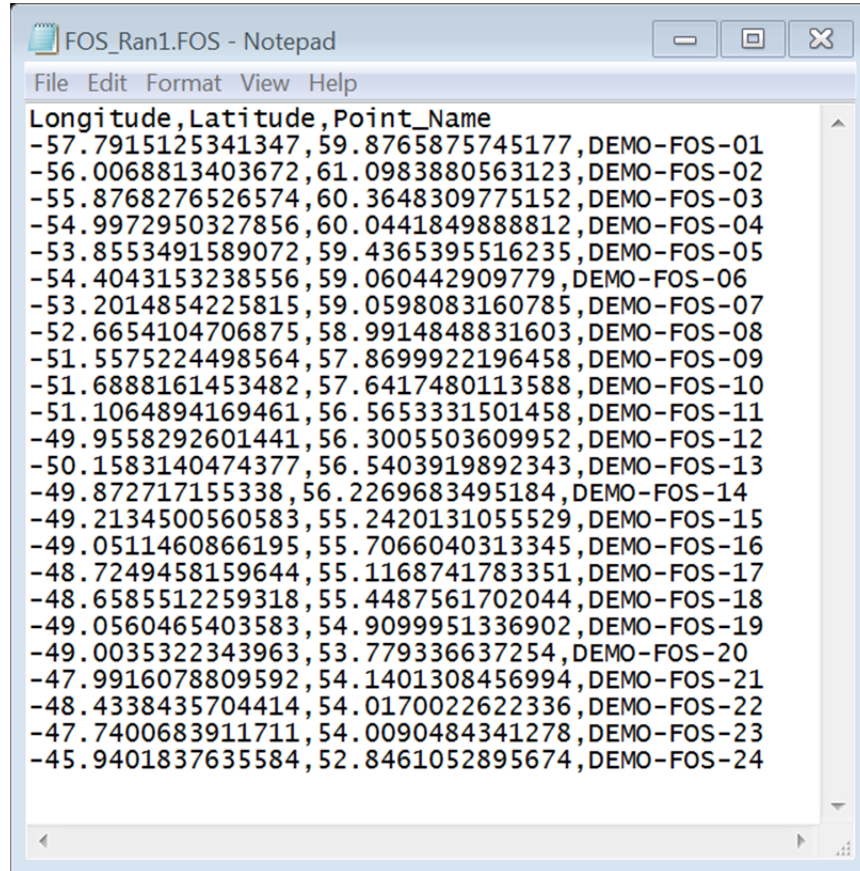| Data Item	Start Col	End Col
⊔ Profile Name	0	0
⊔ Profile Type	0	0
■ Line Name (2D)	90	104
⊔ InLine (3D)	0	0
■ Line Type	88	89
■ Survey Name	106	120
■ Contact Symbol	36	38
■ Segment ID	33	35
⊔ Horizon Name	0	0
■ Fault Name	157	170

Reset   OK   Cancel

Figure 13.3 Definition of field column in a udf file

75

13.3.3 FOS data format

The first line is the head name row (see Figure 13.4). The second line and those thereafter list each FOS with its longitude, latitude, and name. The Three columns must be delimited with commas.
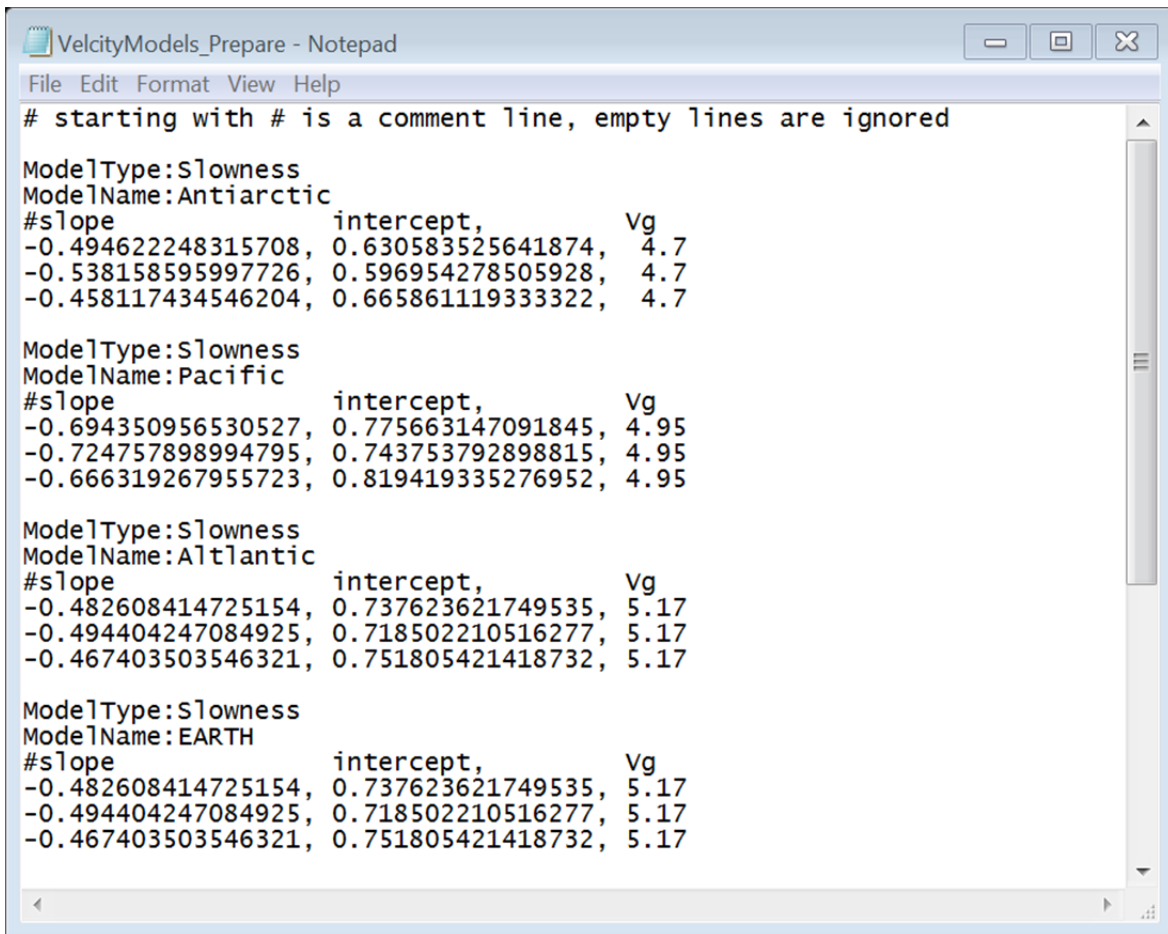
```
FOS_Ran1.FOS - Notepad
File  Edit  Format  View  Help
Longitude,Latitude,Point_Name
-57.7915125341347,59.8765875745177,DEMO-FOS-01
-56.0068813403672,61.0983880563123,DEMO-FOS-02
-55.8768276526574,60.3648309775152,DEMO-FOS-03
-54.9972950327856,60.0441849888812,DEMO-FOS-04
-53.8553491589072,59.4365395516235,DEMO-FOS-05
-54.4043153238556,59.060442909779,DEMO-FOS-06
-53.2014854225815,59.0598083160785,DEMO-FOS-07
-52.6654104706875,58.9914848831603,DEMO-FOS-08
-51.5575224498564,57.8699922196458,DEMO-FOS-09
-51.6888161453482,57.6417480113588,DEMO-FOS-10
-51.1064894169461,56.5653331501458,DEMO-FOS-11
-49.9558292601441,56.3005503609952,DEMO-FOS-12
-50.1583140474377,56.5403919892343,DEMO-FOS-13
-49.872717155338,56.2269683495184,DEMO-FOS-14
-49.2134500560583,55.2420131055529,DEMO-FOS-15
-49.0511460866195,55.7066040313345,DEMO-FOS-16
-48.7249458159644,55.1168741783351,DEMO-FOS-17
-48.6585512259318,55.4487561702044,DEMO-FOS-18
-49.0560465403583,54.9099951336902,DEMO-FOS-19
-49.0035322343963,53.779336637254,DEMO-FOS-20
-47.9916078809592,54.1401308456994,DEMO-FOS-21
-48.4338435704414,54.0170022622336,DEMO-FOS-22
-47.7400683911711,54.0090484341278,DEMO-FOS-23
-45.9401837635584,52.8461052895674,DEMO-FOS-24
```

Figure 13.4 Example of FOS file format

13.3.4 Model Parameter file format

Many functions such as calculating sediment thickness statistics, evaluate the significance of FOS, visualizing Gardiner point, and analyzing uncertainty in the Gardiner tool require a velocity model to transform between TWT (ms) and sediment thickness (metre). In the current version (1.0), a simple data format is developed to store velocity models to make it can work in arbitrary regions of different velocity models. Users can construct, prepare a velocity module file to load it at the start of the application or reload velocity models in a different file at anytime of the application.
As many as required velocity models can be defined in one velocity file. It is a plain text file and an xample is shown in Figure 13.5.


```
VelcityModels_Prepare - Notepad
File  Edit  Format  View  Help
# starting with # is a comment line, empty lines are ignored

ModelType:Slowness
ModelName:Antiarctic
#slope                intercept,           Vg
-0.494622248315708,  0.630583525641874,   4.7
-0.538158595997726,  0.596954278505928,   4.7
-0.458117434546204,  0.665861119333322,   4.7

ModelType:Slowness
ModelName:Pacific
#slope                intercept,           Vg
-0.694350956530527,  0.775663147091845,  4.95
-0.724757898994795,  0.743753792898815,  4.95
-0.666319267955723,  0.819419335276952,  4.95

ModelType:Slowness
ModelName:Altlantic
#slope                intercept,           Vg
-0.482608414725154,  0.737623621749535,  5.17
-0.494404247084925,  0.718502210516277,  5.17
-0.467403503546321,  0.751805421418732,  5.17

ModelType:Slowness
ModelName:EARTH
#slope                intercept,           Vg
-0.482608414725154,  0.737623621749535,  5.17
-0.494404247084925,  0.718502210516277,  5.17
-0.467403503546321,  0.751805421418732,  5.17
```

Figure 13.5 Format of velocity model file

An unlimited number of models can be defined. Every model begins with two lines to describe the model type and the model name. The current version supports velocity types of "slowness" and "polynomial", one of which must be used. The model name is defined by the user.

Empty lines and those starting with "#", are ignored. This allows you to add adequate explanatory notes on your velocity model file (see Figure 13.5)

NOTE: The polynomial models, the polynomial coefficients is used in the conversion between TWT and sediment thickness One polynomial coefficients for conversion from TWT to thickness or vice versa must be stored in one line as illustrated in Figure 13.6. The Gardiner (version 1.0) only supports one file in which users can put arbitrary number velocity models as they required. But users can also prepare many velocity model files and they can load them anytime. It is also important that there is only one velocity file available at certain time. The older one will be cleared after loading the new velocity model file.

```
VelcityModels_Prepare - Notepad
File  Edit  Format  View  Help

ModelType:POLYNOMIAL
ModelName:SUN
# H= a(1)*T+a(2)*T*T+ ...
#a(1) a(2), a(3), ...
0.93225911407069,   -0.109320436489879,   0.0140435927848553
0.984804950546097,  -0.0951837824312761,  0.0153828637490604
0.888029379818056,  -0.126100904777059,   0.0129451155652323

# TWT = b(1)*H + b(2)*H*H + b(3)* H*H*H + ...
#b(1) b(2), b(3), ...
1.73976197154162,   -0.112156521259867,   0.00281987593464223
1.75201525188136,   -0.107831018131895,   0.00316373227246018
1.72740674810697,   -0.116360591441583,   0.00245433461297177
```

Figure 13.6 Polynomial (velocity) model

13.3.5 Velocity sample file format

Preprocessed velocity samples are stored in a plain text file with suffix VelSample. The first line is the column name; the other lines are data (Figure 13.7).

```
VelocitySamples.Vel...
File  Edit  Format  View  Help
Depth(km),Vel(km/s)
0.044,1.625
0.19,1.708
0.373,1.832
0.589,1.925
0.912,2.17
1.249,2.42
1.711,2.524
2.317,2.86
3.154,3.05
4.802,3.25
6.458,3.575
7.675,4.25
0.204,1.725
0.71,1.83
```

Figure 13.7 Velocity sample file

13.3.6 H-TWT file format

This file has an .hTWT suffix and it is used in constructing the relationship between H(TWT) and TWT(H) function. Figure 13.8. shows an example file.
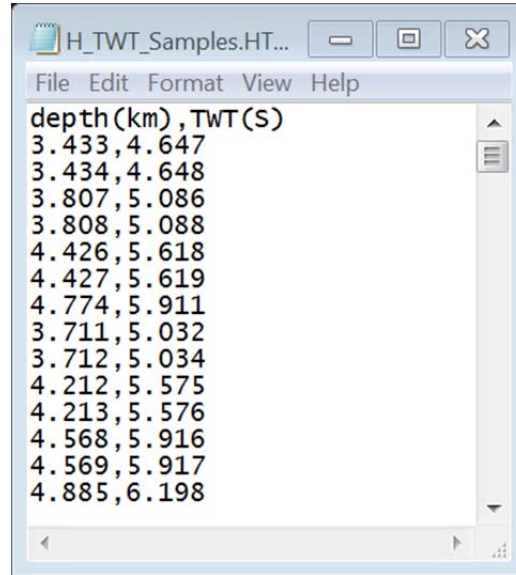


```
H_TWT_Samples.HT...
File  Edit  Format  View  Help
depth(km),TWT(S)
3.433,4.647
3.434,4.648
3.807,5.086
3.808,5.088
4.426,5.618
4.427,5.619
4.774,5.911
3.711,5.032
3.712,5.034
4.212,5.575
4.213,5.576
4.568,5.916
4.569,5.917
4.885,6.198
```

Figure 13.8 H-TWT file format

13.4   Task-oriented Tutorials

The Gardiner tool is easier to set-up and use, while following the step-by-step tutorials

13.4.1 Installation

Users can use setup.exe and follow its hints to install the application. Or, an easy way to do it is to copy the complete folder with its subfolders to your local drive. Open the bin subfolder and double click Gardiner.exe ( ) to start the program. The default velocity models (VelcityModels.ModPara) are loaded automatically into sub folder /dataSamples.

If you want to execute the program from another location, such as your desktop, create a shortcut toGardiner.exe, drag the shortcut to that location, and double click on the short cut, to run the program.

If you received the files by email, please note that the suffixes were changed to prevent the files being blocked from possible firewall. In this situation, change the suffixes of files Gardiner.exZ, CW64.dlZ, and ZedGraph.dlZ to Gardiner.exe, CW64.dll, and ZedGraph.dll while ensuring the files remain in the same folder.

13.4.2 Construct (slowness) velocity model

1) Prepare velocity samples, including resampling and smoothing on your own, and save them in the format as described in the velocity sample file format with suffix "velSample".
2) With the ready-to-use velocity samples, estimate Vg, bootstrapping number.
3) Construct a velocity model, estimate its uncertainty, get parameters for conversion between TWT and sediment thickness.

13.4.2.1   Vg (matrix velocity) estimation

1. As shown in Figure 13.9, select "Matrix Velocity Estimation".
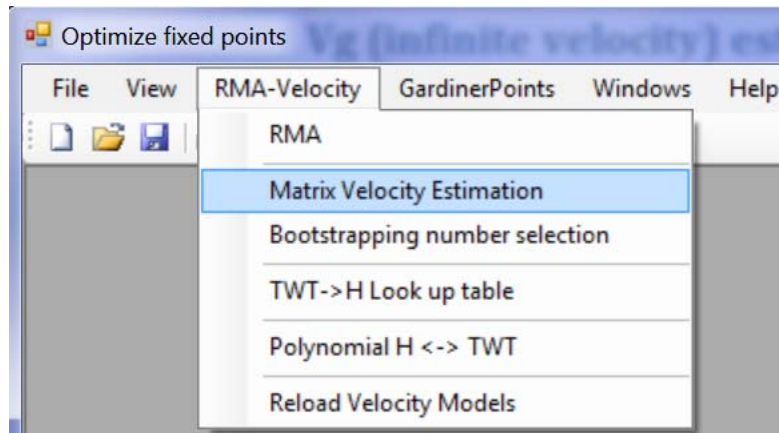
Figure 13.9 RMA-Velocity menu

2. Dialog box "Vg Selection for RMA" (Fig. 13.10) will appear. Click the button **"Select a velocity sample file"** and the Vg range text box will appear. In the Vg range box, three parameters are separated by a vertical line (|). They are the starting, ending, and increment of Vg for looping Vg, to get maximum correlation coefficients. The starting Vg must be greater than the maximum velocity value of your velocity sample file. This maximum velocity value is provided just above the "Select a velocity sample file" button. Usually, the automatically assigned Vg range can be used.
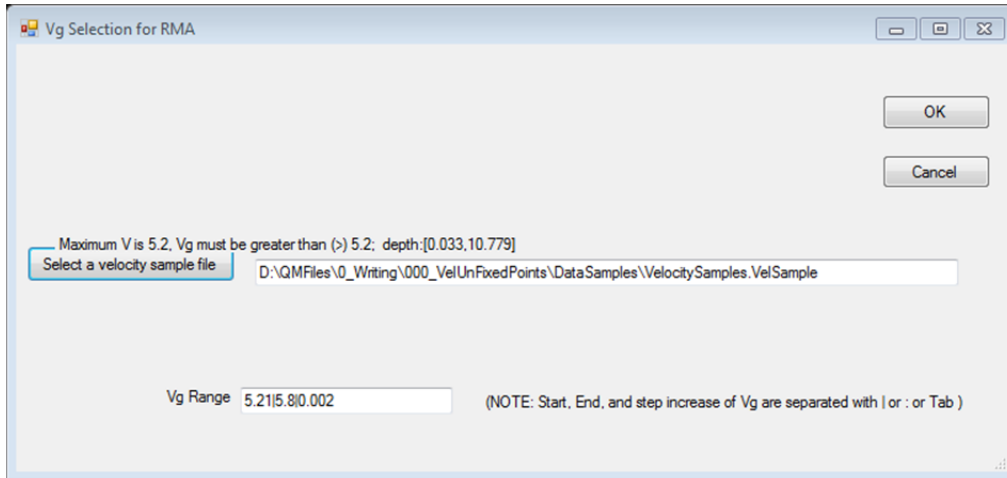
3. Click "OK.

Figure 13.10 Vg Selection for RMA dialog box

4. When a chart window pops up (Figure 13.11), right click on the chart to activate a drop-down menu and select "show point values".

5. However, the cursor over the peak of the red line. The numerical value that appears is the best Vg value at maximum R.
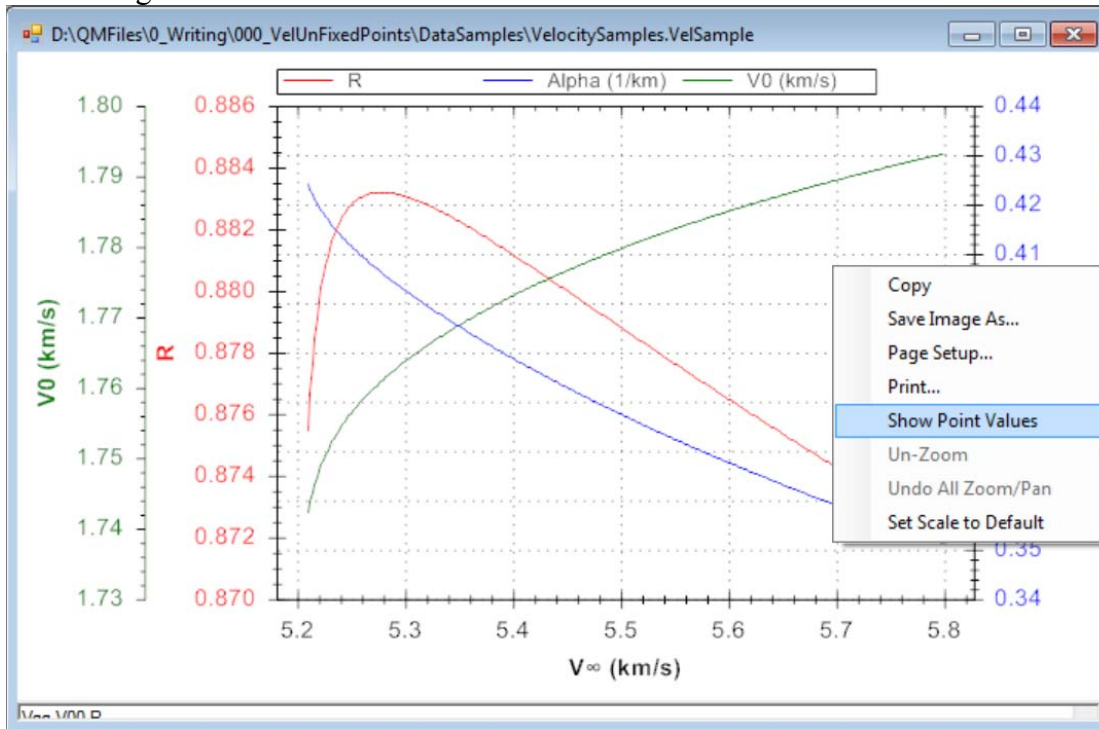

Figure 13.11 Selection of best Vg value

13.4.2.2   Optimal bootstrapping number estimation

To select the suitable bootstrapping number for the modeling, loop a series of bootstrapping number to see the variations of parameters.

1) Input several bootstrapping numbers, delimited with a comma, in the text box (Fig. 13.12). The order must be increasing, but the increment can be irregular.

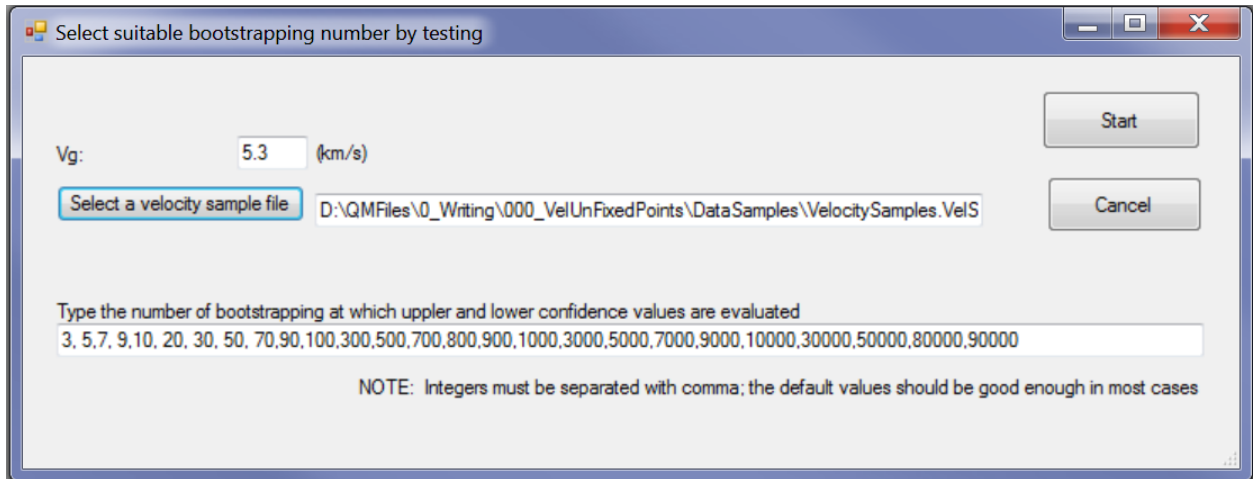2) All numbers will be looped and plotted with sample data file as shown in Figure 13.12

Figure 13.12 Bootstrapping number selection

3) From this resulting plot (Fig. 13.13), 10^4 looks to be an adequate bootstrapping number for this velocity sample dataset
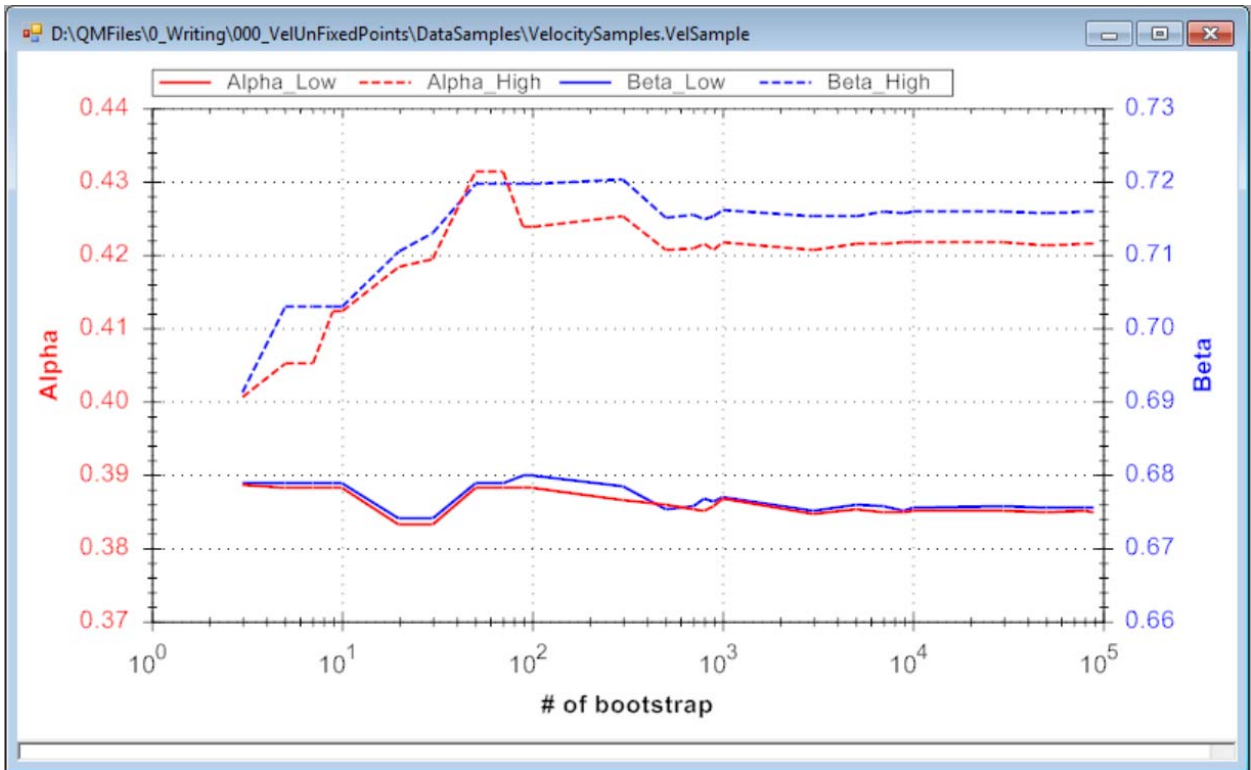
Figure 13.13 Parameter (confidence) bounds and bootstrapping number plot

.

13.4.2.3   Create slowness model

With the Vg and bootstrapping work in hand, the (slowness) velocity model can be constructed.

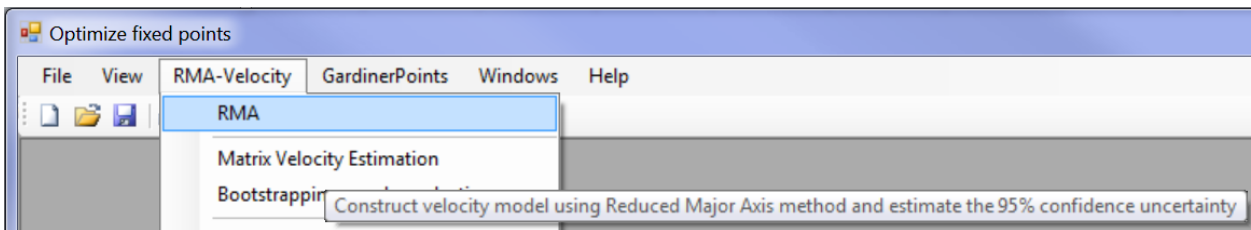1. Select "RMA" from the drop-down menu under "RMA_Velocity" (Fig. 13.14) to start RMA slowness modeling.

Figure 13.14 RMA menu for slowness modeling

2. In the resulting dialog box (Fig. 13.15), insert the values for "Vg", "# of bootstrap), and "Maximum Depth" (for the range of thickness evaluation). The "# of domains for velocity sample distribution in depth" field is used to chart the velocity depth distribution; the default value should be adequate. The default value for "# of domains for residual velocity histogram" is generally suitable
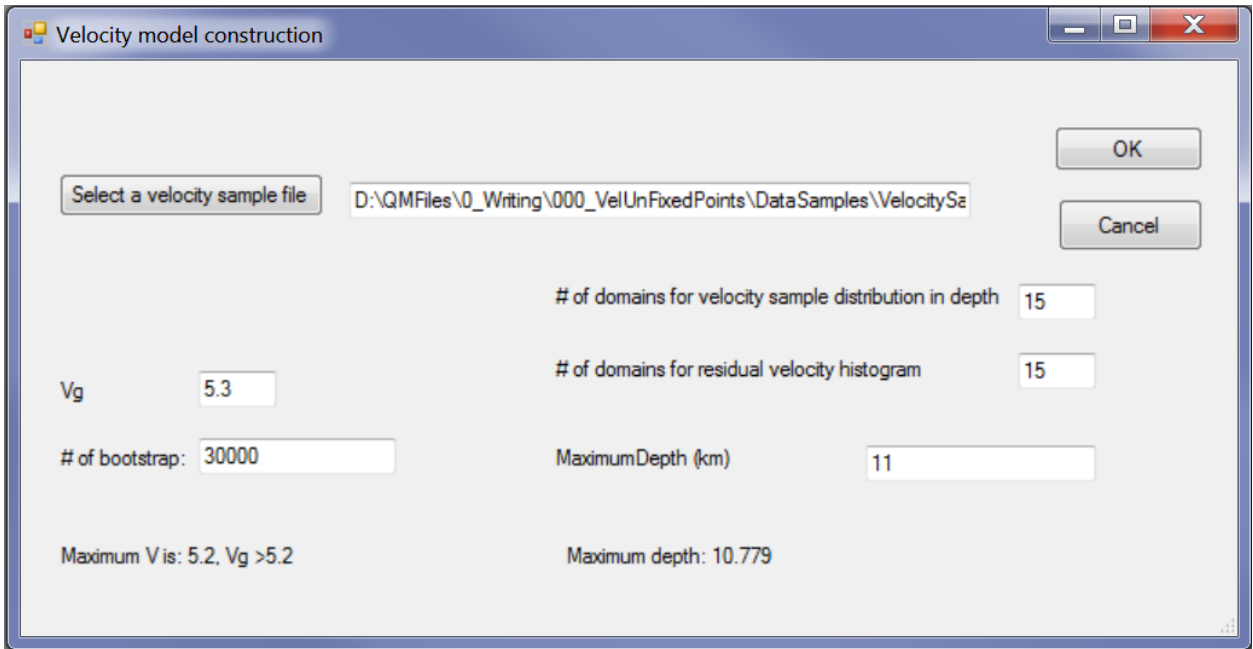
Figure 13.15 RMA velocity modeling dialog and parameters

3. Click "OK" (13.15) to generate the RMA results (Fig. 13.16 . Each child window contains a report area at the bottom edge. Drag the boundary to zoom in. Right click the mouse to copy or save.
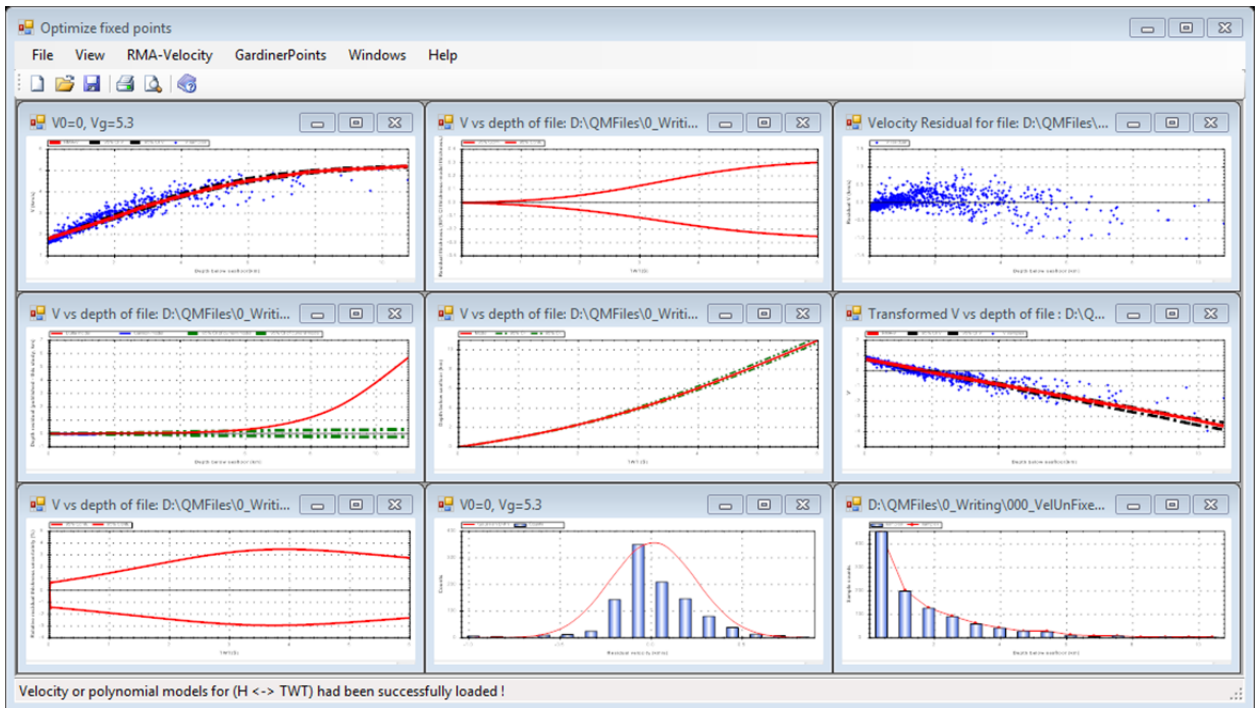

Figure 13.16 RMA results

13.4.3 Construct a polynomial velocity model

It is often used to fit a polynomial function between TWT and sediment thickness from observed TWT and depth pairs. In the polynomial function relationship, it should be constrained that at the starting time (TWT=0), the depth should be zero also (H=0), and vice versa. This means that the intercept of polynomial must be zero with following equation:

$$H(TWT) = \sum_{k=1}^{n} a^k \, (TWT)^k$$

And similarly:

$$TWT(H) = \sum_{k=1}^{n} b^k \, H^k$$

We limit the polynomial order n in the two previous within $[1,10]$ for the dataset will be over fitted with higher n and that has no significance. Select "Polynomial-H<->TWT" from the "RMA-Velocity" drop-down menu (Fig. 13. 17). The parameter dialog box will appear (Fig. 13.18).
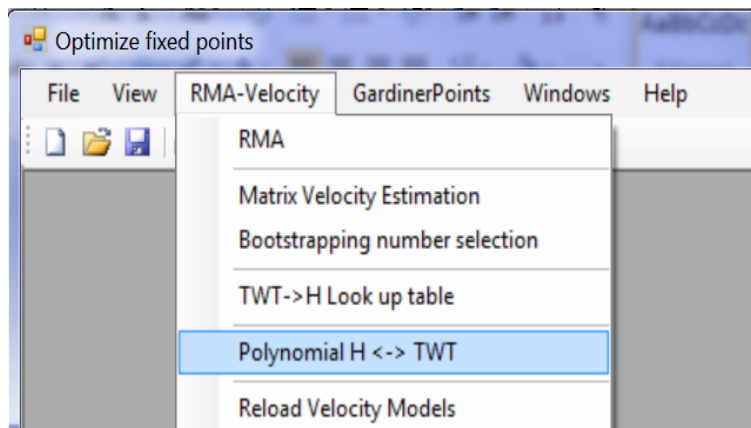

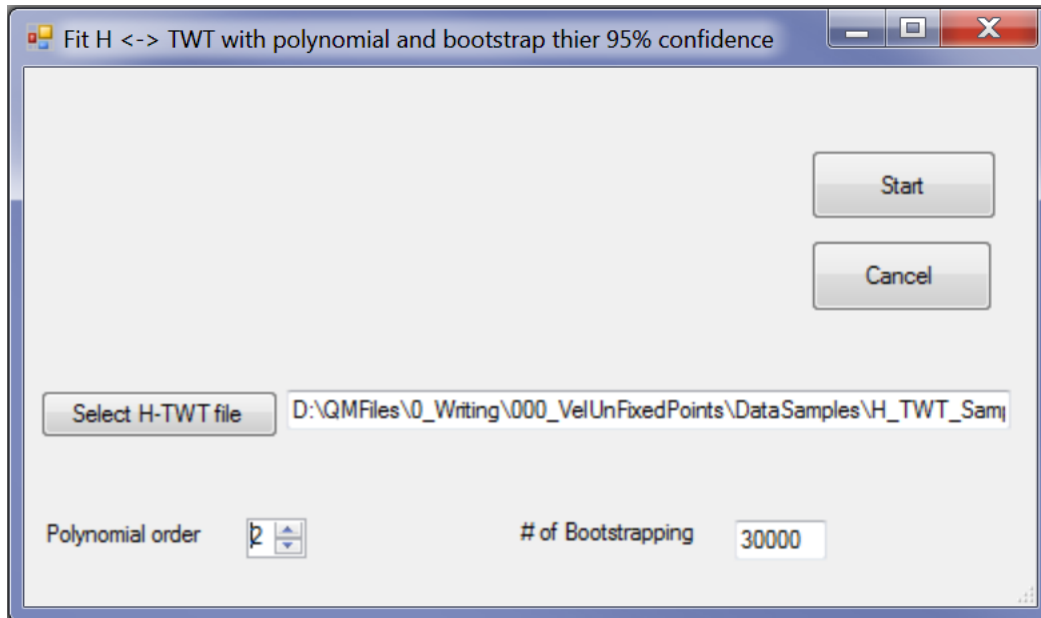Figure 13.17 Fit a polynomial function

Figure 13.18 Parameter dialog box for polynomial fitting of H-TWT and bootstrapping

You must select an H-TWT file (Fig, 13.18). An H-TWT file example is given in the sample data folder. The "Polynomial order" can be input in the text or tuned using the arrows.. The value in "# of bootstrapping" is used to create confidence interval.

Click "Start" to obtain both H(TWT) and TWT(h) charts with reports at the bottom of each chart (Fig, 13.19). Copy the coefficients from these reports and directly paste into the velocity model file.

There are 3 functions for both the H(TWT) and TWT(H) functions because they are required for uncertainty analysis.

Because of the over fitting or other facts in the polynomial model construction, the test by the principal author demonstrated that most of confidence estimation by bootstrapping for polynomial fitting is not stable and it could not give reasonable results.
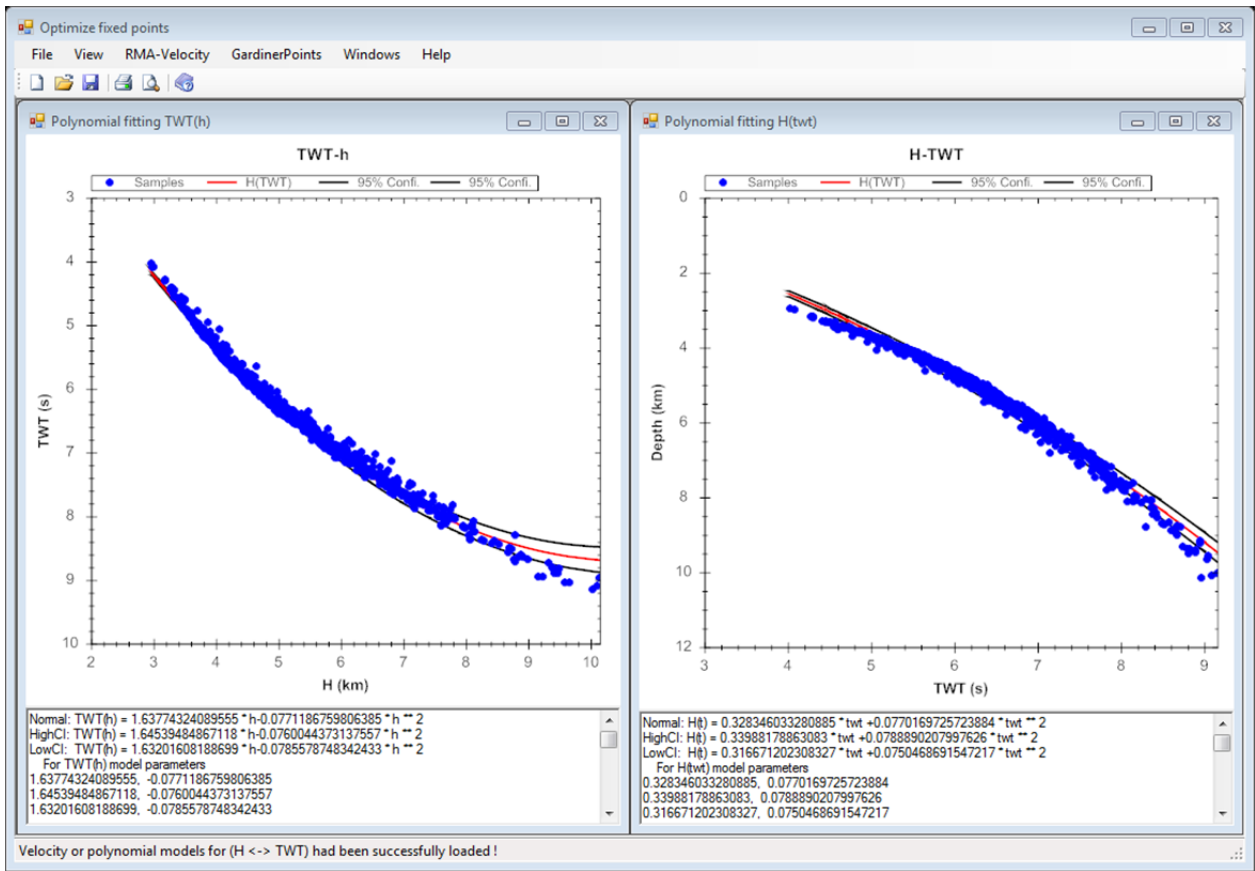
Figure 13.19 Polynomial fitting of H(TWT) and TWT(h)

13.4.4 Create a TWT-H look up table

Sometimes, a look-up table is useful to manually check results. To obtain a look-up table for the selected velocity model:

1. S"TWT_>H Loop up table" from the RMA-Velocity" drop-down menu (Figure 13.20) and then select known velocity model (slowness or polynomial).
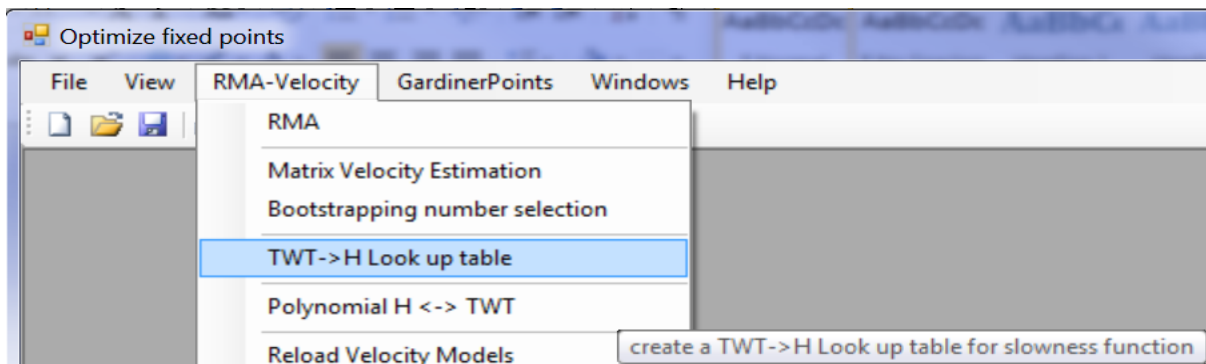

Figure 13.20 Menu selection for look-up table creation

2. In the resulting dialog box (Figure.13-21), insert values for "Start TWT", "Maximum TWT" or "TWT step".

3. Right click on the text box and save the look-up table to report usage. You can create as many look-up tables as you require.
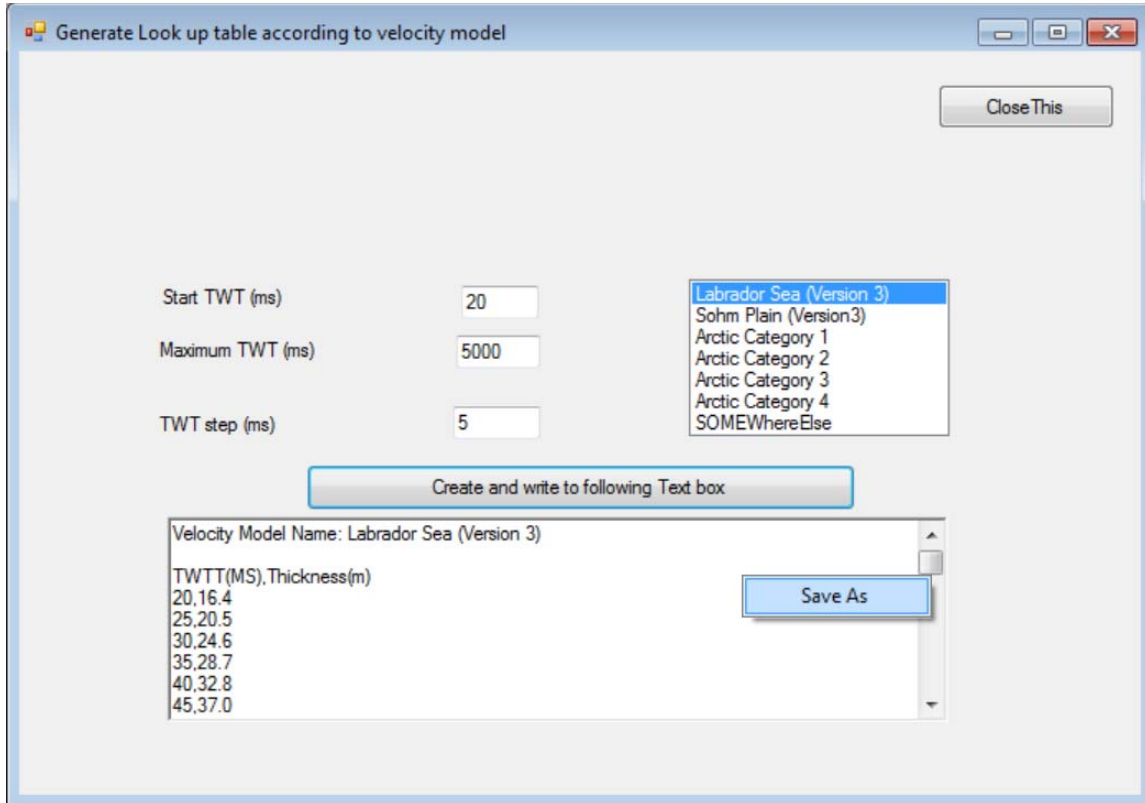

Figure 13.21 Dialog box to create look-up table

13.4.5 Prepare a velocity model file

The velocity model file is used to convert sediment thickness TWT in millisecond to sediment thickness in metres. The sample of file format is shown in VelocityModels.ModPara. The file is self-documented.

For every velocity model in the model file, there are really 3 models: the maximum likelihood velocity model; and two velocity confidence limits. We do not clarify which is which of the lower and higher confidence, but their absolute difference value are used for confidence range analysis.

A predefined velocity model file is attached as a template. The user must create their velocity model file.

When the Gardiner application/tool? Is initiated, a default velocity model file "VelcityModels.ModPara" is loaded automatically. At any time, a user can load his/her

velocity model file to use immediately. The reloading menu is shown in Figure 13.22 and the reloading dialog is shown in Figure13.23.
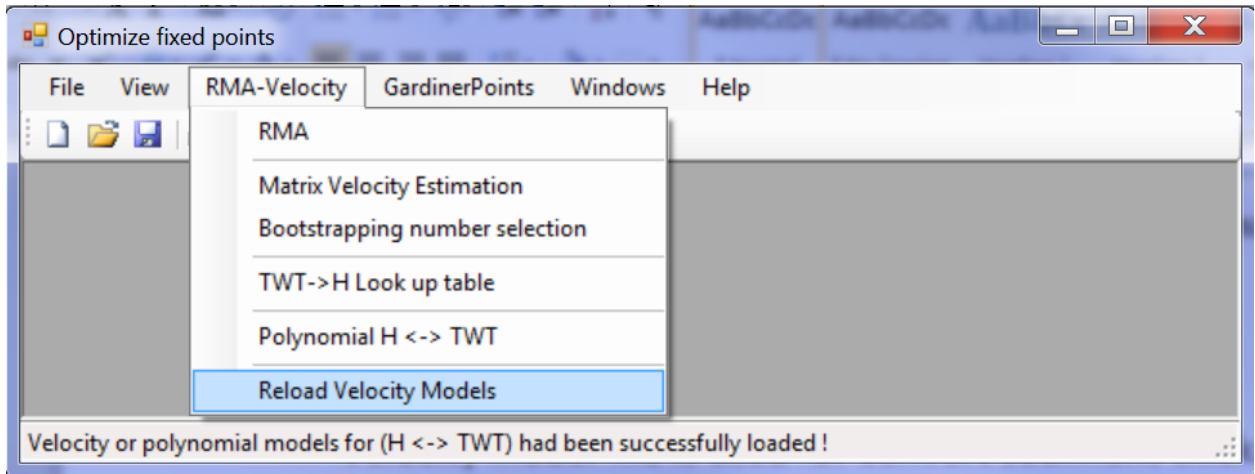
Figure 13.22 Reloading velocity models
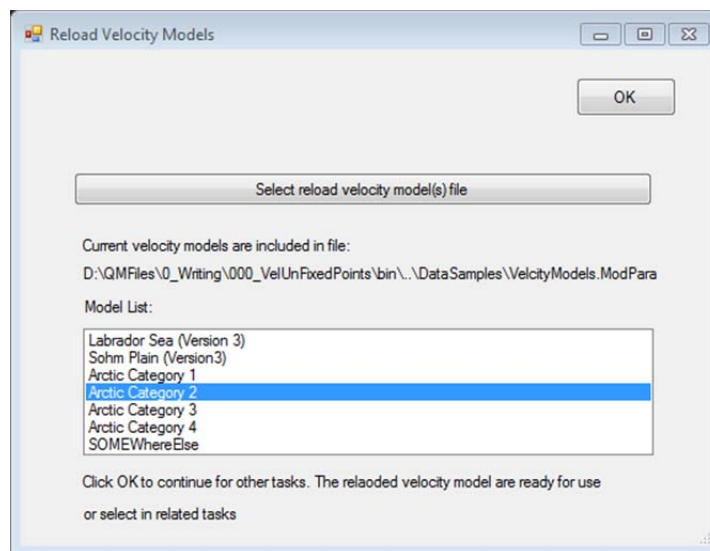
Figure 13.23 Reloading velocity dialog

Select a velocity model file to reload it; the reloaded models will be displayed immediately. Click "OK" to continue.

An easy way to do it automatically is to replace the "VelcityModels.ModPara" that was supplied, when you start the Gardiner application.

13.4.6 Significance of FOS

Evaluating the significance or contribution and non-contribution (where it is used to identify if a CDP is not a Gardiner point candidate) of FOS points is helpful to select and

adjust FOS points (such as increasing points around critical FOS points and focus on only the significant FOS points).

 From the "Gardiner Points" drop-down menu (Figure13.24), select "FOS significance evaluation" and a dialog will appear as shown in Figure 13.25.

The contribution of every FOS can be identified from Figure13.26. It is easy to delete FOS points without contribution to the fixed point or add FOS points near the high contribution points.
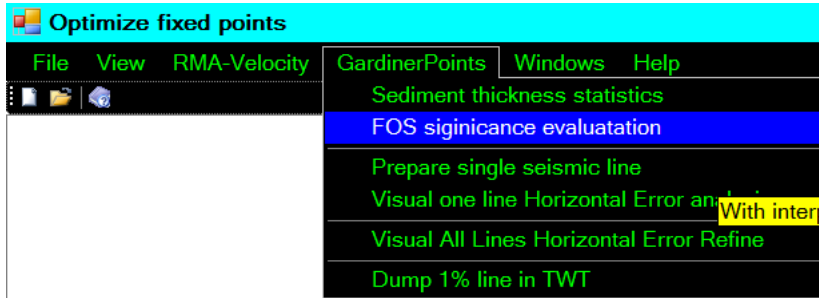
Figure 13.24 FOS significance evaluation
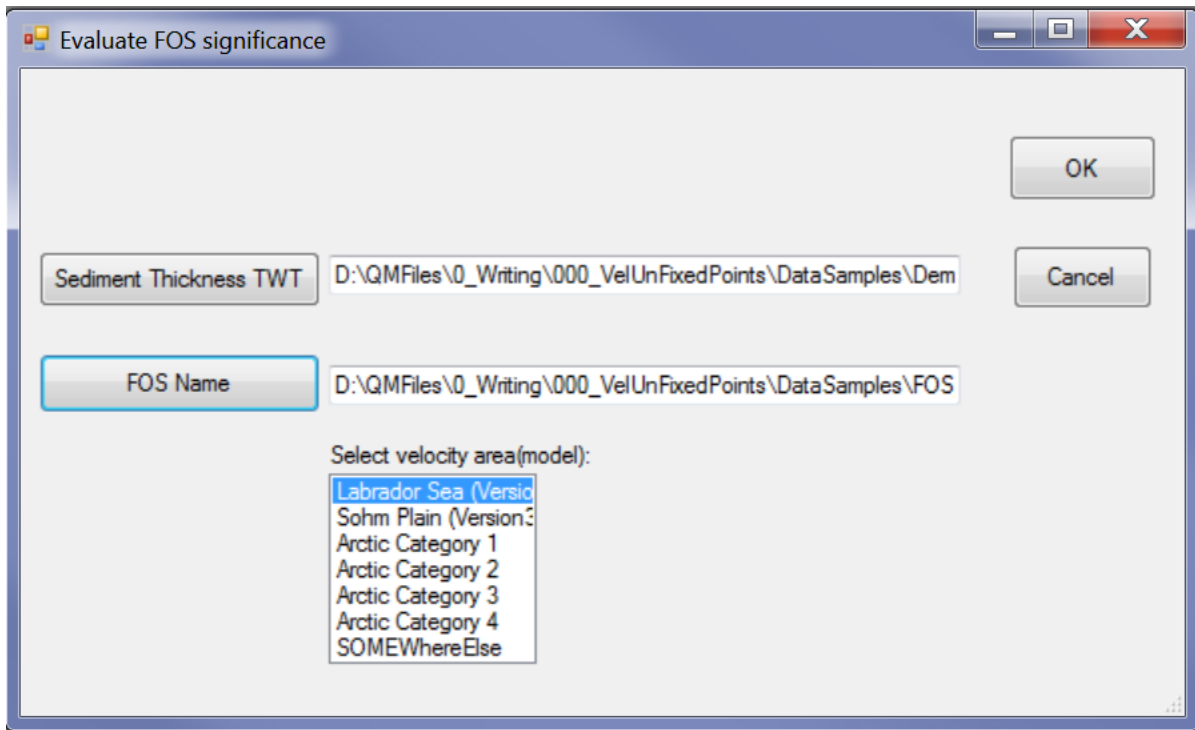
Figure. 13.25 The evaluate FOS Significance dialog box
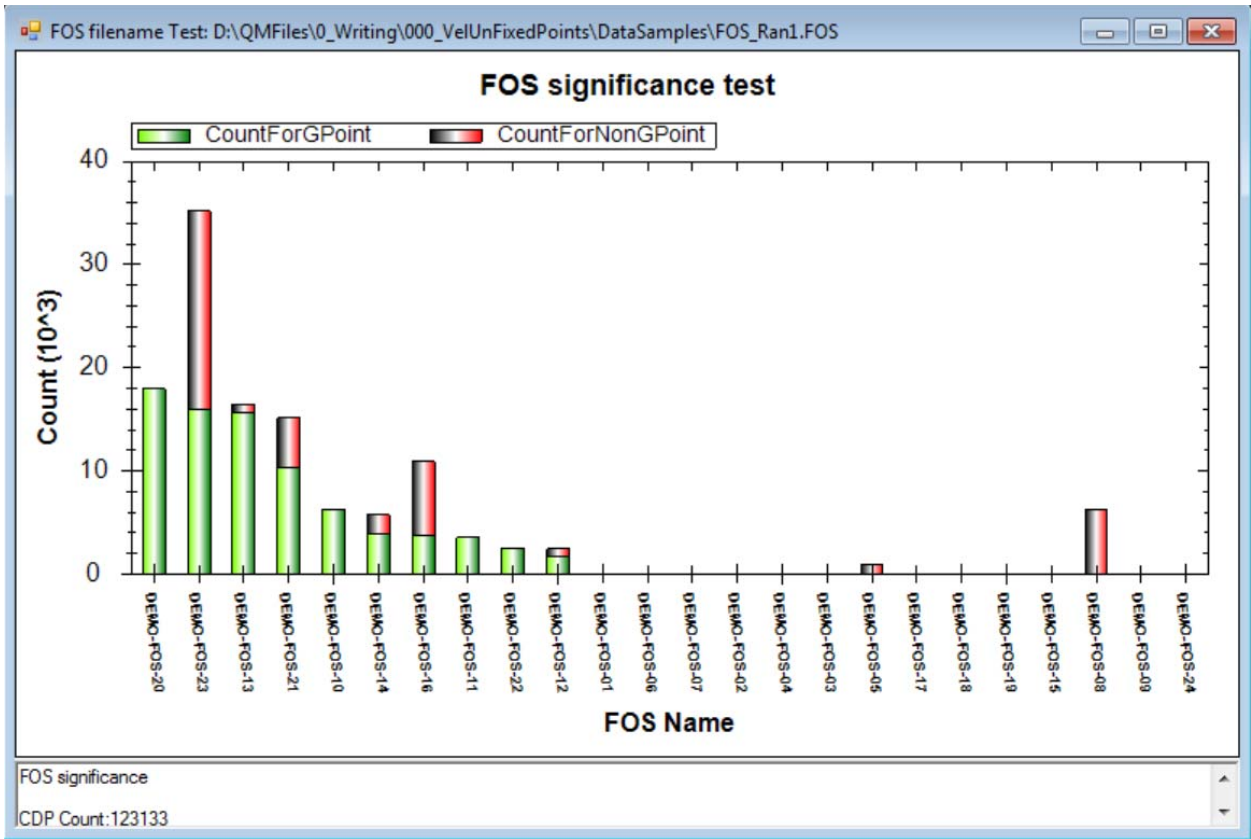
Figure 13.26 FOS significance evaluation results

13.4.7 Distribution of Thickness

The statistical features (mean, standard deviation, etc) and frequency distribution of sedmentary thickness in TWT (milliseconds) and metres (based on a velocity model) are useful to understand many sedimentation features.. Following the steps listed in figures, 13.27 and 13.28, the user can obtain the statistical and distributional information of sediment thickness. The distribution of thickness is shown in Figure13.29.
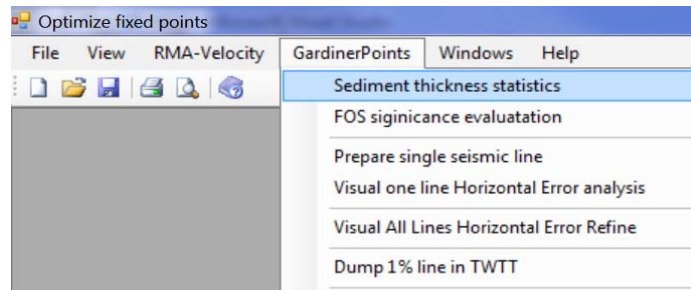
Figure 13.27 Sediment thickness statistics
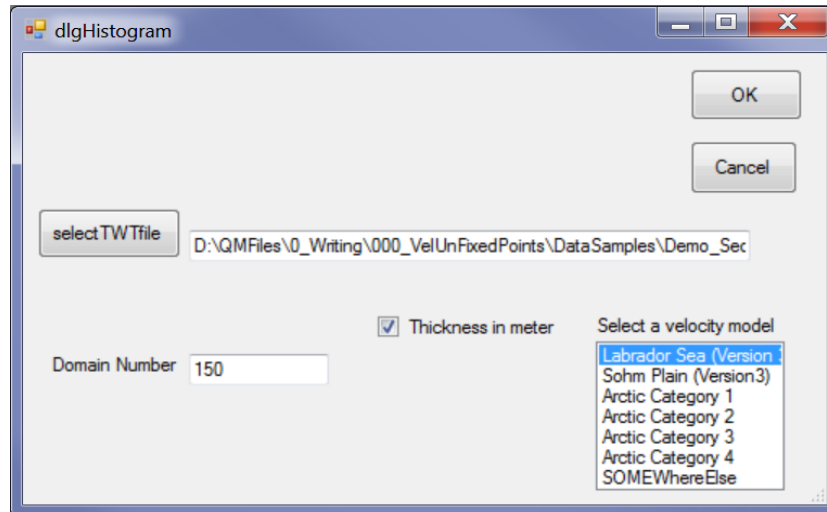
Figure 13.28 Parameter dialog box
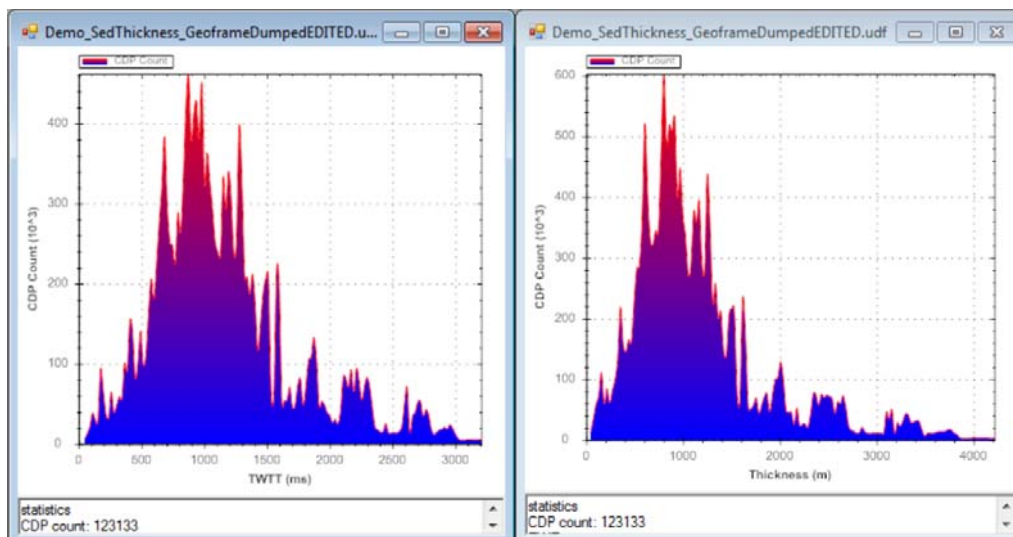
Figure 13.29 Sediment thickness in ms (TWT) and metres

13.4.8 QLine

As described in Chapter 5, QLine is used to optimize fixed point selection. Select "Dump 1% line in TWT" as shown in figures13.30, a dialog form as listed in figure 13.31 13.33, will appear.

In figure 13.31, the "Select a Thickness TWT file" and "select a seafloor TWT file" ask for interpreted sediment thickness in TWT (milliseconds) and seafloor horizon in TWT, respectively. Their format can be found in 13.3.2.

The "Select a FOS file" in figure 13.31 requires a FOS file name when it is clicked. The FOS file format can be found in 13.3.3.

The "Image width(Pixel)" and "Image Height (pixel)" in figure 13.31 define the width and height in pixels of the QLine plot, respectively.

"Select velocity model" in figure 13.31 is used for select a velocity model from the given velocity models in the velocity model file as described in 13.3.5.

User should use the "Select a folder to dump" button in figure 13.31 to select a folder for outputs. Gardiner will create some subfolders and dump reports, QLine in GeoFrame file (see 13.3.2) and QLines images.
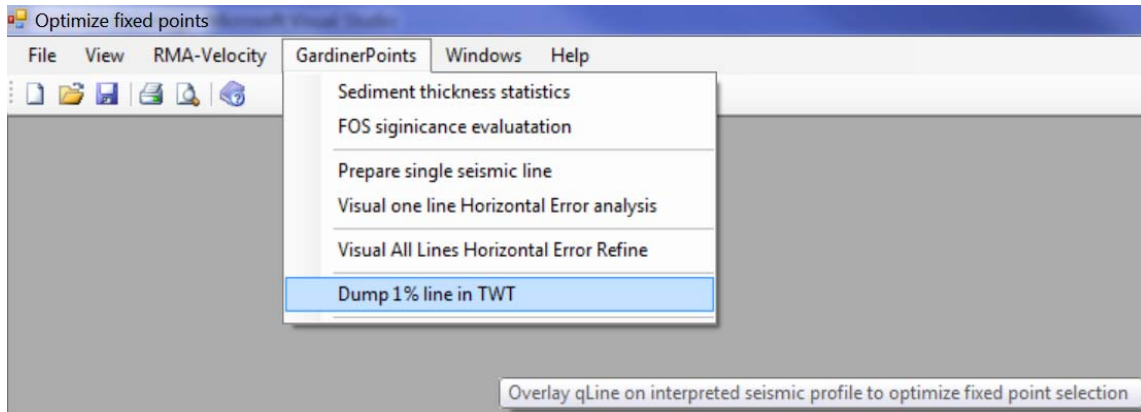
Figure 13.30 QLine menu
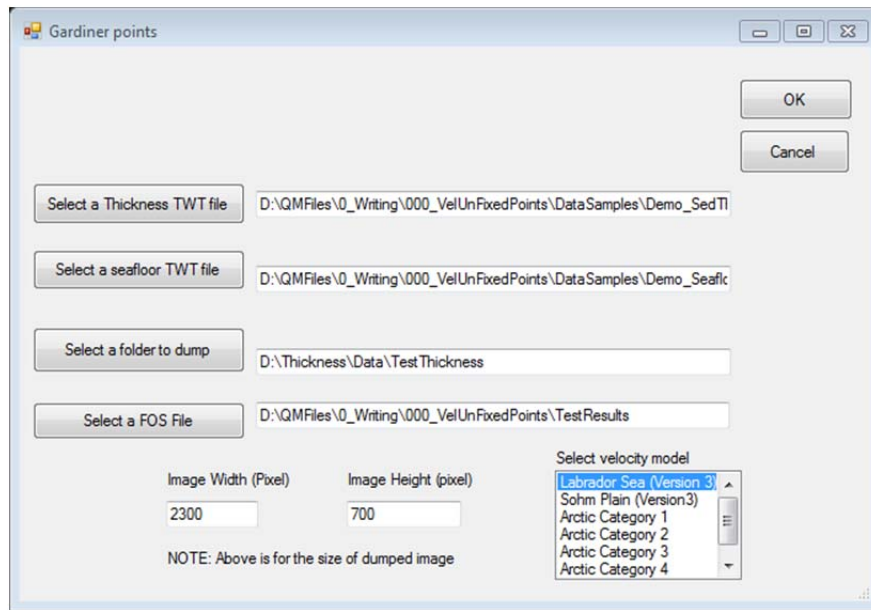
Figure 13.31 QLine dialog

Figure 13.32 QLine results data structure

93
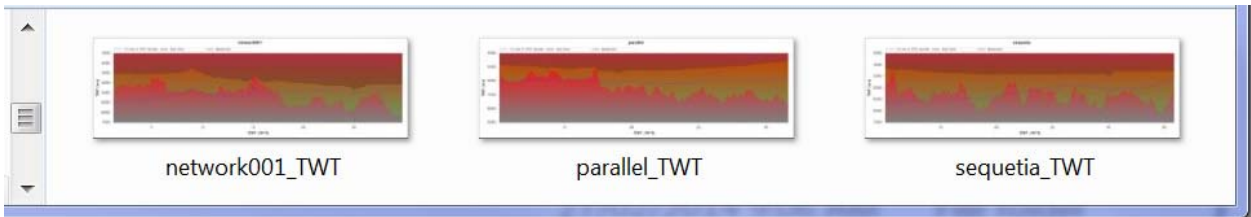
Figure 13.33 The resulting Image folder structure

Figure 13.33 and 13.34 are the sample of output folder structure and QLine image previews, respectively.

13.4.9 Uncertainty

The user can process all lines together or choose line-by-line for uncertainty analysis. Line-by-line analysis is favored by the lead author. The following steps are required:

1. Prepare a single line

Click "Prepare single seismic line item as shown in figure 13.34, a parameter dialog will appear as shown in figure 13.35 for parameter selection.
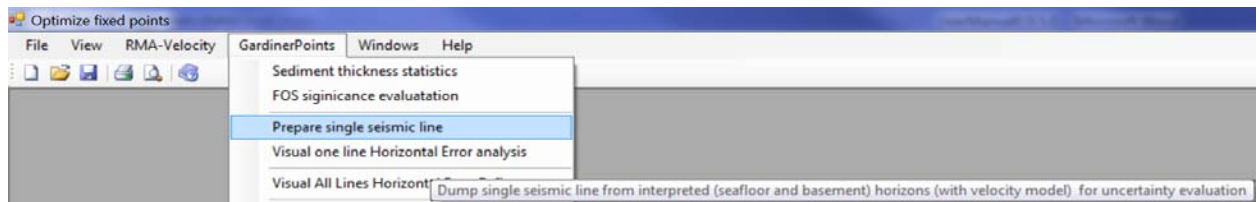
Figure 13.34 menu item

In the dialog form as shown in figure 13.35, select required files, an output folder, and velocity model, then click "OK" to finish single seismic lines preparing. The dumped single seismic lines are in plain text file and one example is shown in figure 13.36.
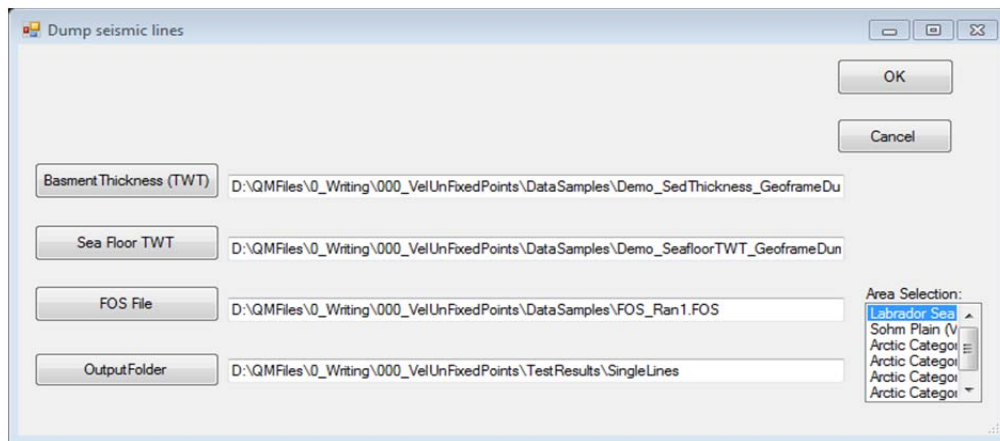
Figure 13.35 parameter dialog
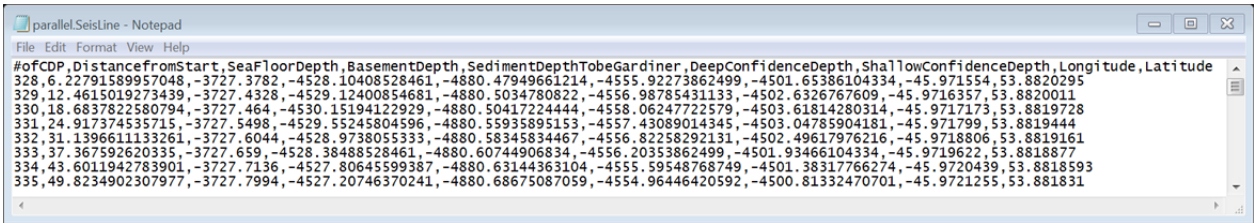
Figure 13.36 One example of text file dumped from this function

The Gardiner software tool is designed to read these single line files. They are comma delimited plain ascii text format.

2. Uncertainty analysis

After preparing the seismic lines, the uncertainty analysis can be done by selecting "Visual one line Horizontal Error analysis" item as shown in figure 13.37. This will require users to select a seismic profile prepared in step 1. Then an interactive graphic user interface as shown in figure 13.38 will appear permitting users for detailed uncertainty analysis for the input seismic line.
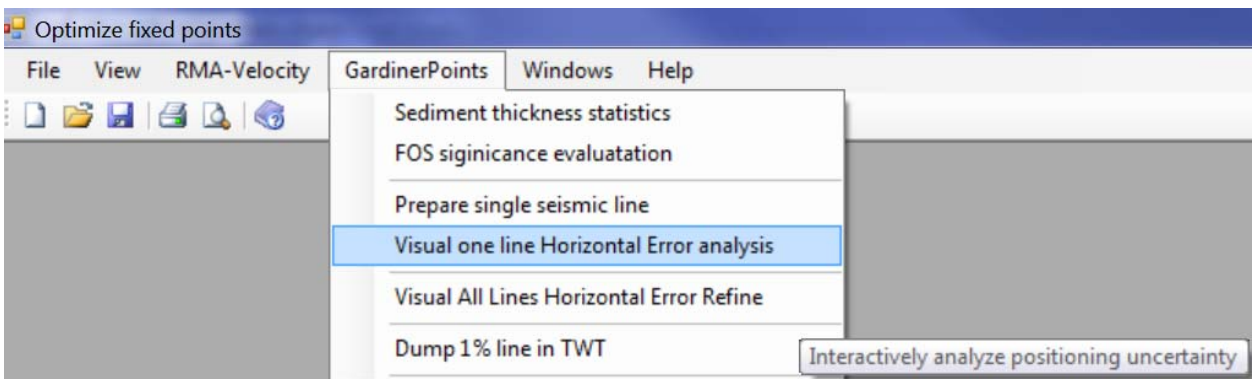
Figure 13.37 Uncertainty analysis menu

In figure 13.38, the "Seafloor and basement identi (m)" two text boxes are the errors caused during the identification of seafloor and basement horizons using seismic profiles, respectively. In the "Seismic nav." box, fill the seismic vessel navigation error which mainly depends on the used GPS or DGPS by the seismic vessel. The "Seismic proc. (m) box means the horizontal error caused during seismic data processing. The "Streamer uncertainty" box requires the error in stream position estimation. And the "FOS identification err." is the error occurred in FOS positioning. The grayed "Vertical err from Velocity (m)" and "Transmitted err. From vertical err" boxes are displayed intermediate errors created during uncertainty evaluation and they are not filled parameter.

The X and Y are "Geodetic distance (m)" and TWT (ms) in figure 13.38.

95

The vertical bars shown in figure 13.38 are movable by mouse as the mouse is over the bar and holding the left button. This way, the uncertainty analyzing domain (between the two bars) can be adjusted.

Another way to tune the analyzing domain is developed by using the MinX, MaxX, MinY and MaxY text boxes as shown in figure 13.38. by filling these values, the analyzing domain can be constrained accurately. The "Update" button is used to update the defined analyzing domain.

User can click the "Add Box Bar" button to add the uncertainty box as shown in figure 13.39. User can also use the "Show" and "Hide" button to control the two bars' visibility.
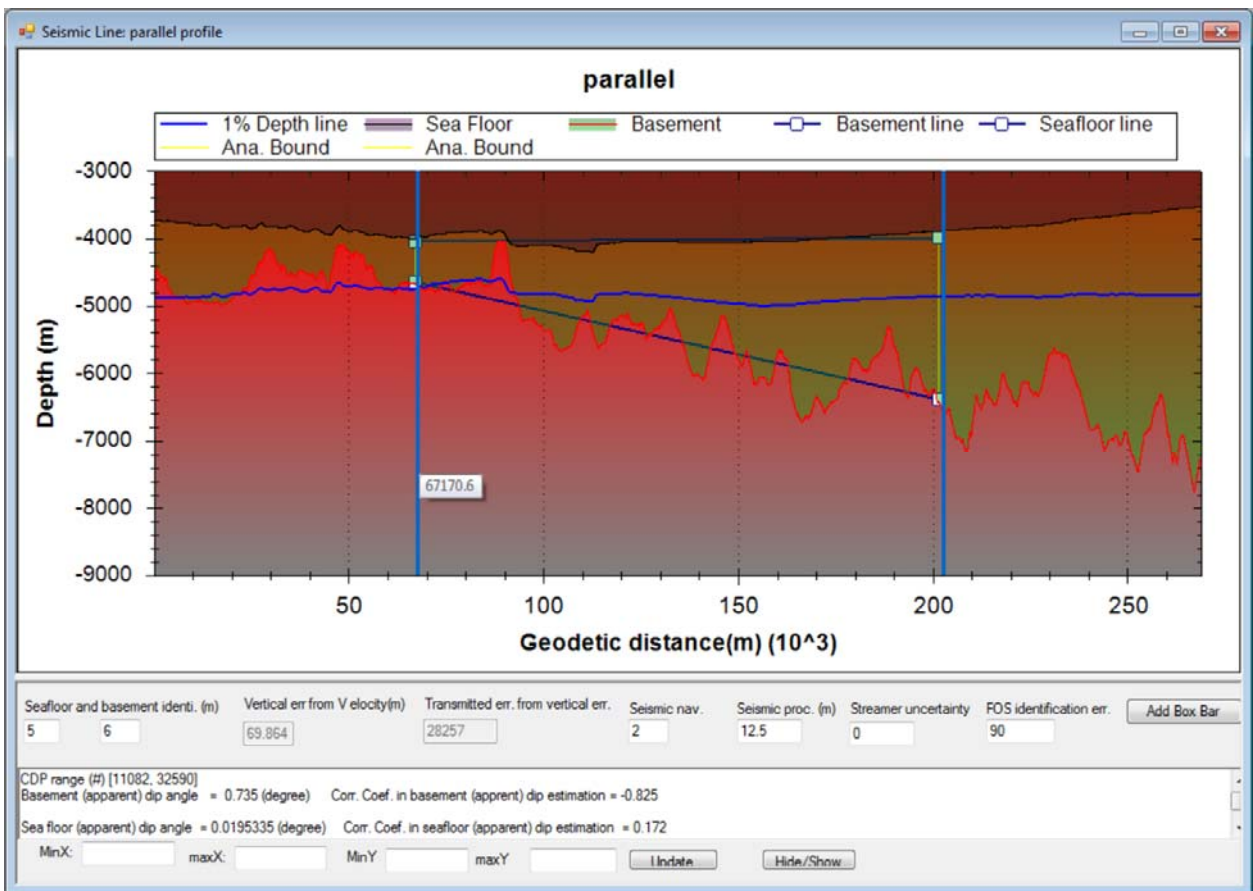
Figure 13.38 Uncertainty interactive graphic user interface

Use the "Hide/Show" toggle button to the bars for better display.

The analyzing report will be updated automatically in the report window as the text box in the bottom of figure 13.39.
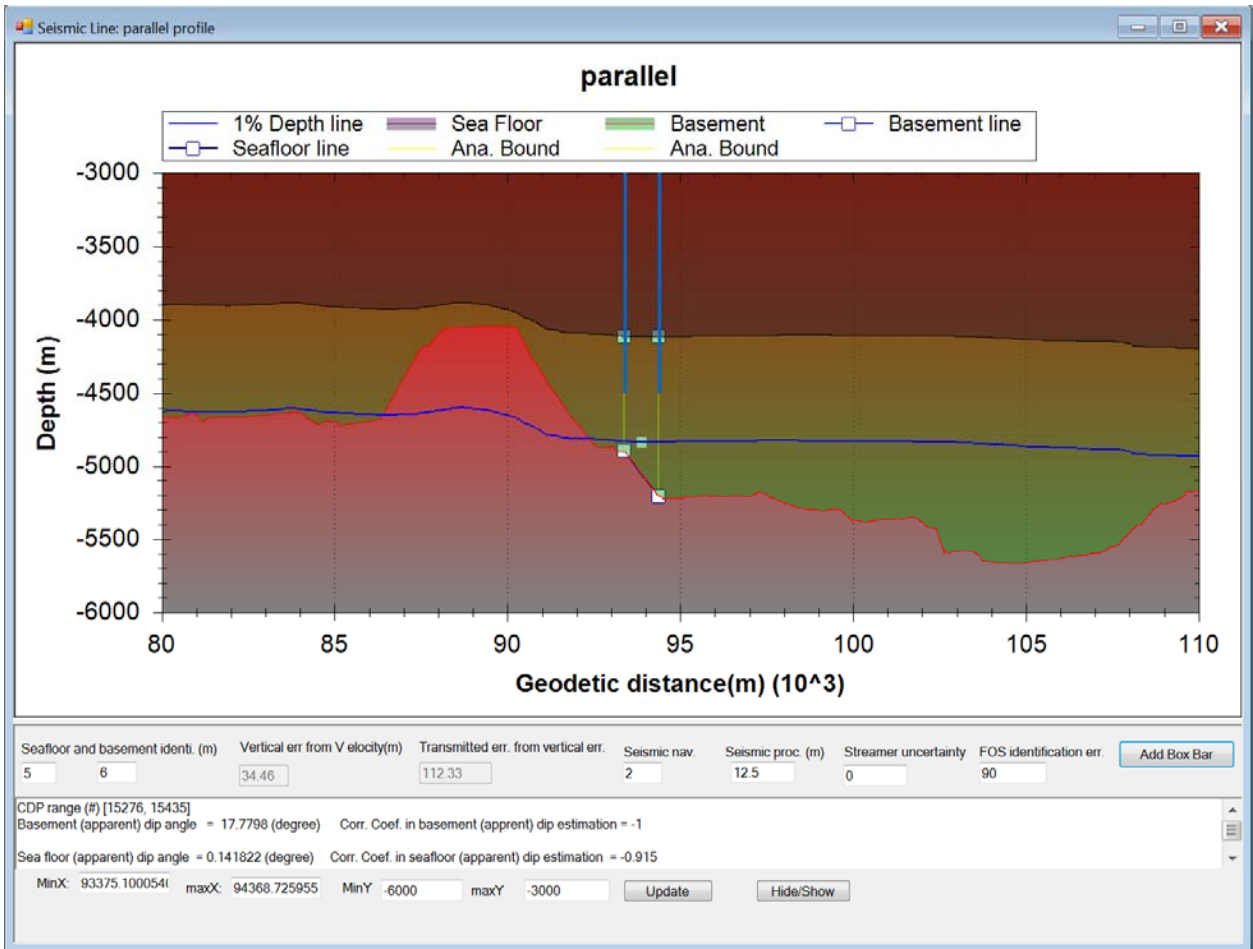
Figure 13.39 Adjusted uncertainty evaluation

14   Appendix 5: Look-up table of two-way time versus depth

The following is a listing of two-way time (in 5 millisecond increments) versus depth below seafloor (in metres) derived by applying Newton's method to the model of the present study (please refer to Section 4.2).

TWT(ms),h(m)	190,160.1	385,332.3	580,513.1
0,0.0	195,164.4	390,336.9	585,517.9
5,4.1	200,168.7	395,341.4	590,522.6
10,8.2	205,173.1	400,345.9	595,527.4
15,12.4	210,177.4	405,350.5	600,532.2
20,16.5	215,181.7	410,355.0	605,536.9
25,20.7	220,186.1	415,359.6	610,541.7
30,24.8	225,190.4	420,364.1	615,546.5
35,28.9	230,194.8	425,368.7	620,551.3
40,33.1	235,199.1	430,373.3	625,556.1
45,37.3	240,203.5	435,377.8	630,560.9
50,41.4	245,207.9	440,382.4	635,565.7
55,45.6	250,212.2	445,387.0	640,570.5
60,49.8	255,216.6	450,391.6	645,575.4
65,54.0	260,221.0	455,396.2	650,580.2
70,58.1	265,225.4	460,400.8	655,585.0
75,62.3	270,229.8	465,405.4	660,589.9
80,66.5	275,234.2	470,410.0	665,594.7
85,70.7	280,238.6	475,414.7	670,599.6
90,74.9	285,243.0	480,419.3	675,604.5
95,79.1	290,247.4	485,423.9	680,609.3
100,83.4	295,251.8	490,428.6	685,614.2
105,87.6	300,256.2	495,433.2	690,619.1
110,91.8	305,260.7	500,437.9	695,624.0
115,96.0	310,265.1	505,442.5	700,628.9
120,100.3	315,269.6	510,447.2	705,633.8
125,104.5	320,274.0	515,451.9	710,638.7
130,108.8	325,278.5	520,456.5	715,643.6
135,113.0	330,282.9	525,461.2	720,648.5
140,117.3	335,287.4	530,465.9	725,653.4
145,121.5	340,291.9	535,470.6	730,658.4
150,125.8	345,296.3	540,475.3	735,663.3
155,130.1	350,300.8	545,480.0	740,668.2
160,134.3	355,305.3	550,484.7	745,673.2
165,138.6	360,309.8	555,489.4	750,678.1
170,142.9	365,314.3	560,494.2	755,683.1
175,147.2	370,318.8	565,498.9	760,688.1
180,151.5	375,323.3	570,503.6	765,693.1
185,155.8	380,327.8	575,508.4	770,698.0

775,703.0	1005,939.7	1235,1191.0	1465,1458.0
780,708.0	1010,945.0	1240,1196.6	1470,1464.0
785,713.0	1015,950.3	1245,1202.2	1475,1470.0
790,718.0	1020,955.6	1250,1207.9	1480,1476.0
795,723.1	1025,960.9	1255,1213.5	1485,1482.0
800,728.1	1030,966.2	1260,1219.2	1490,1488.0
805,733.1	1035,971.6	1265,1224.9	1495,1494.1
810,738.1	1040,976.9	1270,1230.6	1500,1500.1
815,743.2	1045,982.3	1275,1236.2	1505,1506.1
820,748.2	1050,987.6	1280,1241.9	1510,1512.2
825,753.3	1055,993.0	1285,1247.6	1515,1518.3
830,758.3	1060,998.4	1290,1253.3	1520,1524.3
835,763.4	1065,1003.8	1295,1259.1	1525,1530.4
840,768.5	1070,1009.1	1300,1264.8	1530,1536.5
845,773.6	1075,1014.5	1305,1270.5	1535,1542.6
850,778.6	1080,1019.9	1310,1276.3	1540,1548.7
855,783.7	1085,1025.3	1315,1282.0	1545,1554.8
860,788.8	1090,1030.8	1320,1287.8	1550,1560.9
865,793.9	1095,1036.2	1325,1293.5	1555,1567.0
870,799.1	1100,1041.6	1330,1299.3	1560,1573.2
875,804.2	1105,1047.1	1335,1305.1	1565,1579.3
880,809.3	1110,1052.5	1340,1310.9	1570,1585.5
885,814.4	1115,1057.9	1345,1316.6	1575,1591.6
890,819.6	1120,1063.4	1350,1322.4	1580,1597.8
895,824.7	1125,1068.9	1355,1328.3	1585,1604.0
900,829.9	1130,1074.3	1360,1334.1	1590,1610.1
905,835.0	1135,1079.8	1365,1339.9	1595,1616.3
910,840.2	1140,1085.3	1370,1345.7	1600,1622.5
915,845.4	1145,1090.8	1375,1351.6	1605,1628.7
920,850.6	1150,1096.3	1380,1357.4	1610,1634.9
925,855.7	1155,1101.8	1385,1363.3	1615,1641.2
930,860.9	1160,1107.3	1390,1369.1	1620,1647.4
935,866.1	1165,1112.9	1395,1375.0	1625,1653.6
940,871.3	1170,1118.4	1400,1380.9	1630,1659.9
945,876.6	1175,1123.9	1405,1386.8	1635,1666.1
950,881.8	1180,1129.5	1410,1392.7	1640,1672.4
955,887.0	1185,1135.0	1415,1398.6	1645,1678.7
960,892.2	1190,1140.6	1420,1404.5	1650,1685.0
965,897.5	1195,1146.2	1425,1410.4	1655,1691.3
970,902.7	1200,1151.7	1430,1416.3	1660,1697.6
975,908.0	1205,1157.3	1435,1422.2	1665,1703.9
980,913.2	1210,1162.9	1440,1428.2	1670,1710.2
985,918.5	1215,1168.5	1445,1434.1	1675,1716.5
990,923.8	1220,1174.1	1450,1440.1	1680,1722.8
995,929.1	1225,1179.7	1455,1446.1	1685,1729.2
1000,934.4	1230,1185.3	1460,1452.0	1690,1735.5

1695,1741.9	1925,2043.6	2155,2364.1	2385,2704.0
1700,1748.2	1930,2050.4	2160,2371.3	2390,2711.7
1705,1754.6	1935,2057.1	2165,2378.4	2395,2719.3
1710,1761.0	1940,2063.9	2170,2385.6	2400,2726.9
1715,1767.4	1945,2070.7	2175,2392.9	2405,2734.5
1720,1773.8	1950,2077.5	2180,2400.1	2410,2742.2
1725,1780.2	1955,2084.3	2185,2407.3	2415,2749.9
1730,1786.6	1960,2091.1	2190,2414.5	2420,2757.5
1735,1793.0	1965,2098.0	2195,2421.8	2425,2765.2
1740,1799.5	1970,2104.8	2200,2429.0	2430,2772.9
1745,1805.9	1975,2111.6	2205,2436.3	2435,2780.6
1750,1812.4	1980,2118.5	2210,2443.6	2440,2788.3
1755,1818.8	1985,2125.4	2215,2450.9	2445,2796.0
1760,1825.3	1990,2132.2	2220,2458.1	2450,2803.7
1765,1831.8	1995,2139.1	2225,2465.5	2455,2811.5
1770,1838.3	2000,2146.0	2230,2472.8	2460,2819.2
1775,1844.8	2005,2152.9	2235,2480.1	2465,2827.0
1780,1851.3	2010,2159.8	2240,2487.4	2470,2834.7
1785,1857.8	2015,2166.7	2245,2494.8	2475,2842.5
1790,1864.3	2020,2173.7	2250,2502.1	2480,2850.3
1795,1870.8	2025,2180.6	2255,2509.5	2485,2858.1
1800,1877.4	2030,2187.5	2260,2516.8	2490,2865.9
1805,1883.9	2035,2194.5	2265,2524.2	2495,2873.7
1810,1890.5	2040,2201.4	2270,2531.6	2500,2881.5
1815,1897.0	2045,2208.4	2275,2539.0	2505,2889.3
1820,1903.6	2050,2215.4	2280,2546.4	2510,2897.2
1825,1910.2	2055,2222.4	2285,2553.8	2515,2905.0
1830,1916.8	2060,2229.4	2290,2561.2	2520,2912.9
1835,1923.4	2065,2236.4	2295,2568.7	2525,2920.8
1840,1930.0	2070,2243.4	2300,2576.1	2530,2928.6
1845,1936.6	2075,2250.4	2305,2583.5	2535,2936.5
1850,1943.2	2080,2257.5	2310,2591.0	2540,2944.4
1855,1949.8	2085,2264.5	2315,2598.5	2545,2952.3
1860,1956.5	2090,2271.6	2320,2606.0	2550,2960.2
1865,1963.1	2095,2278.6	2325,2613.4	2555,2968.2
1870,1969.8	2100,2285.7	2330,2620.9	2560,2976.1
1875,1976.4	2105,2292.8	2335,2628.4	2565,2984.0
1880,1983.1	2110,2299.9	2340,2636.0	2570,2992.0
1885,1989.8	2115,2307.0	2345,2643.5	2575,3000.0
1890,1996.5	2120,2314.1	2350,2651.0	2580,3007.9
1895,2003.2	2125,2321.2	2355,2658.6	2585,3015.9
1900,2009.9	2130,2328.3	2360,2666.1	2590,3023.9
1905,2016.6	2135,2335.4	2365,2673.7	2595,3031.9
1910,2023.4	2140,2342.6	2370,2681.3	2600,3039.9
1915,2030.1	2145,2349.7	2375,2688.8	2605,3047.9
1920,2036.8	2150,2356.9	2380,2696.4	2610,3056.0

2615,3064.0	2845,3444.2	3075,3844.4	3305,4264.2
2620,3072.1	2850,3452.7	3080,3853.3	3310,4273.5
2625,3080.1	2855,3461.2	3085,3862.3	3315,4282.9
2630,3088.2	2860,3469.7	3090,3871.2	3320,4292.2
2635,3096.3	2865,3478.2	3095,3880.1	3325,4301.6
2640,3104.4	2870,3486.7	3100,3889.1	3330,4310.9
2645,3112.5	2875,3495.3	3105,3898.1	3335,4320.3
2650,3120.6	2880,3503.8	3110,3907.0	3340,4329.7
2655,3128.7	2885,3512.4	3115,3916.0	3345,4339.1
2660,3136.8	2890,3520.9	3120,3925.0	3350,4348.5
2665,3144.9	2895,3529.5	3125,3934.0	3355,4357.9
2670,3153.1	2900,3538.1	3130,3943.0	3360,4367.4
2675,3161.2	2905,3546.7	3135,3952.1	3365,4376.8
2680,3169.4	2910,3555.3	3140,3961.1	3370,4386.2
2685,3177.6	2915,3563.9	3145,3970.1	3375,4395.7
2690,3185.8	2920,3572.5	3150,3979.2	3380,4405.1
2695,3194.0	2925,3581.1	3155,3988.2	3385,4414.6
2700,3202.2	2930,3589.8	3160,3997.3	3390,4424.1
2705,3210.4	2935,3598.4	3165,4006.4	3395,4433.6
2710,3218.6	2940,3607.1	3170,4015.5	3400,4443.1
2715,3226.8	2945,3615.8	3175,4024.6	3405,4452.6
2720,3235.1	2950,3624.4	3180,4033.7	3410,4462.1
2725,3243.3	2955,3633.1	3185,4042.8	3415,4471.6
2730,3251.6	2960,3641.8	3190,4051.9	3420,4481.1
2735,3259.8	2965,3650.5	3195,4061.0	3425,4490.7
2740,3268.1	2970,3659.2	3200,4070.2	3430,4500.2
2745,3276.4	2975,3668.0	3205,4079.3	3435,4509.7
2750,3284.7	2980,3676.7	3210,4088.5	3440,4519.3
2755,3293.0	2985,3685.4	3215,4097.6	3445,4528.9
2760,3301.3	2990,3694.2	3220,4106.8	3450,4538.5
2765,3309.7	2995,3702.9	3225,4116.0	3455,4548.0
2770,3318.0	3000,3711.7	3230,4125.2	3460,4557.6
2775,3326.3	3005,3720.5	3235,4134.4	3465,4567.2
2780,3334.7	3010,3729.3	3240,4143.6	3470,4576.9
2785,3343.1	3015,3738.1	3245,4152.8	3475,4586.5
2790,3351.4	3020,3746.9	3250,4162.1	3480,4596.1
2795,3359.8	3025,3755.7	3255,4171.3	3485,4605.7
2800,3368.2	3030,3764.5	3260,4180.5	3490,4615.4
2805,3376.6	3035,3773.4	3265,4189.8	3495,4625.0
2810,3385.0	3040,3782.2	3270,4199.1	3500,4634.7
2815,3393.4	3045,3791.1	3275,4208.3	3505,4644.4
2820,3401.9	3050,3799.9	3280,4217.6	3510,4654.1
2825,3410.3	3055,3808.8	3285,4226.9	3515,4663.7
2830,3418.8	3060,3817.7	3290,4236.2	3520,4673.4
2835,3427.2	3065,3826.6	3295,4245.5	3525,4683.1
2840,3435.7	3070,3835.5	3300,4254.8	3530,4692.9

3535,4702.6	3765,5158.4	3995,5630.1	4225,6116.2
3540,4712.3	3770,5168.5	4000,5640.6	4230,6126.9
3545,4722.0	3775,5178.6	4005,5651.0	4235,6137.6
3550,4731.8	3780,5188.7	4010,5661.4	4240,6148.3
3555,4741.5	3785,5198.8	4015,5671.9	4245,6159.0
3560,4751.3	3790,5208.9	4020,5682.3	4250,6169.8
3565,4761.1	3795,5219.1	4025,5692.8	4255,6180.5
3570,4770.9	3800,5229.2	4030,5703.2	4260,6191.3
3575,4780.6	3805,5239.3	4035,5713.7	4265,6202.0
3580,4790.4	3810,5249.5	4040,5724.2	4270,6212.8
3585,4800.2	3815,5259.6	4045,5734.6	4275,6223.5
3590,4810.0	3820,5269.8	4050,5745.1	4280,6234.3
3595,4819.9	3825,5280.0	4055,5755.6	4285,6245.1
3600,4829.7	3830,5290.2	4060,5766.1	4290,6255.9
3605,4839.5	3835,5300.4	4065,5776.6	4295,6266.6
3610,4849.4	3840,5310.6	4070,5787.1	4300,6277.4
3615,4859.2	3845,5320.8	4075,5797.7	4305,6288.2
3620,4869.1	3850,5331.0	4080,5808.2	4310,6299.0
3625,4878.9	3855,5341.2	4085,5818.7	4315,6309.8
3630,4888.8	3860,5351.4	4090,5829.3	4320,6320.7
3635,4898.7	3865,5361.6	4095,5839.8	4325,6331.5
3640,4908.6	3870,5371.9	4100,5850.4	4330,6342.3
3645,4918.5	3875,5382.1	4105,5860.9	4335,6353.1
3650,4928.4	3880,5392.4	4110,5871.5	4340,6364.0
3655,4938.3	3885,5402.6	4115,5882.0	4345,6374.8
3660,4948.2	3890,5412.9	4120,5892.6	4350,6385.7
3665,4958.2	3895,5423.2	4125,5903.2	4355,6396.5
3670,4968.1	3900,5433.5	4130,5913.8	4360,6407.4
3675,4978.0	3905,5443.8	4135,5924.4	4365,6418.2
3680,4988.0	3910,5454.0	4140,5935.0	4370,6429.1
3685,4998.0	3915,5464.4	4145,5945.6	4375,6440.0
3690,5007.9	3920,5474.7	4150,5956.2	4380,6450.9
3695,5017.9	3925,5485.0	4155,5966.8	4385,6461.8
3700,5027.9	3930,5495.3	4160,5977.5	4390,6472.6
3705,5037.9	3935,5505.6	4165,5988.1	4395,6483.5
3710,5047.9	3940,5516.0	4170,5998.7	4400,6494.4
3715,5057.9	3945,5526.3	4175,6009.4	4405,6505.3
3720,5067.9	3950,5536.7	4180,6020.0	4410,6516.3
3725,5077.9	3955,5547.0	4185,6030.7	4415,6527.2
3730,5088.0	3960,5557.4	4190,6041.3	4420,6538.1
3735,5098.0	3965,5567.8	4195,6052.0	4425,6549.0
3740,5108.0	3970,5578.1	4200,6062.7	4430,6560.0
3745,5118.1	3975,5588.5	4205,6073.4	4435,6570.9
3750,5128.2	3980,5598.9	4210,6084.1	4440,6581.8
3755,5138.2	3985,5609.3	4215,6094.8	4445,6592.8
3760,5148.3	3990,5619.7	4220,6105.5	4450,6603.7

4455,6614.7	4595,6923.6	4735,7236.1	4875,7551.8
4460,6625.7	4600,6934.7	4740,7247.3	4880,7563.2
4465,6636.6	4605,6945.8	4745,7258.5	4885,7574.5
4470,6647.6	4610,6956.9	4750,7269.8	4890,7585.9
4475,6658.6	4615,6968.0	4755,7281.0	4895,7597.2
4480,6669.6	4620,6979.1	4760,7292.2	4900,7608.6
4485,6680.6	4625,6990.2	4765,7303.5	4905,7619.9
4490,6691.6	4630,7001.4	4770,7314.7	4910,7631.3
4495,6702.6	4635,7012.5	4775,7326.0	4915,7642.6
4500,6713.6	4640,7023.6	4780,7337.2	4920,7654.0
4505,6724.6	4645,7034.8	4785,7348.5	4925,7665.4
4510,6735.6	4650,7045.9	4790,7359.8	4930,7676.7
4515,6746.6	4655,7057.1	4795,7371.0	4935,7688.1
4520,6757.6	4660,7068.2	4800,7382.3	4940,7699.5
4525,6768.7	4665,7079.4	4805,7393.6	4945,7710.9
4530,6779.7	4670,7090.6	4810,7404.9	4950,7722.2
4535,6790.7	4675,7101.7	4815,7416.1	4955,7733.6
4540,6801.8	4680,7112.9	4820,7427.4	4960,7745.0
4545,6812.8	4685,7124.1	4825,7438.7	4965,7756.4
4550,6823.9	4690,7135.3	4830,7450.0	4970,7767.8
4555,6834.9	4695,7146.4	4835,7461.3	4975,7779.2
4560,6846.0	4700,7157.6	4840,7472.6	4980,7790.6
4565,6857.1	4705,7168.8	4845,7483.9	4985,7802.0
4570,6868.1	4710,7180.0	4850,7495.2	4990,7813.4
4575,6879.2	4715,7191.2	4855,7506.5	4995,7824.9
4580,6890.3	4720,7202.4	4860,7517.9	5000,7836.3
4585,6901.4	4725,7213.6	4865,7529.2	
4590,6912.5	4730,7224.9	4870,7540.5	

Acknowledgments

Contact Information

Qingmou Li
Geological Survey of Canada (Atlantic)
1 Challenger Drive
P.O. Box 1006
Dartmouth, NS
CANADA
B2Y 4A2

qli@NRCan.gc.ca   or
Qingmou.Li@NRCan.gc.ca